UNIVERSITY OF CALIFORNIA,
IRVINE

Investigation of metal ion extraction and aggregate formation combining acidic and neutral organophosphorus reagents

DISSERTATION

Submitted in partial satisfaction of the requirements
for the degree of

DOCTOR OF PHILOSOPHY

in Chemical Engineering

by

Alexander David Braatz

Dissertation Committee:
Professor Mikael Nilsson, Chair
Professor Hung Nguyen
Professor A. J. Shaka

2015

DEDICATION

To

My family, friends, and all those who have guided me along the way

TABLE OF CONTENTS:

LIST OF FIGURES

LIST OF TABLES

ACKNOWLEDGEMENTS

I would like to express the deepest appreciation to my committee chair, Professor Mikael Nilsson, who selected me to work on this project and expressed confidence that I could perform well in the field of nuclear science, which until the beginning of grad school was unknown to me. I am grateful for his advice and friendly counsel, his enthusiasm towards the field, and the unending support when certain models and analysis methods were being uncooperative. Without him, I would have never been able to present my accomplishments in this thesis. I would also like to thank my committee members, Professor A. J. Shaka for his guidance through the years at group meeting and Professor Hung Nguyen for suggesting I apply for graduate school in the first place. I would also like to express my gratitude to Dr. Mark Antonio and Dr. Ross Ellis who have guided my experiments while at Argonne National Laboratory. Before I began working with them, X-ray studies were an unknown science to me and it has truly been an honor working with them.

Throughout my PhD career, both past and present students have been there for me through it all. Michael, Ko, Jeremy, Leila, Andy, Tro, Christian, Rose, Edward, Randy, Amber, Quynh, Jonathan, Ted, and Cory provided help and camaraderie throughout the years. They have been the best colleagues that anyone could hope for and will be greatly missed. I would also like to thank those undergraduate researchers, Tim Anderson and Steven Bui, who have helped me during the life of this project and have hopefully learned as much from me as I did from them.

I would like to thank the UCI TRIGA® Reactor Facility and Dr. George Miller for his help and support with reactor runs and suggesting that I pursue an operator license. I have learned many things throughout the years and I hope to take the lessons I've learned to other facilities.

My parents and family have been the most essential support group for me as I have been working on my PhD. They have been very encouraging and supportive of my choice of career path and have been there for me in my times of need. I am grateful for their unlimited time and love.

Last but not least, I would like to thank Mallory who has been the rock that I could lean on during my time as a PhD student. She has always been supportive and has believed in me through every hurdle, even when I did not. Without her, none of this would have been possible. She is and will always be in my heart and mind as my best friend.

I would like to thank the U.S. Department of Energy for funding through the Nuclear Energy University Program, NEUP contract No. 120569 and DE-NE0000156. The work completed at Argonne National Lab and the use of the Advanced Photon Source was supported by the U.S. Department of Energy, Office of Science, Office of Basic Energy Sciences, Division of Chemical Sciences, Biosciences and Geosciences under contract No. DE-AC02-06CH11357.

CURRICULUM VITAE

Alexander D Braatz

2010 B.S. in Chemical Engineering, University of California, Irvine

2012 M.S. in Chemical Engineering, University of California, Irvine

2015 Ph.D. in Chemical Engineering, University of California, Irvine

Field of Study

Synergistic solvent extraction system investigations for used nuclear fuel processing.

Publications

1. Braatz, A.; Nilsson, M. A SANS study of Aggregation Phenomena in the TBP-HDBP Solvent Extraction System. (*In preparation)*
2. Braatz, A.; Antonio, M.; Nilsson, M. A SAXS study of Aggregation in the TBP-HDBP Solvent Extraction System. (*In preparation)*
3. Braatz, A.; Antonio, M.; Nilsson, M. Structural Study of Complexes Formed by Acidic and Neutral Organophosphorus Reagents. (*In preparation)*
4. Nilsson, M., Braatz, A., Jackson, A., Vo, Q., Nguyen, H. D., Zalupski, P., Ellis, R., Antonio, M. (2015). Microemulsions and Aggregation Formation in Extraction Processes for Used Nuclear Fuel. In *Proceedings from 13IEMPT. OECD/NEA 13th Information Exchange Meeting on Actinide and Fission Product Partitioning and Transmutation*, (pp. 129-137). Seoul, South Korea.
5. Nilsson, M., Braatz, A., Jackson, A., Zalupski, P., Ellis, R., Antonio, M. (2014). Microemulsions and Aggregation Formation in Extraction Processes for Used Nuclear Fuel. In *Proceedings from the International Solvent Extraction Conference. ISEC' 2014*, (pp. 551-556). Würzburg, Germany.
6. Braatz, A.; Nilsson, M. Fluorescence studies of metal complexes in synergistic extraction systems combining dibutyl phosphoric acid and tri-*n*-butyl phosphate. *J. Radioanal. Nucl.Chem.* 2014.DOI 10.1007/s10967-014-3487-1
7. Braatz, A. D.; Ellis, R.; Antonio, M.; Nilsson, M. Investigation of Metal Ion Extraction and Aggregate Formation Combining Acidic and Neutral Organophosphorus Reagents. Global 2013, Salt Lake City, Utah, September 29-October 3, 2013, 1490-1494.
8. Ellis, R. J.; Anderson, T. L.; Antonio, M. R.; Braatz, A.; Nilsson, M. A SAXS Study of Aggregation in the Synergistic TBP-HDBP Solvent Extraction System. *J. Phys. Chem. B.* 2013, 117, 5916-5924.
9. Anderson, T. L.; Braatz, A.; Ellis, R. J.; Antonio, M. R.; Nilsson, M. Synergistic Extraction of Dysprosium and Aggregate formation in Solvent Extraction Systems Combining TBP and HDBP. *Solvent Extr. Ion Exch.* 2013, 31, 617-633.

ABSTRACT OF THE DISSERTATION

Investigation of metal ion extraction and aggregate formation combining acidic and neutral organophosphorus reagents

By

Alexander David Braatz

Doctor of Philosophy in Chemical Engineering

University of California, Irvine, 2015

Professor Mikael Nilsson, Chair

Advanced nuclear fuel cycles are dependent on successful chemical separation of various elements present in the used fuel. Numerous solvent extraction systems have been developed for this purpose. In these solvent extraction systems, aggregation phenomena can interfere with the efficiencies of the processes and decrease the successfulness of the separation. The predictability of these phenomena have been challenging due to the lack of a fundamental understanding of the mechanism that drives these aggregate formations. Previous research has shown that these aggregates may be linked to a synergistic effect, whereby the extraction of metal ion into the organic phase is enhanced with mixtures of extraction reagents compared to each reagent used alone. To investigate the aggregation more closely and to probe the possibility of a link between aggregation and synergy, combined solutions of tri-*n*-butyl phosphate (TBP) and dibutyl phosphoric acid (HDBP) in *n*-dodecane were chosen as the organic phase to be contacted with an aqueous phase containing a single metal ion from the lanthanide series in nitric acid.Distribution ratios of the metal ions between the phases as well as water uptake and nitric acid extraction into the organic phase were used to investigate this aggregation phenomenon more closely and to understand the extraction behavior of this binary extractant system.Additionally, X-ray and

neutron scattering and X-ray absorptiontechniques were used to investigate the macromolecular phase behaviors of the organic phase, with scattering yielding information regarding aggregate size and shape and absorption yielding information on the complex environment of the extracted metal ions. The combination of these techniques provide a more complete picture of the organic phase and may shed light on the link to synergy and mixed complexes. Our studies show that the complexes resulting from extraction of lanthanides into TBP:HDBP system differ from those that have been previously explored in these types of systems. This finding coupled with the formation of elongated rod-like aggregate structures formed in the organic phase may suggest that the complexes formed by the extraction of lanthanides by TBP:HDBP may be incorporated into the micellar structures and indicate a link between synergy and aggregate formation.

Chapter 1: Introduction and Background

1.1 Nuclear Energy and Fuel Management

Nuclear reactors have the ability to produce vast amounts of energy while yielding low carbon emissions and minimal air pollution. These two properties alone make nuclear energy an attractive option to provide enough power to satiate the worldwide energy demand that has been increasing for the past decade due to the increase in industrial and domestic utilization. In nuclear power plants, energy is produced by the process of fission, where a heavy atom is split into two lighter nuclei. During this process, a large amount of energy is released from the splittingofthese heavy nuclei, typically uranium for commercial power plants. A typical reaction of this type proceeds as described in equation 1.1 below.

$$^{235}\mathrm{U} + \mathbf{neutron} \rightarrow \mathbf{fission\ products} + 2.5\ \mathbf{neutrons} + \mathbf{200MeV} \qquad 1.1$$

During the neutron irradiation process, neutron capture (n,γ) reactions may also take place and produce other actinides in addition to the fission products produced by the splitting of the heavy nuclei. These fission products and other actinides contaminate the used nuclear fuel with both short lived isotopes that emit very strong radiation and long lived isotopes that remain radioactive for hundreds of thousands of years before their radiation levels return to natural background. When fuel has reached the end of its useful life in the reactor, it is removed and placed into cooling pools on site since the decay of radioactive elements creates excessive heat.[1] Management of the fuel is essential to avoid potential environmental and societal disasters since the fuel remains radiologically hazardous on a timescale of well over a hundred thousand years.[2-4] One solution to this problem requires specialized, secure geological waste repositories, similar

to the well know and controversial Yucca Mountain High-Level Waste Repository. It is important to note that approximately 96% of the used nuclear fuel is reusable if purified, and a few countries such as France, Japan and the UK are currently or have in the past utilized purification methods to this end.[3-6] The Blue Ribbon Commission on America's Nuclear Future (BRC), formed by the United States Government to investigate the current state of domestic used nuclear fuel management, determined that recycling of used fuel would greatly reduce the quantity of uranium required for fabrication of fuel assemblies compared to a non-recycling reference case.[3] However, a need for a geological repository is still very present for used fuels that cannot be recycled or waste streams that contain constituents that cannot be used in the fabrication of new fuel elements. The report also determined that utilization of recycle processes would increase the sustainability of the fuel cycle as a whole and provides for significant front-end waste reductionsuch as waste from mining and enrichment processes. The commission is vehement on its stance that waste treatment must progress further so future generations of Americans will not suffer from the impact of the current used fuel inventory, toalsoregain lost influence and leadership in nuclear technologies as a whole, and finallyto retain the option of future nuclear energy usage for future generations.

Though the BRC outlined strategies for management of used fuels, the path forward has yet to be decided by the federal government. Currently, there are no efforts in the United States to recycle any of the current 72,000 metric tons of used fuel that continues to accumulate at a rate of ~2,200 tons per year.[3,7] Additionally, efforts to establish a politically viable and environmentally suitable final repository location have been largely unsuccessful and the efforts to complete the Yucca Mountain repository have been, as of now, canceled. Continued research regarding potential treatment methods and a fundamental understanding of each process is of

theutmost importance to allow policy makers a basis with which to make an informed decision. This research does not go without a substantial financial commitment, though the needs of the nation far outweigh the costs. One current research thrust into potential solutions to the used fuel problem and the focus of this thesis is the investigation of solvent extraction systems designed for the separation of the metals present in used nuclear fuels.

1.2 Solvent Extraction

In the early nineteenth century, large advancements in chemistry brought about the synthesis and characterization of numerous pure inorganic and organic compounds. During this period of time, it was discovered that many inorganic salts, such as iron, mercury and gold chlorides, could be dissolved in alcohols and ethers and subsequently recrystallized.[8] As time progressed, it was discovered that the introduction of organic reagents dissolved into another organic liquid could increase the efficiency of extracting a desired component from aqueous solutions, and thus modern solvent extraction was born. Solvent extraction is a proven technique that is used in industry for the separation and partitioning of nonvolatile solutes (e.g., metal ions). It has current and widespread uses in the pharmaceutical industry, the production of precious metals, base metals, rare-earth metals, and in the chemical treatment of used nuclear fuel.[9-13] Solvent extraction involves the use of a biphasic (liquid-liquid) solution system: an aqueous phase containing a target solute, such as a metal ion, is contacted with an immiscible organic solvent containing an amphiphilic molecule, referred to as an extractant. With vigorous contact and efficient phase disengagement, the targeted solute is bound selectively to the extractant and is removed to the organic phase, separating it from the remaining aqueous solutes. A simplified example of a generic solvent extraction system is shown in Figure 1. An example of such a process designed for the separation of uranium and plutonium from the rest of the material in

used nuclear fuel is the PUREX (Plutonium, Uranium, Reduction, EXtraction) process used in France, Japan and the UK.[5,6]The PUREX process relies on tri-*n*-butyl phosphate, TBP, to selectively extract U and Pu away from the fission and corrosion products as well as other minor actinides (Figure 2a).

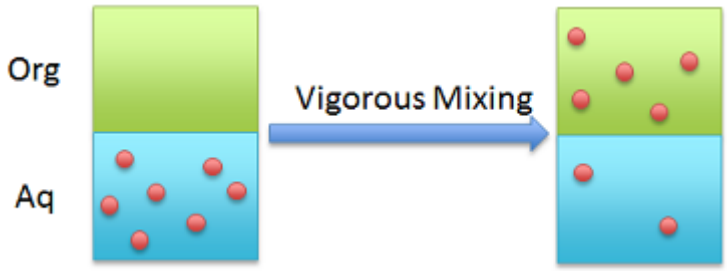

Figure 1: Example of a generic solvent extraction scheme. The red dots represent the solute of interest to be extracted, i.e. metal ions in this case.

The extraction of metal ions using TBP has been studied extensively over the years and the extraction behaviors of various metal ions from moderately concentrated nitric acid solutions are well characterized, at least on an empirical level.[14-17]

1.3 Neutral Extraction Reagents

In the early days of used nuclear fuel processing, experiments carried out at Oak Ridge National Lab investigated TBP and other similar neutral organophosphorus compounds extensively and ultimately replacedthe ethers and ketones used previously for raw material processing from mining and nuclear fuel processing.[18]

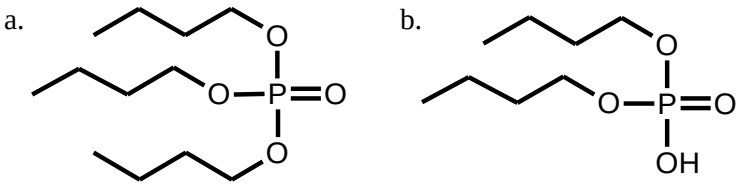

Figure 2: Structure of tri-*n*-butyl phosphate (TBP) (a.) and dibutylphosphoric acid (HDBP) (b.).

For practical purposes, most neutral organophosphorus compounds are relatively similar in their extraction behavior and the type of complexes they form, though as a general rule the extraction power increases markedly as the number of carbon-phosphorus direct bonds increases. Namely,

the distribution ratios expected for extraction by neutral organophosphorus reagents should follow the general trend; phosphate <phosphonate<phosphinate< phosphine oxide.[18] Although phosphinates and phosphine oxides show great promise in terms of their high extractability and have been viewed as potential extractants,[19] they do suffer from low stability and are therefore impractical as effective extractant reagents.[18]

TBP (Figure 2a), the most studied of the organophosphorus extractants and the extractant of interest for this present work, coordinates to metal ions via a solvation mechanism.[20] For such solvation mechanisms, the neutral metal nitrate species is recovered through displacement of water molecules from the inner-coordination sphere of the aquated cation (M^{n+}), which is favored by high nitric acid concentrations as shown in Eq. 1.2. Stripping of the organic phase is then accomplished through contacting the loaded organic phase with an aqueous solution of low nitric acid concentration, thus forcing the reverse reaction.

$$\mathbf{M^{n+} + n NO_3^- + m\overline{TBP} \rightleftarrows \overline{M(NO_3)_n(TBP)_m} + water} \qquad 1.2$$

A bar over a species in the above equation and all following equations indicates that it is present in the organic phase.

1.4 Acidic Extraction Reagents

During the extraction of highly radioactive materials, as would be the case in the PUREX process and all other proposed processes for the separation of used nuclear fuel, the TBP will inevitably degrade by radiolysis and hydrolysis. The primary degradation product of TBP is dibutylphosphoric acid, HDBP(Figure 2b), which is an effective extraction reagent at low aqueous acidity.[21] In addition to being an effective extractant, it has been noticed that HDBP

may also increase the chance of third phase formation (explained in greater detail in a later section) in the process streams, further complicating the extraction. In contrast to the solvating mechanism present for the extraction of metal ions with TBP, HDBP is a cation exchanging, chelating extractant. It must be deprotonated to form the DBP^- anion in order to effectively extract metal ions, which is achieved by a chelating mechanism wherein DBP^- binds to the inner-coordination sphere of the metal ion in the process as a monodeprotonated dimer type species.[20,22] Equation 1.3 shows the reaction for the acidic reagent extraction.

$$\mathbf{M^{n+} + n\overline{(HDBP)_2} \rightleftarrows \overline{M(DBP)_n(HDBP)_n} + nH^+ + water} \qquad 1.3$$

In this scheme, metal extraction is favored for low nitric acid concentrations (where the deprotonated anion prevails) and stripping at high (where the associated acid would be reformed). For example, under the moderately high acid PUREX loading condition, HDBP is almost completely ineffective as an extractant. This, however, is not always the case. At very high acid concentrations HDBP may instead act as a neutral solvating extractant, as seen with the extraction of UO_2^{2+} with HDBP.[23] It is important to note that under the low acid PUREX stripping condition, HDBP is capable of exchanging its H^+ ion for the polyvalent metal cations, including U(VI) and Pu(IV, VI), thus retaining them in the organic phase and reducing the selectivity for U(VI) and Pu(IV, VI) over metal ions of other valence states.[24] This is the main reason why the organic solvent in PUREX needs to be cleaned periodically to remove HDBP.The exact composition of the extracted complex in Eq. 1.2 and 1.3 may vary depending on the metal and the diluent used for the extraction. The examples given by Irving and Edgington[20] for U(VI), that is, UO_2^{2+}, extraction suggests that n = 2 and m = 2 (in both Eq. 1.2

and 1.3), whereas for a trivalent metal ion *n* would be equal to 3 to completely neutralize the charge of the metal ion.

1.5 Synergy

In addition to the single extractants having differing mechanisms, combinations of neutral and acidic extractants may result in an enhancement in extraction, commonly referred to as synergy, which is unexpected based upon a simple additive mechanism. Traditionally, past studies have tried to explain synergism by the formation of mixed complexes where both extractants are coordinated to the metal ion.[13,20,25] This causes the metal ion to be completely dehydrated and thus more lipophilic which improves its extraction into the organic phase. An example of such a synergic reagent pair is that of thenoyltrifluoroacetone (HTTA) and TBP or tributylphosphineoxide (TBPO) for the extraction of the uranyl ion from a nitric acid solution that was investigated by Irving.[22]The linear O=U=O cationis believed to have five to seven coordination sites, and upon extraction with HTTA only four are occupied. This leaves the uranyl group coordinatively unsaturated with the remaining coordination sites being occupied by water and/or nitrate. When TBP or TBPO is added to the system, it is postulated that the remaining water and nitrate coordinated to the metal center is replaced by the adduct forming, neutral extractant which in this case is either TBP or TBPO. Measuring the distribution ratio for the extraction of uranium from nitric acid while the total concentration of (HTTA)+(TBP/TBPO)is kept constant, the distribution of uranium increases to approximately60 for TBP and 1,000 for TBPO from a value of 0.07 for HTTA alone, as shown in Figure 3. At the peak distribution value in this system, the extracted complex is assumed to be $UO_2(TTA)_2B_{1\text{ or }2}$, where B denotes either TBP or TBPO.[13] The decrease observed as one goes to higher

concentrations of TBP or TBPO is due to the decrease of the concentration of TTA^- in the organic phase which prevents U(VI) – TTA complexes from forming.

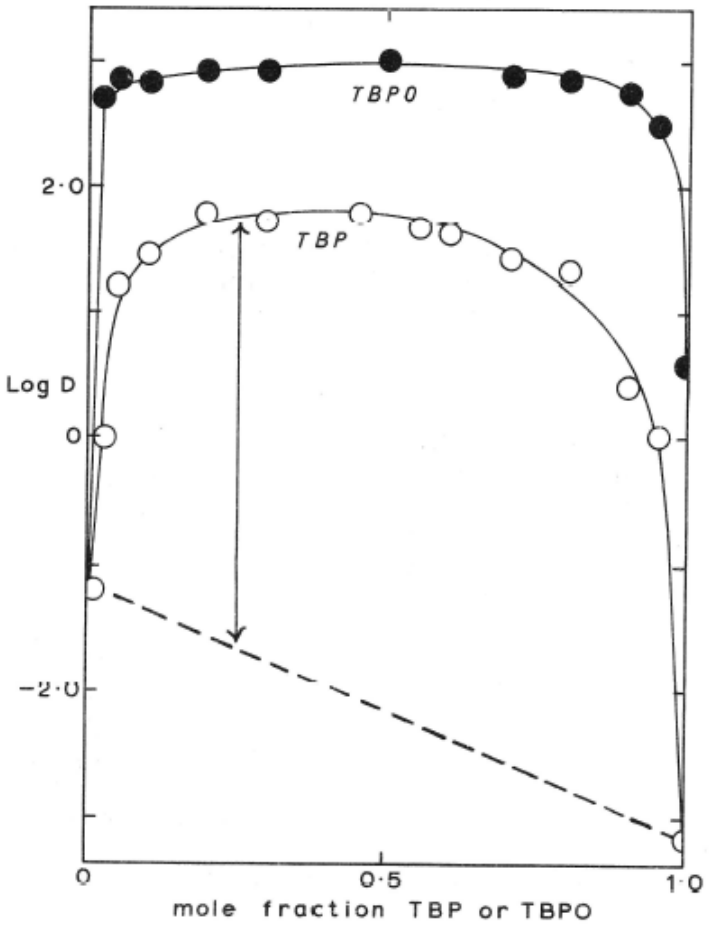

Figure 3: The distribution of uranium(VI) between 0.01 M nitric acid and mixtures of HTTA and TBP or TBPO at a constant total molarity of 0.02 M in cyclohexane. Figure reproduced from reference 20.

In addition to HDBP being a degradation product of TBP, it has also been observed that combination of TBP and HDBP are synergistic in extraction. Hahn and Vander Wall[26] suggested the following mechanism for the extraction of aquated U(VI) using a combination of TBP and HDBP, as denoted in equation 1.4.

$$\mathbf{UO_2^{2+} + 2NO_3^- + 2\overline{HDBP} + 2\overline{TBP}} \rightleftarrows \overline{\mathbf{[UO_2(DBP)_2 \bullet [UO_2(NO_3)_2(TBP)_2]}} + \mathbf{2H^+ + water} \quad (1.4)$$

The authors also suggested another possible mechanism of formation of these mixed complexes where HDBP replaces TBP and nitrate in an already existing U(VI)-nitrate-TBP complex according to equation 1.5.

$$\mathbf{2\overline{UO_2(NO_3)_2(TBP)_2} + \overline{(HDBP)_2}} \rightleftarrows \overline{\mathbf{(UO_2)_2(DBP)_2(NO_3)_2(TBP)_2}} + \mathbf{2HNO_3 + 2\overline{TBP}} \quad (1.5)$$

The extraction mechanism in Eq. 1.5 is similar to the generally accepted synergistic extraction mechanism combining two reagents where one works as a phase transfer reagent while the other binds in the bulk organic phase after the metal has been transferred.[27]Recent works however, have taken an overall different approach to explaining the synergistic effect, namely that organic phase pre-organization and aggregate formation may play some role in synergistic extraction.[28-30]

1.6 Aggregate Formation

Under certain conditions, many of the amphiphilic extraction systems display self-assembly into aggregates that brings about the formation of "third phase". Third phase is a heavy organic phase that typically causes disruptions to the extraction process.[31]An example of third phase formed by extracting 10^{-2} M Dy from 0.2 M HNO_3 into a 0.5/0.5 M TBP:HDBP mixture is shown in Figure 4.

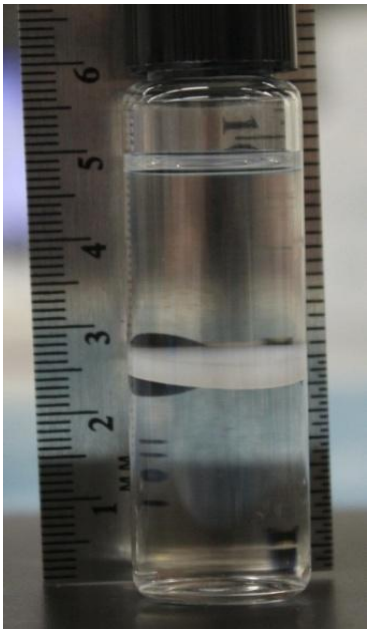

Figure 4: Example of third phase formation upon extracting 10^{-2} M Dy from 0.2 M HNO_3 into a 0.5:0.5 M TBP:HDBP solution in *n*-dodecane.

Approximately two decades ago, Osseo-Asare postulated that the third phase formation from TBP was due to reverse micelles in the organic phase that would grow into large aggregates until they coalesced into a heavy organic phase separate from the bulk organic phase.[29] Since then, the nature of these reverse micelles and the third phase has been studied very closely and works carried out by Chiarizia et al. at Argonne National Laboratory and by Nave et al. at the French CEA have shown that TBP does indeed form reverse micelles in the organic phase, incorporating water and mineral acid.[32-35]A telltale sign of reverse micelle formation in organic phases is the uptake of significant amounts of water that must reside in the polar cores of the aggregates. Additionally, it has been noticed that HDBP may also increase the chance of third phase formation when combined with TBP in PUREX process streams. The formation of these reverse micelles and larger aggregates was studied and a model was presented describing the observed phenomena using other neutral organophosphorus ligands, for example stereoisomers of TBP,

tri(2-ethylhexyl) phosphate (TEHP), tri-n-octyl phosphate (TOP), and tri-n-octylphosphine oxide (TOPO).[36,37]

1.7 Scope of Thesis

In a recent review by Lumetta et al.[38], similar combinations of acidic and neutral reagents for actinide and lanthanide extraction were investigated. The systems scrutinized in this compilation were mostly of more recent works and includes examples of extraction systems combining diamides with phosphoric acid reagents;[39] combinations of HDEHP and CMPO (octyl(phenyl)-N-N,-diisobutyl-carbamoylmethyl-phosphine oxide)[19,40]as well as CMPO and TBP (TRUEX solvent); and combinations of heterocyclic nitrogen donors (2,2':6',2"-terpyridine) and lipophilic carboxylic acids (2-bromodecanoic acid).[41]These systems showed a synergic enhancement in distribution ratios ranging from several orders of magnitude to no enhancement, depending on the conditions of the extraction system. These extraction systems also displayed tendencies of changes in the extraction mechanism when parameters such as aqueous acidity or the molar ratio between the reagents were varied. More recent studies by Dourdain et al. have investigated combinations of trioctylphosphine oxide (TOPO) and HDEHP and have shown that there may be a link between the formation of aggregates and the preorganization of the organic phase and synergy.[30] Ultimately, the nature of synergy and when it is observed may not have one simple answer and observations of metal ion distribution ratio alone and treatment of the data by slope analysis may not be enough to elucidate the extraction mechanism.

In this thesis, I have investigated this proposed possibility of a link between the formation of aggregates and synergy in the TBP/HDBP extractant system. To accomplish this, we investigated the system with a multistep approach as follows:

1. We investigated the physicochemical properties of extraction using an organic phase consisting of 1 M total TBP:HDBP in *n*-dodecane from aqueous phases containing 2M or 0.2M $HNO_3$and a metal ion from the lanthanide series. The physicochemical properties provided a baseline for phase behavior in the system for comparison to previous research with these extractants and will be discussed in greater detail in chapter 2.
2. We investigated the molecular aspects of complex formation in the organic phase upon extraction with TBP:HDBP through use of X-ray absorption spectroscopy, and Time-resolved laser induced fluorescence spectroscopy to help determine the origin of synergistic phase characteristics and to investigate if the previously proposed models for synergistic extraction apply under these conditions. This will be described in greater detail in chapter 3.
3. We investigated macromolecular behavior of the organic phase with use of scattering techniques, such as small angle X-ray scattering and small angle neutron scattering, to characterize and gain an improved understanding of the structure of the reverse micelles formed, how and why they form and their role on the metal extraction, both with the single extractant systems and with mixtures of TBP:HDBP, as described in chapter 4.

Chapter 2: Physicochemical Properties of Extraction

The first step in the investigation of the TBP/HDBP extraction system involves investigation of the physicochemical properties of this system. The major properties of interest are the distribution of metal ion between the two phases, the water uptake into the organic phase, and the extraction of mineral acid into the organic phase. These studies will provide a baseline which allows us to compare to previous, published studies on these extraction systems.

2.1 Experimental Procedures

Liquid-liquid extraction experiments using TBP and HDBP in various ratios in *n*-dodecane were carried out at room temperature. Aqueous solutions of 10^{-4} M and 10^{-3} M La^{3+}, Dy^{3+}, and Lu^{3+} in 0.2 or 2 M HNO_3were prepared. Two separate studies were carried outwith 0.2 M HNO_3: one with no addition of a background electrolyte and one with the addition of ammonium nitrate to increase the total nitrate concentration to 2 M. It was found early on, however, that the addition of the background electrolyte did not affect the distribution ratio, water uptake or acid uptake significantly so it was omitted from most of the experiments presented in this thesis. Organic solutions contained a total of 1 M extractant concentration (TBP + HDBP) but in varying molar ratios (4:0, 3:1, 2:2, 1:3, and 0:4 TBP:HDBP). The *n*-dodecane was obtained from Alfa Aesar to > 99% purity, the TBP was obtained from Acros Organic to >99% purity and the HDBP from Aldrichto >97% purity. The organic chemicals were all used without any further purification. The TBP and HDBP were checked for impurities using an in-house gas chromatography method and it was found that the TBP had 0.1% HDBP as the only impurity. The HDBP contained 2% TBP and less than 1% H_2MBP. These impurities were accounted for in the calculations of the final TBP:HDBP ratios used. The H_2MBP was assumed to be removed in the pre-equilibration step as described below. An experiment comparing purified HDBP by the copper precipitation

method[42]to non-treated HDBP, as in the work presented here, showed no difference between the distribution of lanthanum(III) and water at 10^{-4} M metal ion concentration and using similar organic and aqueous phases as in this work.[43]Stocks of the various trivalent lanthanides were obtained by dissolving the respective lanthanide oxides, 99.999% (Ln_2O_3) provided by Michigan Metals & Manufacturing, in nitric acid. These solutions were subsequently standardized for their Ln^{3+} concentrations, acidity, and excess nitrate concentration by a combination of neutron activation analysis, ion exchange, and potentiometric titration. Concentrated nitric acid (15.8 M) was supplied by Fisher Scientific. Ammonium nitrate (chosen to avoid excessive neutron activation of sodium-23 and potassium-41 solutions to adjust salt concentration were made by recrystallization of the solid salt supplied by Fisher Scientific. Water used to dilute concentrated solutions was obtained from an in-house source of ultrapure (18.2 MΩ-cm) water. The aqueous phase was pre-equilibrated by contacting with an equal volume of pure *n*-dodecane for 15 minutes, followed by centrifugation to promote complete phase disengagement. The organic phases were pre-equilibrated, abbreviated as PEQ when shown on figures, by contacting the organic phase with an equal volume of aqueous solution containing nitric acid equivalent to the aqueous phase that the organic phase would be extracting from, but without the metal ion. Samples of pre-equilibrated organic and aqueous phases were taken for blanks to observe any water and acid uptake in the absence of metal ion. Samples of non-pre-equilibrated, i.e. "dry" organic phases, were taken for blanks for water and acid uptake. Samples of non-pre-equilibrated aqueous phase were taken for initial Ln^{3+} and nitric acid content determination. After the pre-equilibration, phases of equal volume were contacted for 15 minutes by vigorous shaking on a vortex mixer followed by 5 minutes of centrifugation. Samples of each phase were taken for metal ion and nitric acid analysis. The metal concentration was measured by neutron activation

analysis using the UC Irvine 250 kW TRIGA® reactor. The metal ion in each sample was activated to produce a radioactive nuclide (lanthanum-140, dysprosium-165, and lutetium-176m) and the samples were measured with use of a Canberra HPGe detector. All Lu^{3+} samples were further analyzed by ICP-MS (Agilent 7500CX) due to the lower activation of Lu^{3+} compared to Dy^{3+} and La^{3+}. The water content in the organic phase was analyzed using a Karl-Fischer titrator, Metrohm model 831 KF Coulometer controlled by Tiamo 2.0 software. The Karl-Fischer measurements were checked for accuracy using standardized solutions of 1mg water per 1 g solution, HYDRANAL® Water Standard 1.0 obtained from Fisher Scientific. The nitric acid concentration in the organic phase was measured by stripping a sample of the organic phases with twice the volume of ultrapure water, collecting the water and repeating the procedure for a total of 3 times. The collected strip solution was quantitatively transferred to a titration vessel and titrated with standardized NaOH using an automated potentiometric titrator; Metrohm model 836 Titrando controlled by Tiamo2.0 software. The NaOH was obtained from Fisher Scientific as a 50 w/w solution in water and the dilute NaOH solutions used for the titration were standardized by dry potassium hydrogen phthalate (KHP), supplied from Fisher Scientific (>99.9%). The HDBP, however, contributes to the acidity of the strip solution and this introduces large errors in the potentiometric determinations of acid concentration. To improve accuracy of the nitric acid uptake, aliquots of the strip solutions were collected and analyzed for total nitrate concentration using ion chromatography, Metrohm model 850 Professional IC.

2.2 Distribution of Metal Ions

2.2.1 Results of Extraction Study

The results for the distribution studies are shown in Figure 5a and 5b. Under these conditions, no third phase or precipitation was observed in the organic phases for all metals at 10^{-4} M

concentrations, though slight clouding of the organic phase was observed for 10^{-3} M Dy when contacted with aqueous phases consisting of 0.2 M $HNO_3$and Lu at 10^{-3} M when contacted with either aqueous acidity. Though clouding would indicate the onset of third phase formation, a simple mass balance accounted for all the metal in both phases for the extraction of Dy. ICP-MS was employed for the 10^{-3} M Lu extraction and the data for these experiments is represented as the distribution ratio calculated from the initial starting aqueous concentration and the remaining concentration of metal left post contact in the aqueous phaseby subtracting the post contact from the pre-contacted values and assuming all of the remaining metal not present in the aqueous phase after contact was present in the organic phase.For the low acid system (Figure 5b), a non-linear tread for all metal ions is observed, indicating an interaction between the two extracting reagents and the possibility of a slight synergistic effect between the TBP and HDBP. The only exception to this would be the extraction of Lu from the 0.2 M HNO_3 solution which shows a pronounced synergy with a maximum at 0.75 M TBP, though taking a look at the aqueous phase concentrations shows that there is effectively complete extraction for organic phases with any HDBP and essentially no extraction from the 1 M TBP phase.[44] At high acidity (Figure 5a), the distribution trends are more linear so that, at thiscondition, only a weak synergistic effect, if any, is produced by the TBP-HDBP mixture. Again, we do see a deviation from this trend when looking at the extraction of Lu from the 2 M HNO_3 aqueous system and looking at the aqueous phase concentrations wesee complete extraction with phases containing any HDBP and almost no extraction for 1 M TBP phases. It was also found that metal ion uptake into the organic phase using 0.2 M HNO_3 with or without the addition of 1.8M NH_4NO_3 showed no difference in the observed trend.[45] From Figure 5 it is clear that when using low nitric acid and high HDBP concentration the extraction is almost 100%.

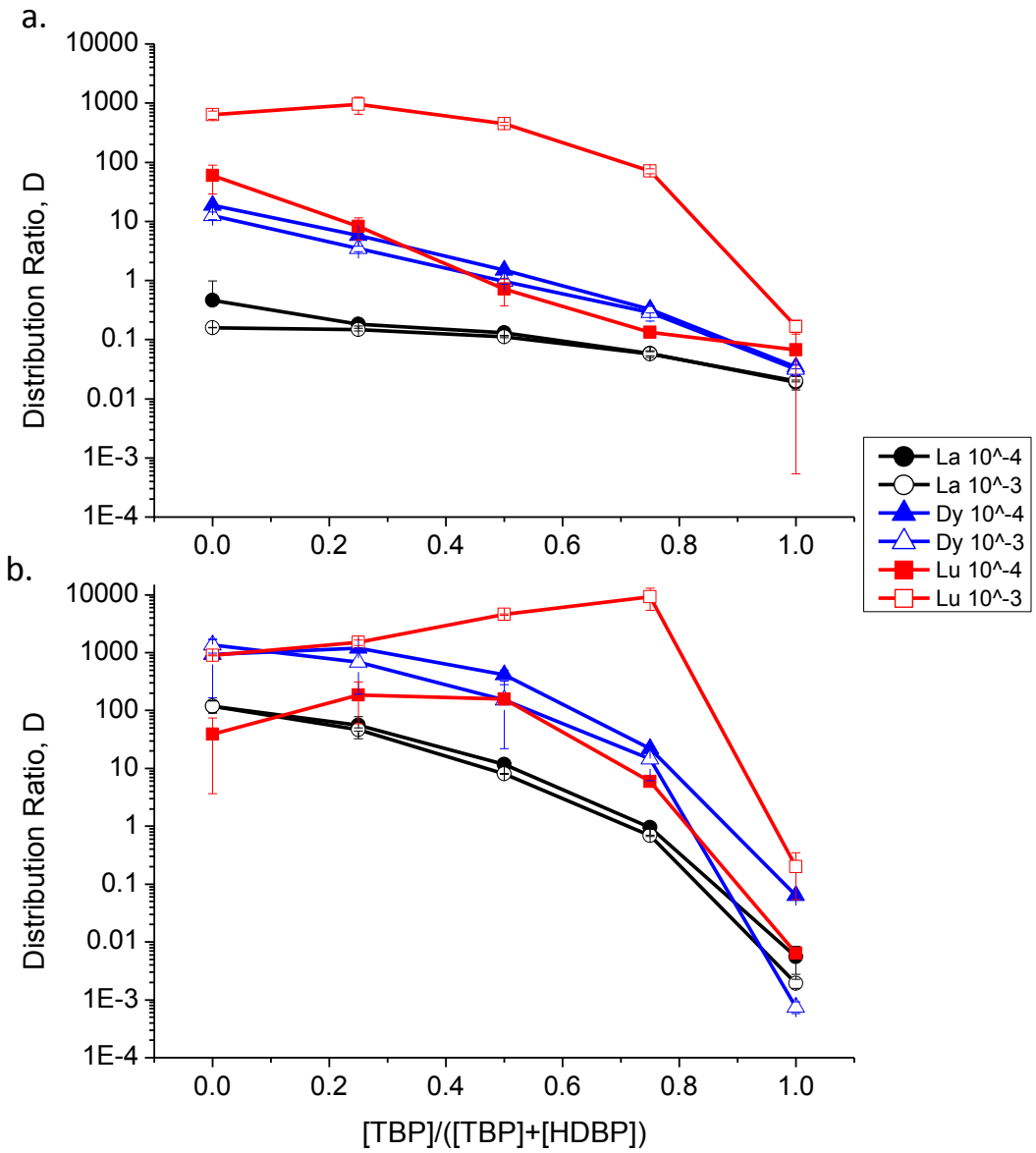

Figure 5: Distribution ratios for 10^{-4} M and 10^{-3} M Ln^{3+} at varying ratios of TBP:HDBP. Extraction from 2M HNO_3 is shown top (a) and extraction from 0.2M HNO_3 is shown bottom (b). The error bars represent the standard deviation of triplicate measurements.

In fact, at high HDBP concentration (above 0.75 M) the distribution ratios, $D = [Ln^{3+}]_{org}/[Ln^{3+}]_{aq}$, are on the order of 100 to 10,000, namely 99% to 99.99% extracted, though the uncertainties in the distribution ratios values become large due to the small signal obtained from the Ln left in

the aqueous phase. Figure 5also shows a comparison between the distributions of metal ions of different ionic radii, $r_{La(III)}>r_{Dy(III)}>r_{Lu(III)}$.The distribution trends of Dy are significantly higher than those of La at both acid concentrations, and the distribution ratios of Lu are higher still, which is most likely due to the lanthanides with a higher Z number having higher surface charge density due to their smaller ionic radii, thereby binding stronger to HDBP.[46] This trend has been seen previously with many other acidic organophosphoric reagents and is typical of similar systems.[18] It is also interesting to note that the distributions of each metal ion at different metal concentration but at the same acidic conditions are relatively similar for La and Dy extraction. This indicates that the metal ion extraction below the onset of third phase is independent of metal concentration which is not surprising considering the 1M extractant reagent concentration being significantly higher than the investigated metal ion concentrations used in this work.

2.2.2 Discussion of Extraction

The uptake of lanthanum and dysprosium at 1 M HDBP (TBP:HDBP mole ratio of 0) at 2 M HNO_3 correlates to distribution (D) values of approximately 1 and 10, respectively. Considering the third order dependency of the extraction constant on the hydrogen ion concentration for trivalent metal ions according to equation 1.3, this value should be 1000 times less than the D of the respective metal ions at a nitric acid concentration of 0.2 M. As discussed above, the uncertainties in the distribution ratios are large and D-values for the high nitric acid extraction are slightly higher than expected. One viable explanation is that the extraction of trivalent lanthanides by HDBP does not proceed solely via cation exchange but rather by a solvation mechanism, possibly involving coordination of the P=O group to the metal ion. This has been observed for HDEHP (di-2-ethylhexyl-phosphoric acid, shown in Figure 6) during the extraction

of trivalent metal ions in contact with fairly acidic solutions[47]and it is probable that HDBP would behave in a similar manner due to its structural similarities.

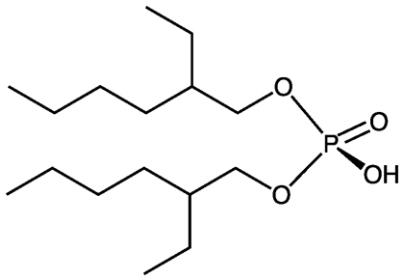

Figure 6: Structure of HDEHP (di-2-ethylhexyl phosphoric acid).

The extraction of lutetium differs from the other two metals for two reasons, the first of which being its strong disposition to form third phases upon contact and a complete extraction of metal ions into the organic phase. The second reason is the formation of small crystals in the organic phase, that were discovered when Bragg peaks indicating high degrees of order in the system were observed in SAXS experiments of 1.25 x 10^{-3} M Lu extractions, shown in appendix A1 of this thesis. Figure 7 shows a photograph from an optical microscope of the crystals formed in solution.

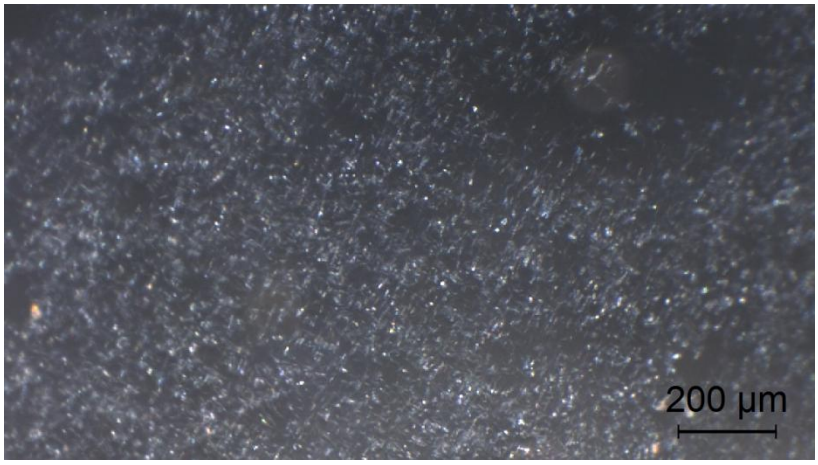

Figure 7: Photograph of a 1.25 x 10^{-3} M Lu extraction into a 1:3 TBP:HDBP organic solution.

Similar observations of crystal growth have been reported in the process of solvent extraction of lanthanide ions by HDEHP.[48-51]Both of these reasons may contribute to the complete extraction observed for 10^{-3} M Lu at either acid concentration.

The extraction trends observed at 0.2 M nitric acid shows a non-linear $[Ln]_{org}$ dependence although, in comparison to other synergistic extraction systems, it is not as pronounced with the exception of lutetium extraction. An example of this phenomenon was discussed earlier in chapter 1 section 5 for the extraction of Uranium by HTTA and TBP or TBPO. In this example, TTA acts as an acidic reagent while TBP or TBPO acts as a neutral extractant. One important difference from our study is that TBP and TBPO have a marked affinity for U(VI) and readily coordinate to the divalent uranyl(VI) ion, UO_2^{2+}; however, they do not have a strong affinity for trivalent lanthanides, such as those investigated in our present work.

Furthermore, the difference in the trends observed for the high and low acid conditions could be attributed to an interaction between the two extracting reagents in the organic phase. Zangen et al.[25] investigated neutral organophosphorus reagents combined with acidic chelating reagents for the extraction of actinides and lanthanides. Zangen noticed that combining dibutylbutylphosphonate (DB[BP]), a neutral reagent, with di[para(1,1,3,3-tetramethylbutyl)-phenyl]phosphoric acid (HDOφP) resulted in non-linear extraction trends for trivalent lanthanides and Am(III) from 0.3 M HCl. All metal ions showed a non-linear trend but the synergisticenhancement varied between the different metal ions. Lutetium and thulium showed no enhancement between pure HDOφP and mixtures with DB[BP], whereas the lighter lanthanides and Am(III) showed an enhancement of between 2 and 4 at approximately an equimolar ratio of the two reagents. At higher DB[BP] concentrations, there was a decreasing trend which Zangen called “antisynergistic.” This antisynergism was explained by an adduct

formation between the neutral and acidic reagent, resulting in a decrease in available ligand to complex the metal ion. While we do not observe a similar trend in our studies for 0.2 M HNO_3, the trend is more linear for the 2 M HNO_3 system. Furthermore, with the low loadings of metal ions in our systems (10^{-4} and 10^{-3} M) and the total ligand concentration of 1 M, it is unlikely that the decrease in metal uptake with increasing TBP concentration is due to adduct formation with HDBP.

2.3 Extraction of Water

Water uptake into an organic phase is a useful tool to determine if reverse micellular aggregates are present. Figure 8 shows the results obtained for the water uptake into the organic phase. It is interesting to note that the data show very little difference between the two different metal ion concentrations for all metals, which indicates that at these low concentrations of metal ion the extraction of metal does not affect the uptake of water into the organic phase. Additionally, there seems to be little difference in water uptake trend betweenthe different metal ions or between the water uptake with or without metal ionswhich indicates that water uptakeinto theorganicphase is dependent on the TBP:HDBP concentration alone under these conditions which differs from the metal ion distribution trends presented earlier. Figure 8 alsoshows that there is very little water present in the organic phases before contact with the aqueous solution.Comparing the water extraction trends, a clear synergistic trend is observed for all metal ions investigated at low nitric acid concentration.Atlowacid,the maximum water uptake into the organic phase was achieved at a 2:2 mole ratio of TBP:HDBP.

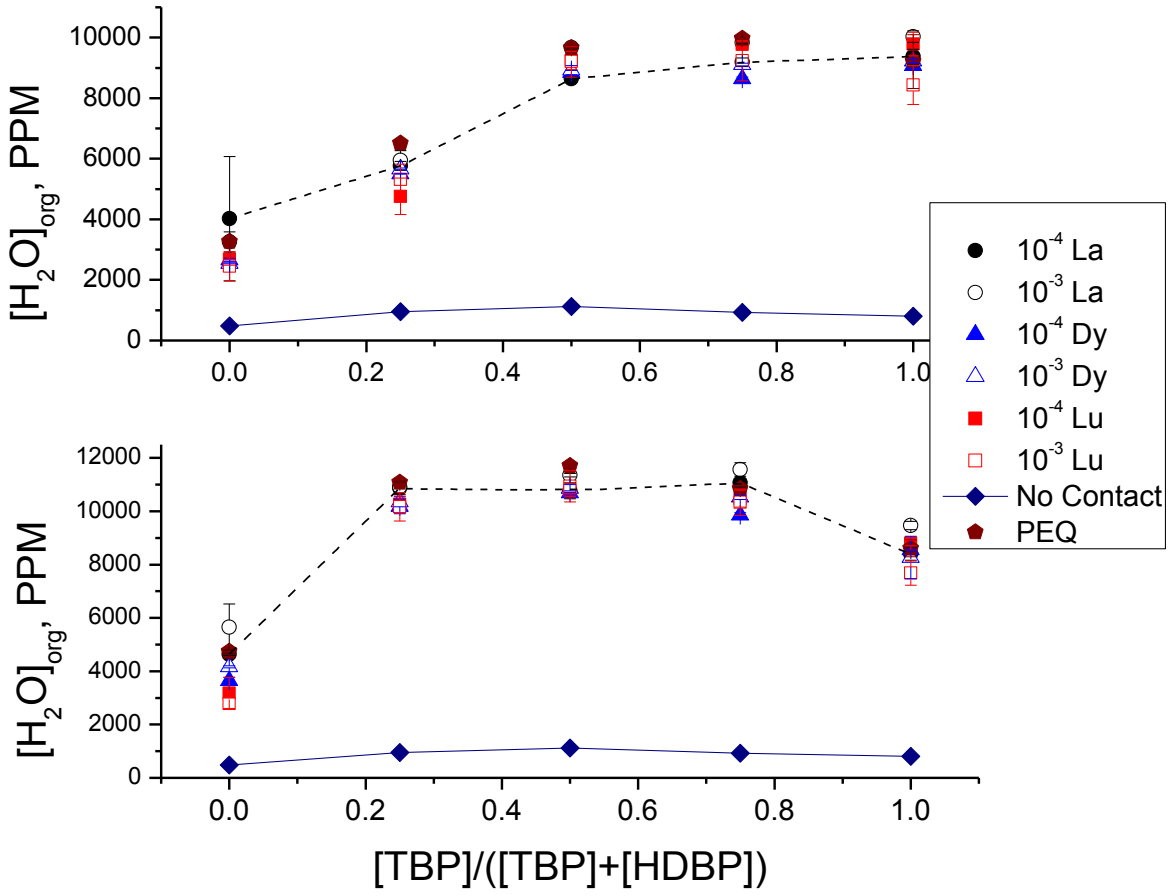

Figure 8: Water uptake into the organic phase for all metal ions investigated. Water uptake from 2M HNO_3 is shown top and water uptake from 0.2M HNO_3 is shown bottom. The PEQ water uptake represents the water taken into the organic phase from an equivalent aqueous phase without metal ion. Dry phase measurements were obtained from the representative organic phase sans contact with an aqueous phase.

At high acid, the synergistic water uptake into the organic phase is not as pronounced and seems to follow a much more linear trend that increases with increasing TBP concentration. The stark contrast in water uptake between the uncontacted organic phase and the organic phases that have been contacted with an aqueous phase indicates the presence of reverse micelles in the system that solubilize water in the organic phase similarly to how oils can be solubilized into aqueous phases with surfactants. The synergistic water uptake into the organic phase for the 0.2 M

HNO_3may indicate the presence of larger aggregates forming when mixtures of TBP and HDBP are present at the proper ratio.

2.4 Mineral Acid Extraction

In contrast to the uptake of water and metal ion, the nitric acid uptake into the organic phases follows a linear trend, showing an increase in acid uptake with an increase in the TBP concentration in the system, as shown in Figure 9.The potentiometric titrations and ion chromatograph determinations show an identical trend, though potentiometric titrations may yield larger uncertainties due to the protons released from HDBP during the titration, as described in the experimental section.It is also important to note that utilizing ion chromatography to determine acid uptake into the organic phase will yield higher acid uptake in the organic phase when ammonium nitrate is used since small amounts of ammonium nitrate may be extracted into the organic phase after contact. This is a known activity effectwhen utilizing ammonium nitrate to maintain ionic strength.[45]The trend observed for the nitric acid uptake into the organic phase has been well described in literature. The extraction of nitric acid by TBP has been studied by several groups over the last 50 years.[31,52] Early studies by Alcock et al.[31] for a range of different nitric acid concentrations and TBP concentrations suggested the following mechanism:

$$\mathbf{HNO_3 + \overline{TBP} \rightleftarrows \overline{(HNO_3)TBP}}, \qquad \mathbf{K = \frac{[HNO_3TBP]_{org}}{[HNO_3]_{aq}[TBP]_{org}} = 0.16M^{-1}} \qquad 2.1$$

This equation and the value of K (0.16 M^{-1}) was found to have good agreement with the experimental data for moderate nitric acid concentrations, ~4-7 M HNO_3, at all TBP concentrations up to 100% TBP.

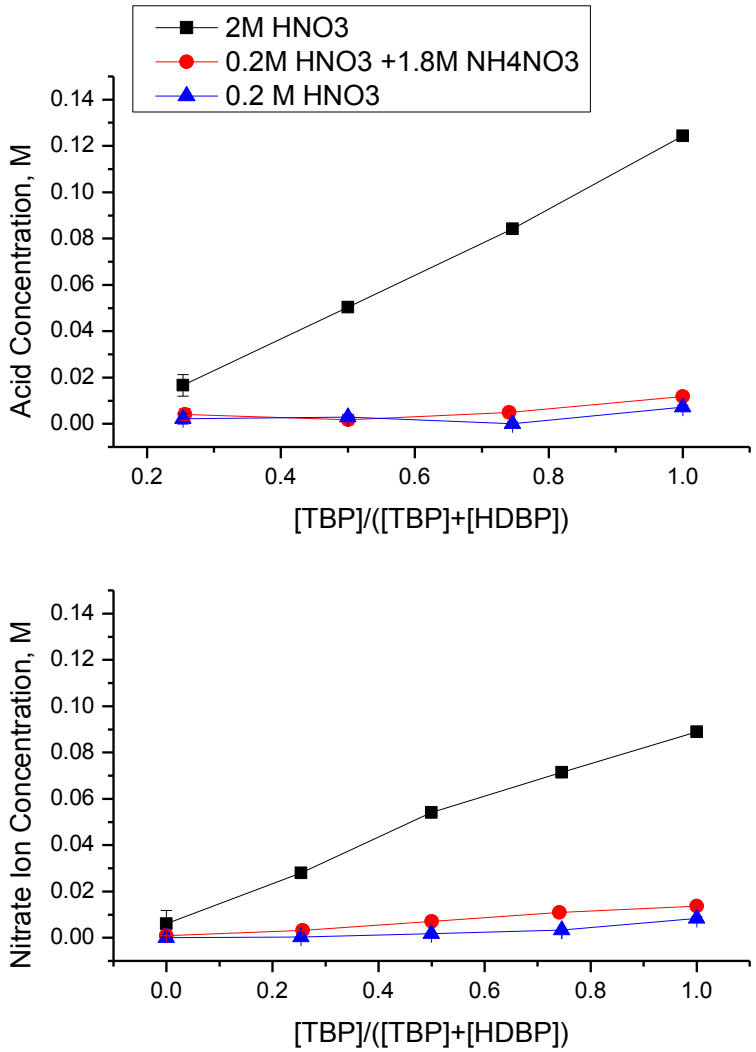

Figure 9: Comparison between acid uptake into the organic phase (top) and nitrate ion concentration in the organic phase (bottom) after extraction of 10^{-3} M Dy from 2 M HNO_3, 0.2 M HNO_3, or 0.2 M HNO_3 + 1.8 M NH_4NO_3.

Eq. 2.1 also agrees well with extraction data for a large range of nitric acid concentrations using a dilute TBP solvent (1.9%). Higher TBP concentrations show some deviations from Eq. 2.1 that the authors suggested were due to non-idealities. The deviations shown at higher nitric acid

concentrations were ascribed by Alcock et al.[31] to the possible formation of 2:1 and 3:1 HNO_3:TBP species, whereas other studies[53] have suggested the formation of HNO_3:TBP complexes of up to 4:1 stoichiometry. Chiarizia et al.[34] studied the extraction of nitric acid by 20% TBP in *n*-dodecane and found that, up to 10 M HNO_3, the ratio of TBP to HNO_3 in the organic phase suggested that the complex formed was predominantly the 1:1 complex. An additional 1:2 HNO_3:TBP complex has also been observed by Chaiko et al.[54] The trends shown in Figure 9 indicate that there is a strong possibility that TBP is the sole reason for the uptake of nitric acid and that HDBP may not participate in the extraction of nitric acid under the conditions used in this study.

2.5 Conclusions

The observed nonlinearity in the extraction of trivalent lanthanides from 0.2 M HNO_3 solutions seems to indicate some sort of interaction between the two extraction reagents and possibly synergy in this system. It is interesting to note that the distribution of metal ions into the organic phase does not seem to deviate with metal ion concentration which indicates that below the onset of third phase the extraction is independent of metal concentration. In view of the water uptake into the organic phase, a clear synergistic trend is observed when contacted with 0.2 M HNO_3 while a more linear trend is observed when contacted with a 2 M HNO_3 aqueous phase. It is also interesting that the identity or concentration of metal ion does not affect the water uptake into the organic phase indicating that the water uptake is dependent solely on the aqueous acidity and organic phase composition. Finally, the uptake of mineral acid into the organic phase is linear and increasing with increasing TBP concentration. This finding is unsurprising since it is well known that TBP will extract mineral acid into the organic phase.The combination of these three studies serves to indicate that the TBP/HDBP system does, in fact, form aggregates in the

organic phase and these aggregates may play a part in the apparent synergistic trends in water uptake and metal ion distribution that we are observing, though further investigation into the complex environment and macromolecular structures are necessary to adequately describe this system fully.

Chapter 3: Complex Centered Structural Investigation

In an effort to investigate the molecular aspects of the complexes formed in the organic phase upon extraction, we now turn to the more complex oriented techniques of EXAFS, XANES, and TRLIFS.

3.1 X-ray Absorption Theory

Before we begin discussing the results of these experiments, it is useful to understand the theory behind the technique of X-ray absorption spectroscopy, XAS. XAS is a unique tool that can be used to study the local structure surrounding selected elements that are contained within a material. The materials typically chosen for this type of investigation can be crystals with high degrees of long range order or systems with little order, such as those in the solutions systems under current investigation.

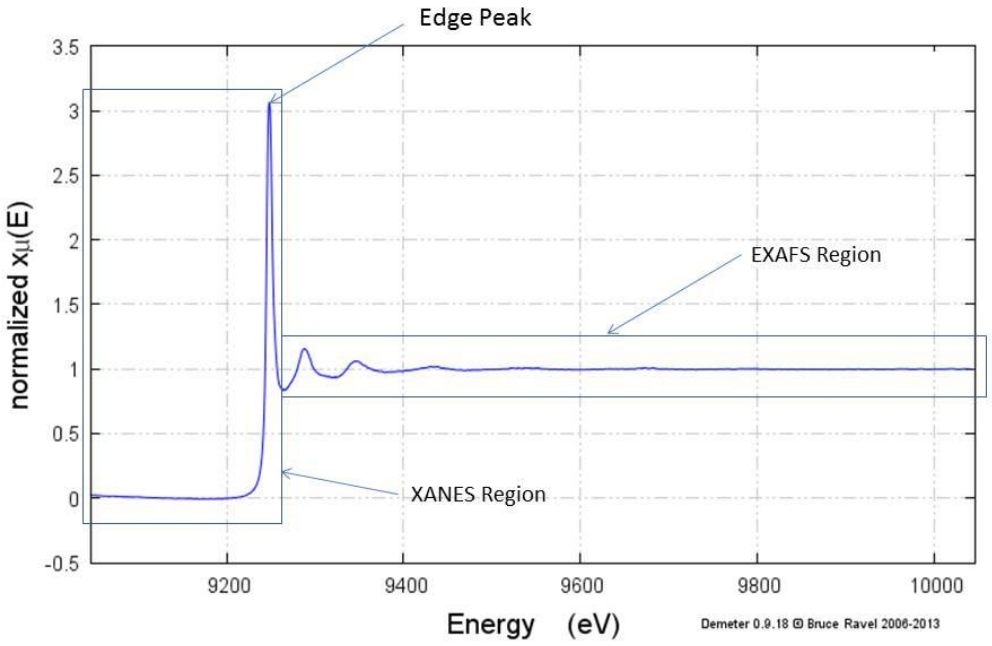

Figure 10: Normalized example XAS data indicating the regions of interest. Figure produced using the Athena program of the Demeter software package.

A single experiment can be split into two regions of interest to allow for easier interpretation of the collected data, the XANES (X-ray absorption near-edge spectroscopy) which lies approximately 30 eV or so before the absorption edge and the EXAFS (extended X-ray absorption fine structure) which extends after the absorption edge, as shown in Figure 10. XANES can yield information about oxidation state and coordination chemistry (i.e. octahedral/tetrahedral geometries) and the EXAFS is used to determine interatomic distances, coordination number and species of the neighboring atoms in the system. The parameter of interest from these types of experiments is the absorption coefficient μ(E), which describes the probability that an X-ray will be absorbed. The data can be collected with two different geometries to obtain μ(E), the first of which is by transmittance where $\mu(E) = Ln(I_0/I)$ where I_0 is the incident beam intensity and I is the measured intensity upon transmittance.

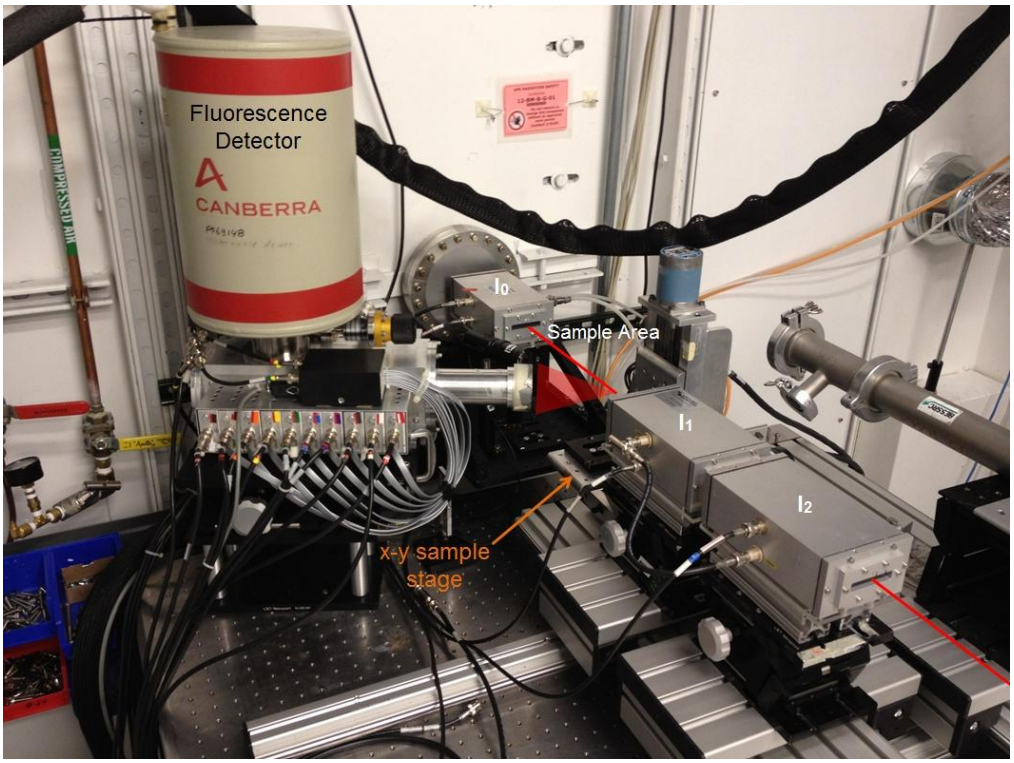

Figure 11: A typical EXAFS experimental set up currently used at 12-BM-B at the Advanced Photon Source.[55]

The second experimental geometry is fluorescence, where $\mu(E) \propto I_f/I_o$ where I_f is the total fluorescence intensity. The set up used for these experiments at beamline 12-BM-B is shown in Figure 11.The data collected as intensities must first be converted to μ(E) using the above relationships. The data is collected over several scans and then averaged together and normalized so further processing can take place. This step is referred to as data minimization. Once the data has been minimized it must then be converted to χ(E) since we are mainly interested in oscillations well above the absorption edge for EXAFS. χ(E) represents the fractional change in absorption coefficient that is induced by the presence of neighboring atoms by the following equation:

$$\boldsymbol{\chi(E) = \frac{\mu(E) - \mu_o(E)}{\mu_0(E)}} \qquad 3.1$$

where $\mu_o(E)$ is a smooth background function measuring the absorption of an isolated atom. Since EXAFS is best understood in terms of the wave behavior of the photo-electron created by the absorption process, it is common to convert the X-ray energy to *k*, the wave number of the photo-electron, which has dimensions of 1/distance and is defined as:

$$\boldsymbol{k = \sqrt{\frac{2m(E - E_o)}{\hbar^2}}} \qquad 3.2$$

where E_0 is the absorption edge energy and *m* is the electron mass. This gives the primary quantity for EXAFS as χ(*k*), the oscillations as a function of the photo-electron wave number, as represented by the standard EXAFS equation:

$$\chi(\mathbf{k}) = S_0^2 \sum_i \frac{N_i f_i(\mathbf{k}) e^{-2k^2\sigma^2}}{kr_i^2} \sin(2kr_i + \delta_i(\mathbf{k})) \quad 3.3$$

where $\delta_i(k)$ is the partial wave phase shift, N_i is the number of neighboring atoms, r is the distance to the neighboring atoms from the central absorber, $f_i(k)$ is the scattering amplitude, $S_o{}^2$ is the scale factor, and σ^2 is the Debye-Waller factor, which is the mean square variation of distances about the average, r_j. This equation can then fit to experimental $k^3\chi(k)$ versus k using any number of mathematical procedures and will be explained in a later section in more detail. The use of $k^3\chi(k)$ is to simply emphasize the oscillations that would normally decay quickly with increasing k and to yield a consistent amplitude over the range of k that we are interested in.

3.2 Experimental Procedures

To conduct XAS experiments on the TBP/HDBP system, only the organic phases containing the extracted complexes are necessary. Samples were created identically as described in section 2.1 of this thesis, though the concentration of metal ion was increased to 1.25×10^{-3} M for each Ln^{3+} to ensure that sufficient signal could be obtained. The Ln^{3+} L_3-edge data were obtained for solutions contained in micro X-ray cells (SPEX 3577) with Kapton® film windows, 0.0003" (SPEX 3511), mounted as shown in Figure 12.

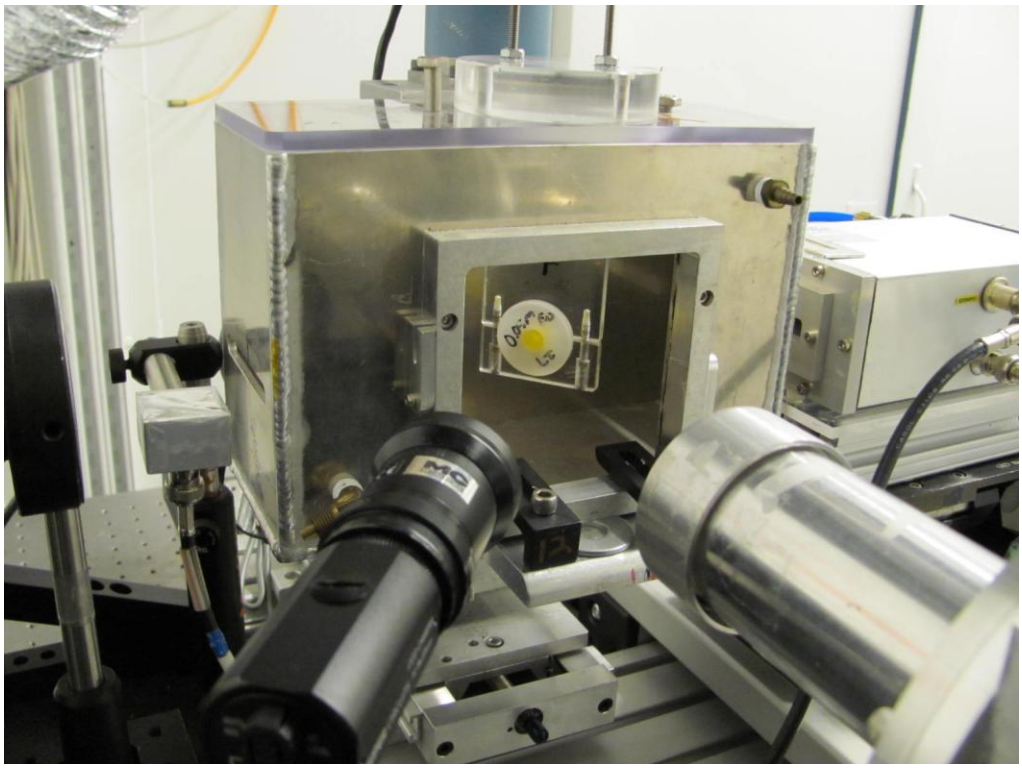

Figure 12: SPEX 3577 X-ray cells with Kapton window mounted at a 45° angle from the incident beam.

All measurements were made at the Advanced Photon Source beam line 12-BM-B (Agronne National Laboratory) using a 13 element fluorescence detector (Canberra) in the configuration as shown in Figure 11 and Figure 12.Data was collected as intensity and converted to total absorption coefficient, μ(E), by the equation: $\mu(E) \propto I_f/I_o$, where I_f is the measured total fluorescence intensity and I_0 is the incidence beam intensity. All data collected was first minimized and averaged over the number of individual scans of each sample. Every sample was scanned a minimum of 2 times for samples that contained sufficient signal and a maximum of 6 times for those samples containing lower Ln3+ concentrations. The EXAFS data was analyzed in a consistent fashion using EXAFSPAK[56] and, also, by use of Athena[57]. The conventional metrical analysis of the metal $k^3\chi(k)$ EXAFS was performed with a fixed scale factor ($S_o{}^2 = 0.9$) in a series of step-wise fits of increasing complexity and numbers of O and P coordination shells, using theoretical phase and amplitude functions calculated with FEFF8.0.[58]All of the

EXAFS spectra were fit with either a four parameter model: Ln-O interatomic distances, r; O coordination number, CN; Ln-O Debye-Waller factor, σ^2; energy threshold parameter, $\Delta E0$ – for the one-shell (Ln-O), or a six parameter model -the previously mentioned four plus the Ln-P interatomic distances, r; P coordination number, CN – for the two shell (Ln-O and Ln-P). To determine the validity of the models chosen, an additional 7 parameter model adding a Ln-P Debye-Waller Factor was used to determine the "goodness of fit," a statistical analysis used to determine the significance of adding the additional parameter. The goodness of fit calculation first requires calculating the number of independent points of the data set utilizing equation 3.4.

$$\mathbf{N_I = \left(\frac{2\delta k \delta R}{\pi}\right) + 2} \qquad 3.4$$

In the above equation, δk and δR refer to the difference between the maximum k or R and the minimum.[59] Typically, the model with the lowest value of χ^2/υ, where υ is the number of degrees of freedom of the fit given by $\upsilon = (N_I) - (\#\text{ of parameters})$, is the most appropriate fit statistically. An F_x test was employed to determine the addition of parameter was statistically significant utilizing Equation 3.5.

$$\mathbf{F_x = \frac{\upsilon(\chi_a^2 - \chi_0^2)}{b\chi_0^2}} \qquad 3.5$$

where b is the difference between the number of parameters used in the two fits, χ_0^2 is the value of χ^2 for the fit with the larger number of parameters, χ_a^2 is the value of χ^2 for the fit with the smaller number of parameters, and υ is the number of degrees of freedom in the fit with the larger number of parameters. The probability of obtaining a given value of χ^2 by chance for the

fit with the larger number of parameters is given by $P(F_x, b, \upsilon)$ and was determined using the FDIST function of Excel, as previously employed in a similar manor by Lukens et al.[60] The usual criteria for judging the reduced value of χ^2 to be significantly different is that $P(F_x, b, \upsilon) < 0.05$. For all our samples, $P(F_x, b, \upsilon) >> 0.05$ indicating that the 7 parameter model did not yield a statistically significant improvement over the 6 parameter model. As a result, only the 6 parameter model will be discussed in further detail in this thesis.

XANES fitting and analysis was completed using the Athena program of the Demeter software package. Principal component analysis and linear combination fitting were completed with use of WinXAS to yield further insight into the nature of the complexes formed.[61]

3.3 EXAFS Result

The $k^3\chi(k)$ EXAFS data for the complexes formed by extraction from aqueous phase into an organic phase containing TBP, HDBP or a mix of both are shown in Figure 13.The corresponding FT (Fourier transforms) and fits are shown in Figure 14. L_3-edge X-ray absorption spectroscopy for the lanthanide elements was chosen due to the easily accessible X-ray energies (approx. 6–9 keV) at synchrotron radiation user facilities and for the wealth of published absorption spectra involving L_3-edge EXAFS of lanthanides.[62]

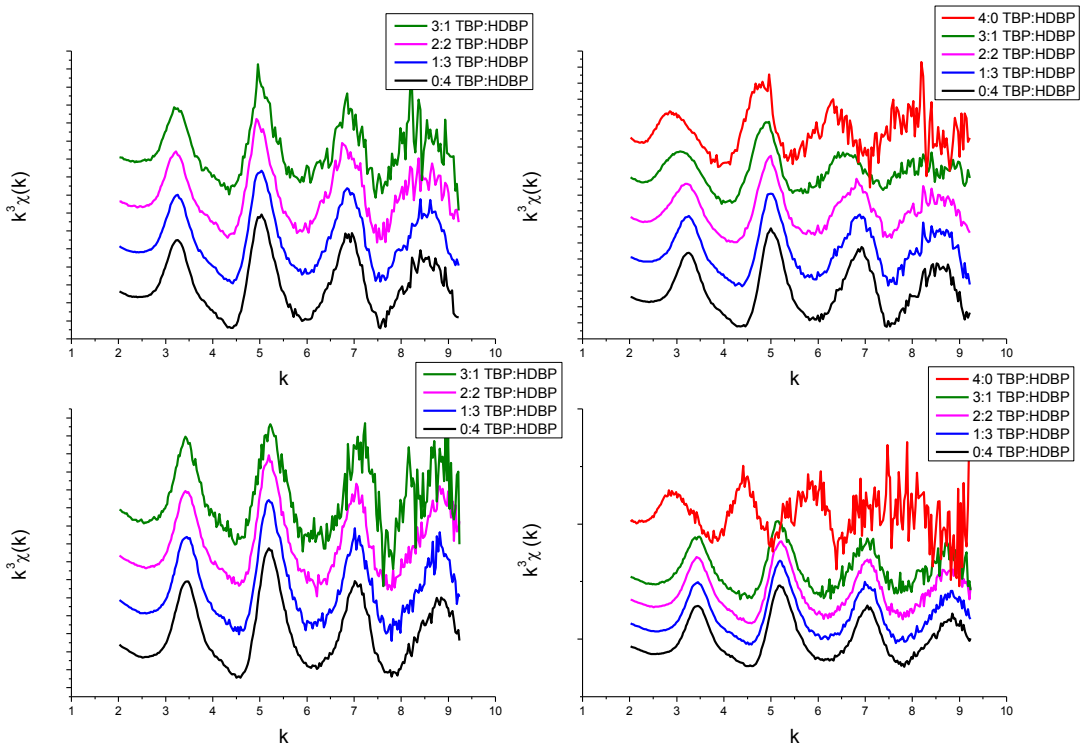

Figure 13: $k^3\chi(k)$ EXAFS data of organic phases extracting from aqueous phases containing $1.25x10^{-3}$ M Dy in 0.2 M HNO_3 (top left), $1.25x10^{-3}$ M Dy in 2 M HNO_3 (top right), $1.25x10^{-3}$ M Lu in 0.2 M HNO_3 (bottom left), and $1.25x10^{-3}$ M Lu in 2M HNO_3 (bottom right).

Unfortunately, EXAFS experiments involving La^{3+} proved to be uninformative due to the closeness of the L_2 and L_3-edges, yielding insufficient fine structure information. This data will be included in the appendix A2 and A3 for completeness, though no additional analysis could be completed with reasonable accuracy with our current experimental configuration. The FT data of the organic phases show two peaks of physical significance: an intense peak at 1.8-1.95 Å attributed to the nearest O neighbor, and a medium peak at 3.3-3.45 Å attributed to the distant P atoms.

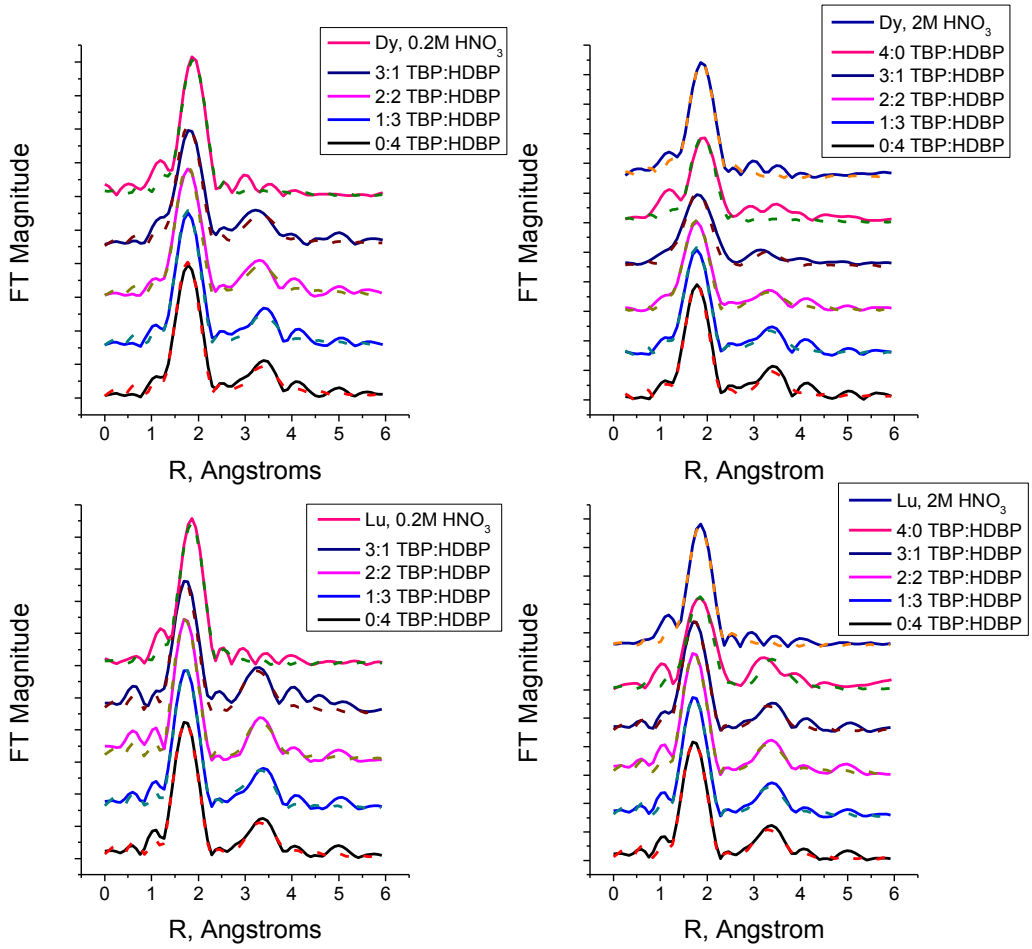

Figure 14: Fourier transformdataof the $k^3\chi(k)$ EXAFS and the corresponding fits (dashed lines).

Based on the appearance of the Ln-O and Ln-P interactions in the FT data, all of the Ln $k^3\chi(k)$ EXAFS for the organic phases were fit using a two shell (O and P) backscattering model, with the exception of the 1 M TBP samples which showed no distant Ln-P interactions due to the low metal ion concentration in the organic phase yielding insufficient signal to differentiate the peak from noise. Metrical results of the fits are collected in Table 1, Table 2, and Table 3.

Table 1: Ln-O and Ln-P EXAFS fit data for Dy^{3+} and Lu^{3+} extraction from 2 M HNO_3 into the organic phase. R is the interatomic distance, CN is the coordination number, σ^2 is the Debye-Waller Factor, ΔE is the energy threshold values.

2M HNO_3									
Organic Composition		**r/Å**	**err**	**CN**	**err**	**σ^2/Å^2**	**err**	**ΔE/eV**	**err**
0:4 TBP:HDBP	Dy-O	2.25	0.002	5.8	0.2	0.0053	0.0004	-2.6	0.3
	Dy-P	3.80	0.005	3.2	0.2				
	Lu-O	2.19	0.002	6.8	0.2	0.0061	0.0003	0.3	0.2
	Lu-P	3.75	0.004	4.4	0.2				
1:3 TBP:HDBP	Dy-O	2.25	0.003	5.7	0.2	0.0061	0.0004	-2.9	0.3
	Dy-P	3.80	0.005	3.2	0.2				
	Lu-O	2.19	0.002	6.7	0.8	0.0057	0.0003	0.2	0.2
	Lu-P	3.76	0.004	4.2	0.3				
2:2 TBP:HDBP	Dy-O	2.26	0.003	5.9	0.2	0.0087	0.0005	-4.4	0.3
	Dy-P	3.80	0.006	2.9	0.3				
	Lu-O	2.18	0.002	6.7	0.2	0.0056	0.0004	0.1	0.3
	Lu-P	3.75	0.004	4.2	0.3				
3:1 TBP:HDBP	Dy-O	2.30	0.005	7.4	0.4	0.0147	0.0009	-4.4	0.5
	Dy-P	3.86	0.013	3.6	0.5				
	Lu-O	2.19	0.003	6.9	0.3	0.0071	0.0006	-0.2	0.4
	Lu-P	3.76	0.007	4.1	0.4				
4:0 TBP:HDBP	Dy-O	2.38	0.008	6.6	0.6	0.0096	0.0014	-2.7	0.8
	Lu-O	2.31	0.011	8.1	1.0	0.0111	0.0019	-0.3	0.9

The results of the fit indicate that Dy and Lu are six-coordinate with O atoms with organic phases containing any concentration of HDBP, though Lu and Dy do indicate closer to 8 coordinate with O atoms when extracted by 1M TBP alone from 2M HNO_3 though the errors associated with the coordination number determination are high due to low metal ion concentrations in the organic phase. There is an increase in the O coordination number from 6 with 100 % HDBP to 8 for 100% TBP as the TBP concentration is increased to its final concentration of 1M TBP. The 8 O CN is lower than but consistent with the 9 O coordinate TBP-trisolvates of Ln(III), which have 6 O atoms from three bidentate inner-sphere nitrate anions and 3 O atoms from three solvating TBP molecules.[63,64]

Unfortunately, the concentration of metal ion was too low with the extraction from 0.2 M HNO_3 by TBP alone to obtain a sufficient signal so the Ln-O coordination number for the 1 M

TBP organic phase is solely from the 2M HNO_3 extractions. The EXAFS data for the extraction of Ln^{3+} from 0.2 M HNO_3 is shown in the appendix A4. The results of the fit for the Ln-P coordination numbers indicate Dy and Lu are between 3-5-coordinate with P, though the errors are high due to low fluorescent signal obtained as we move further away from the metal ion center because of the $1/r^2$ dependence of the EXAFS signal strength (Eq 3.2).

Table 2: Ln-O and Ln-P EXAFS fit data for Dy^{3+} and Lu^{3+} extraction from 0.2 M HNO_3 into the organic phase. R is the interatomic distance, CN is the coordination number, σ^2 is the Debye-Waller Factor, ΔE is the energy threshold values.

0.2M HNO_3									
Organic Composition		**r/Å**	**err**	**CN**	**err**	**σ^2/Å^2**	**err**	**ΔE/eV**	**err**
0:4 TBP:HDBP	Dy-O	2.25	0.003	5.9	0.2	0.0055	0.0004	-2.4	0.3
	Dy-P	3.80	0.006	3.2	0.3				
	Lu-O	2.19	0.002	6.7	0.2	0.0056	0.0003	0.5	0.2
	Lu-P	3.75	0.004	4.3	0.2				
1:3 TBP:HDBP	Dy-O	2.25	0.002	5.9	0.2	0.0052	0.0004	-2.4	0.3
	Dy-P	3.81	0.005	3.2	0.2				
	Lu-O	2.19	0.002	6.8	0.2	0.0054	0.0004	0.4	0.3
	Lu-P	3.75	0.005	4.3	0.3				
2:2 TBP:HDBP	Dy-O	2.25	0.003	6.1	0.3	0.006	0.0005	-3	0.4
	Dy-P	3.77	0.007	3.5	0.3				
	Lu-O	2.18	0.002	6.2	0.2	0.0039	0.0004	-0.1	0.3
	Lu-P	3.74	0.005	4.1	0.3				
3:1 TBP:HDBP	Dy-O	2.26	0.005	5.5	0.4	0.0058	0.0009	-1.8	0.6
	Dy-P	3.78	0.009	3.6	0.5				
	Lu-O	2.18	0.006	6.5	0.5	0.0056	0.0009	-0.3	0.7
	Lu-P	3.71	0.010	5.1	0.7				

In previous EXAFS research with the related di-*n*-alkylphosphoric acid HDHP(di-*n*-hexylphosphoric acid), the Nd^{3+} and Yb^{3+} coordination environments in the 0.3 M HDHP solutions after contact with 0.01 M $Ln(NO_3)_3$ in 0.1 M HNO_3 reveals P CNs of 5–6.[65]

Table 3: Ln-O EXAFS fit data for Dy^{3+} and Lu^{3+} in either 2 M or 0.2 M HNO_3.

Aqueous Phase		r/Å	err	CN	err	σ^2/Å^2	err	ΔE/eV	err
2M HNO3	Dy-O	2.36	0.003	8.3	0.3	0.0085	0.0006	-3.5	0.4
	Lu-O	2.30	0.003	8.2	0.3	0.0073	0.0005	-0.3	0.3
0.2M HNO3	Dy-O	2.36	0.003	8.9	0.3	0.0078	0.0005	-2.8	0.4
	Lu-O	2.31	0.002	8.7	0.3	0.0073	0.0004	-0.2	0.3

In general, metal ions extracted from aqueous solutions by dialkylphosphoric acids are known to have as many as four different types of speciation, and variations between different extractants and conditions are not unusual.[23,66]

3.4 EXAFS Discussion

Comparison of the predicted distances based upon the sum of the Ln^{3+} and O^{2-} ionic radii and experimental distances as obtained from the EXAFS fit (Table 1,2 and 3) yields good correlation and provides support for the EXAFS-determined O coordination numbers for all samples.[67] Table 4 shows the calculated interatomic Ln-O distances calculated using the effective ionic radii, tabulated by Shannon.[67] The calculated values shown in Table 4 indicate that our experimentally determined values match more closely with a 6 coordinate in oxygen structure for samples that contain HDBP. The distances calculated in Table 4 also support the 8 oxygen coordination with the 1 M TBP extractant concentration when compared to the experimentally determined distance of approximately 2.38 Å.

Table 4: Ln-O and Ln-P interatomic distances calculated for various coordination numbers. Interatomic distances are given as Å.

CN	VI	VII	VIII	IX
Dy-O	2.312	2.37	2.447	2.503
Lu-O	2.261	-	2.397	2.452
Dy-P	3.78	3.84	3.917	-
Lu-P	3.73	-	3.86	-

In addition, there is precedent in the literature for a 6 O coordination of lanthanides in complexes with similar dialkylphosphoric acids, such as HDEHP and Cyanex-272 (bis-(2,4,4-trimethylpentyl) phosphinic acid).[68,69] For organic phases that contain TBP alone, it was found that Dy^{3+} and Lu^{3+} is likely eight coordinate with O, which is more consistent with the known aqua ions of the Ln^{3+} series and to be expected due to TBP being a neutral extraction reagent and thus extracting by a solvation mechanism as opposed to an ion exchange mechanism.[70] With this in mind, 6 O coordination of Ln^{3+} with HDBP and TBP is consistent with precedent, as is the apparent 8 O coordination with TBP alone. The question that arises with regard to the coordination number is the source of the O, as EXAFS alone only yields coordination numbers and interatomic distances. This O could arise from the HDBP ligand alone in a monomer or monodeprotonated dimer form. We could also be observing monodentate or bidentate bonding of the HDBP to the metal ion with either water and/or nitrate ions. We could also be observing a mixed complex system with HDBP and TBP, which has been suggested in literature as the possible mechanism for synergism, or some combination of all of those possibilities contributing to the inner coordination sphere about the metal. For insights into the source of these oxygen atoms we turn to the analysis of the more distant Ln-P interactions.

The results in Table 1 and 2 show the Ln-P distances span the range from 3.7-3.8 Å. Again, comparing experimental interatomic distances with predicted distances calculated in Table 4, we obtain good correlation and once again provide support for our EXAFS fits.[67] To rule out the possibility of a bidentate binding of HDBP to the metal ion, we must simply look at the interatomic distances of the Ln-O and Ln-P interactions. Gannaz, *et al.* observed that the interatomic distances of the Ln-O interaction would be too long and the Ln-P distances would be too short for a bidentate bound HDEHP extractant around Eu^{3+}.[65] Applying a similar model to

our system yields the same effect, that the interatomic distances for Ln-O and Ln-P interactions are more in line with a monodentate model, as shown in Figure 15, since a bidentate bonding of the HDBP molecules about the metal centers does not match the experimental interatomic distances. The O-P-O angle is fixed at 109.5, assuming the phosphate group maintains a perfect tetrahedral geometry.

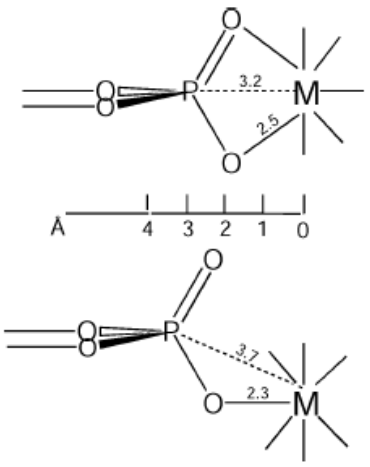

Figure 15: Model depicting a bidentate, edge sharing of two phosphate O with M (top) and a monodentate binding of one phosphate O with M. Figure reproduced from Gannaz, et al. [65]

A value of 6 P would be consistent with the coordination of three monodeprotonated dimers to $Ln^{3+}$to form a neutral species $Ln(HDBP{\cdot}DBP)_3$[68,69] or due to a mixed complex system of $Ln(DBP)_3{\cdot}TBP_3$ that maintains charge neutrality but still yields 6P coordination. The EXAFS determined coordination numbers for the Ln-P interaction, however, do not show 6 P but rather a range of coordination numbers from 3-5 P. This suggests a different speciation than those previously explored in these types of systems. A study utilizing HDEHP and bis(2,4,4-trimethyl-pentyl)oxothiophosphinic acid observed a similar 4 P interaction that was attributed to the formation of a dinuclear species.[71] To determine if the complex is $Ln(HDBP{\cdot}DBP)_3$, $Ln(DBP)_3{\cdot}TBP_3$,or a mixture of both possibilities or perhaps even a dinuclear species that yield less than 6 phosphorus atoms in the second coordination shell, further analysis must be carried out with the obtained EXAFS spectra.

3.5 XANES

Utilization of XANES can yield further insight into the coordination environment of the Ln(III) ions in the TBP:HDBP systems and lend further support for the observed coordination of 6 oxygen atoms about the metal centers. The normalized L_3-edge XANES for all samples are shown in Figure 16. The intense L_3-edge peaks are characteristic of dipole-allowed (2p-to-5d) electronic transitions for Ln(III)[72]and the responses are essentially equivalent, which suggests that the Ln(III) coordination environments in the TBP/HDBP organic systems are consistent across the latter half of the period.

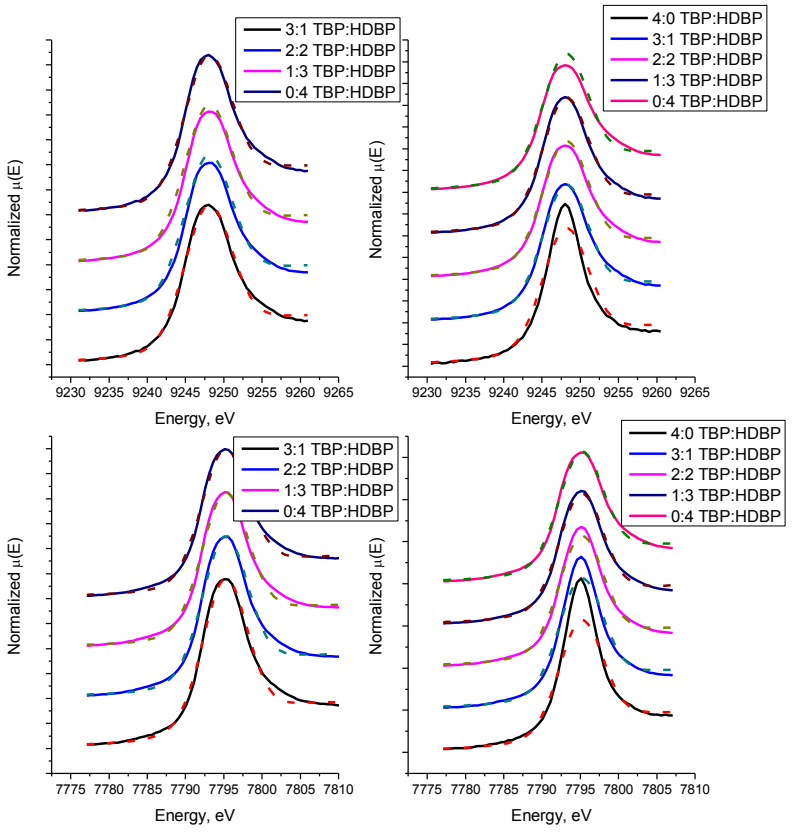

Figure 16: Normalized L_3-edge peaks for Lu in 0.2 M HNO_3 (top left), Lu in 2 M HNO_3 (top right), Dy in 0.2 M (bottom left), and Dy in 2 M HNO_3 (bottom right). Corresponding fits are shown as dashed lines.

Quantitative details were extracted from the XANES region by use of curve fitting with a Lorentzian to the L_3-edge peak. The results of the XANES fits, in terms of peak heights, centers, and full widths at half-maximum (FWHM), are listed in Table 5 for all conditions investigated. The results of the fit show that the FWHM increases with increasing atomic number, Z, as expected from the tabulations of the natural widths by Krause and Oliver.[73]

Table 5: Metrical data for the XANES fitting for organic phases containing either Dy^{3+} or Lu^{3+}.

Dy						
0.2M HNO3						
Sample	**Center**	**err**	**FWHM**	**err**	**Height**	**err**
3:1 TBP:HDBP	7795.1	0.24	6.45	0.13	17.5	3.3
2:2 TBP:HDBP	7795.1	0.22	6.48	0.09	16.6	2.07
1:3 TBP:HDBP	7795.2	0.19	6.53	0.06	15.9	1.28
0:4 TBP:HDBP	7795.1	0.34	6.74	0.19	16	4.83
2M HNO3						
Sample	**Center**	**err**	**FWHM**	**err**	**Height**	**err**
4:0 TBP:HDBP	7795.1	0.12	5.11	0.04	16.9	0.64
3:1 TBP:HDBP	7795.2	0.14	5.55	0.04	16	0.75
2:2 TBP:HDBP	7795.2	0.17	5.99	0.05	15.7	0.92
1:3 TBP:HDBP	7795.2	0.18	6.31	0.06	15.8	1.1
0:4 TBP:HDBP	7795.1	0.22	6.53	0.07	15.9	1.54
Lu						
0.2M HNO3						
Sample	**Center**	**err**	**FWHM**	**err**	**Height**	**err**
3:1 TBP:HDBP	9248	0.51	6.97	0.24	17.3	5.53
2:2 TBP:HDBP	9248.1	0.6	6.99	0.25	16.6	5.55
1:3 TBP:HDBP	9248.2	0.34	7.14	0.09	17.3	2.19
0:4 TBP:HDBP	9248.1	0.41	7.2	0.13	16.4	2.88
2M HNO3						
Sample	**Center**	**err**	**FWHM**	**err**	**Height**	**err**
4:0 TBP:HDBP	9248	0.25	5.48	0.07	16.5	1.36
3:1 TBP:HDBP	9248.1	0.46	6.67	0.14	16.4	2.98
2:2 TBP:HDBP	9248.1	0.66	6.87	0.21	16.2	4.63
1:3 TBP:HDBP	9248.1	0.55	7.03	0.18	16.2	4.07
0:4 TBP:HDBP	9248	0.4	7.22	0.12	16.4	2.65

The experimental widths are larger than the natural widths due to broadening typically associated with beamline optics and instrumental resolution. In addition, the apparent decrease of the FWHM with increasing TBP concentration is attributed to a change in the coordination environment about the metal centers, which can also be seen with the EXAFS data showing a trend of slightly increasing O coordination number as TBP concentration increases.

Further investigation of the XANES region and further evidence of the six O coordination environments can be obtained by taking the second derivative of the L_3-edge peak. The differentiation is done to remove the edge step in a convenient manner, which improves the ease of visualization of the response. The second derivative data for both metal ions at all conditions are shown in Figure 17. For the extraction from low nitric acid, there is evidence of two minima in the 2nd derivative of the L_3-edge peak for all conditions investigated. This double minima is evidence of crystal field splitting and also indicative of an octahedral geometry, namely a complex containing 6 ligands about a metal center, assuming monodentate binding.[74] For the high acid data, an evolution in the crystal field splitting is apparent in the 2nd derivative data as the concentration of TBP increases. This evolution lends direct and independent support to the coordination number changing from 6 to 8 in O as the concentration of TBP is increased.

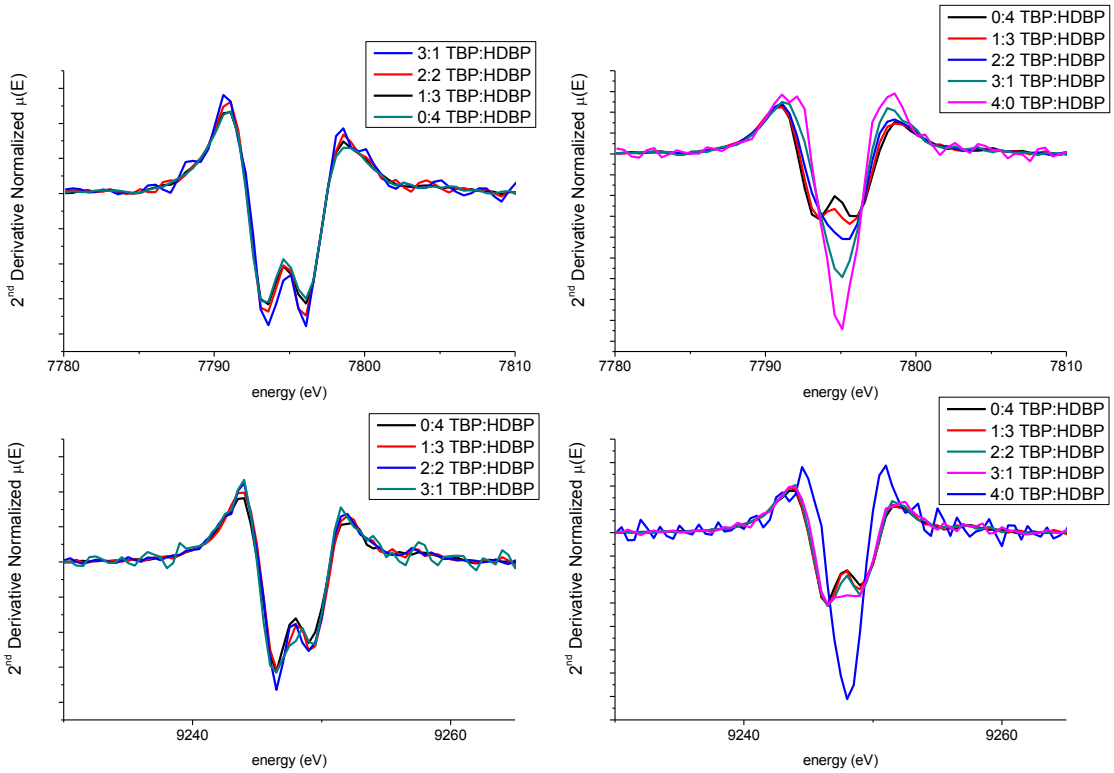

Figure 17: 2nd derivatives of the normalized L_3-edge peaks for Dy in 0.2 M (top left), and Dy in 2 M HNO_3 (top right), Lu in 0.2 M HNO_3 (bottom left), Lu in 2 M HNO_3 (bottom right).

3.6 Principal Component Analysis and Linear Combination Analysis

Further analysis of the EXAFS and XANES data may be carried out through use of principal component (factor) analysis (PCA) and linear regression analysis. PCA and linear regression analysis can be utilized to further probe the binary extractant system after extraction from 2 M HNO_3 only since the data for 0.2 M HNO_3 does not form a complete set with both single extractant reference solutions. The 1 M TBP and 1 M HDBP organic phases were used as reference phases and compared against the mixed phases. For PCA, all five data sets for each metal ion extracted from 2 M HNO_3 were first analyzed identically as above. The data was truncated at k = 9.25 $Å^{-1}$ to reduce the possibility of adverse effects of the experimental noise at high k on the PCA. The results were the same for both metal ions investigated, namely that two

principal components accounted for all the data. This result, though purely mathematical in nature, is consistent with the notion that the single extractant systems with HDBP and TBP alone are the so-called end-member species. Most importantly, the implication of the PCA results is that the EXAFS data for the binary extractant system are adequately described as an arithmetic sum of the EXAFS data for the two single extractant systems, meaning mixed complexes are unlikely in the extraction of metal ions by mixtures of these two extractants.

To strengthen this treatment of the data, Linear combination fitting was implemented on the primary, normalized spectra, I_f/I_0 vs. energy (keV), of the binary extractant systems using again the spectra for the single component extraction as the two limiting end members. The results of the linear combination analysis, as shown in Table 6, show similar results to the PCA analysis, namely that the binary extractant mixtures are simple additions of the end member species.

Table 6: LCF percentages of the pure components Ln-TBP or Ln-HDBP extraction from 2 M HNO_3.

Organic Phase Composition	Dy-TBP %	Dy-HDBP %	Lu-TBP %	Lu-HDBP %
0.75 M TBP/0.25 M HDBP	44.23	55.77	0	100
0.5 M TBP/0.5 M HDBP	0	100	0	100
0.25 M TBP/0.75 M HDBP	0	100	0	100

Additionally, the linear combination analysis shows that the predominant species formed is one with only HDBP. Two such possibilities with a 6O and 6P coordination environment and a 6 O and 4 P coordination environment are shown in Figure 18.This finding is in line with the well-known fact that TBP does not tend to extract trivalent metal ions at these low acid concentrations and is also supported by findings that similar acidic organophosphorus reagents form classical molecular monodeprotonated dimers to extract trivalent metals in ideal, non-associating diluents.[68,69] Whether or not the molecular scenario depicted in Figure 18 is relevant to the supramolecular micellar nature of the systems studied here is open to question. But based upon

the metrics of the aggregation provided by the analysis of the SAXS as described in chapter 4 of this thesis, it may be the case that the species depicted in Figure 18 does not populate the bulk organic diluent in a homogeneous and random distribution as shown. Instead, this species and others like it may be confined to the nano-scale size polar cores of reverse micelles and aggregates of them that also contain significant concentrations of water and nitric acid. It may also be the case that the 6 O may not all be donated from the extractants and may come from water or nitrate.

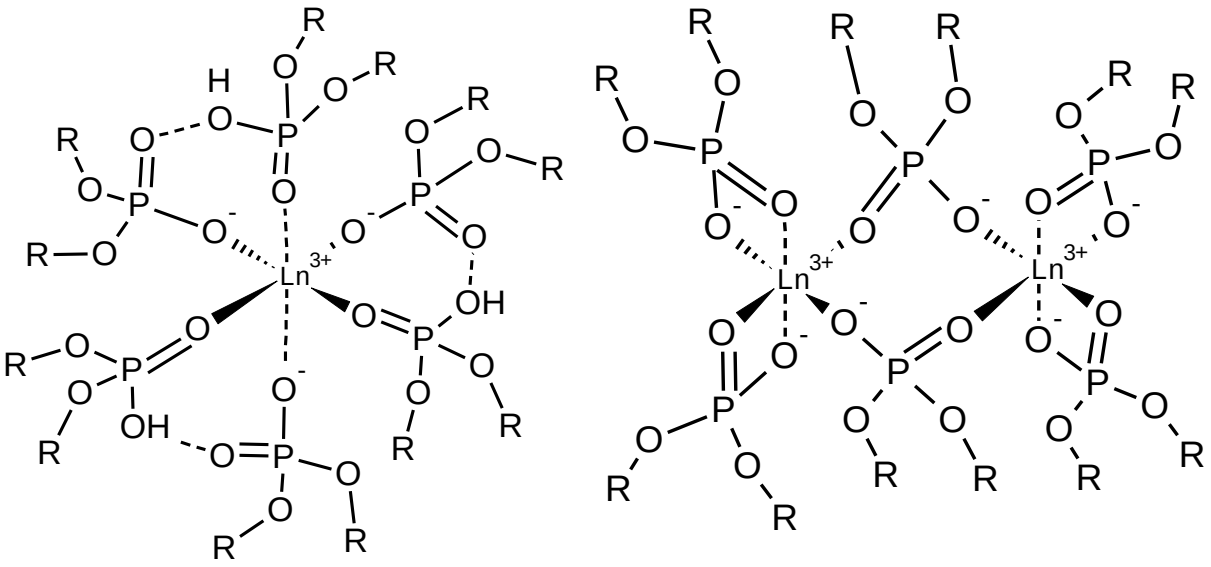

Figure 18: Structure of a generic Ln^{3+} complex with 6 O and 6 P coordination (left) and 6 O and 4 P coordination (right).

3.7 Note on Ce(IV) EXAFS

In an effort to collect EXAFS data on a light Ln^{3+}, extraction of Ce^{3+} were performed in an identical manner as described in the preceding sections. EXAFS experiments were conducted at beamline 12-BM-B under the same conditions as all experiments. Cerium was expected to yield sufficient data since the L_3 and L_2 edges are further apart than for La. Unfortunately, an unexpected phenomena occurred during the collection of EXAFS data on this system. The L_3 edge of Ce(III) is expected to be identical to all other trivalent lanthanides. However, during the second scan of the organic samples a second peak after the first L_3 edge peak was observed.

Several more scans of this sample were conducted and the double edge peak structure became more pronounced as time progressed. Figure 19 shows the variation of peak shape of the Ce EXAFS with each successive scan.

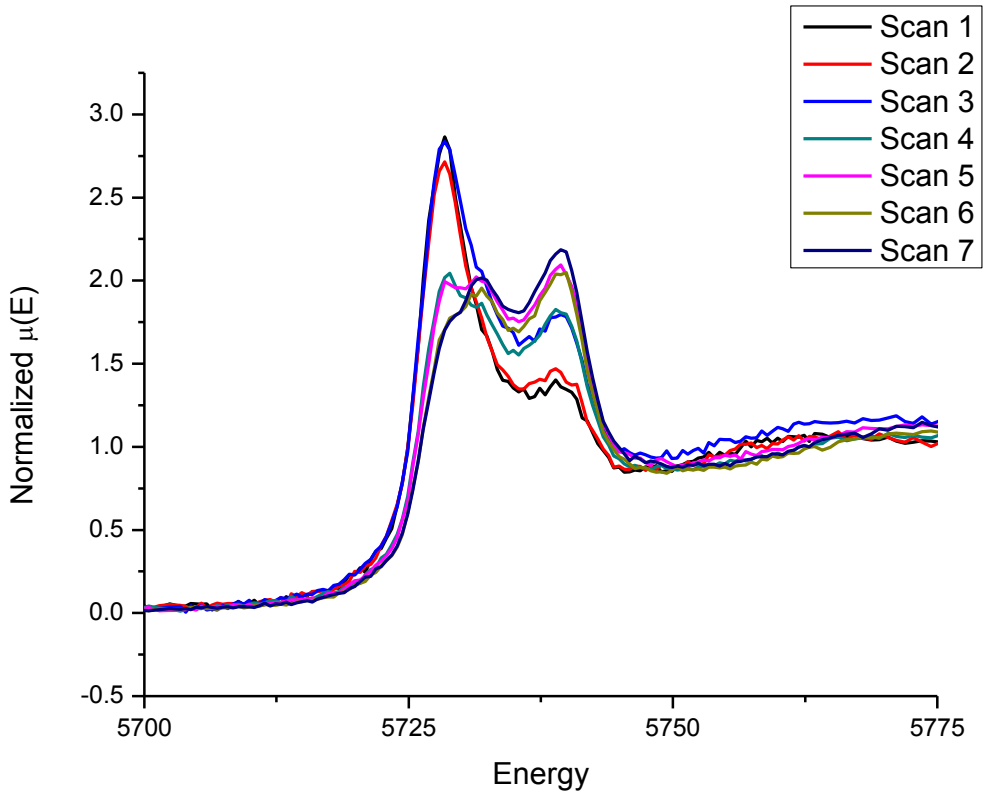

Figure 19: L_3 edge of 1.25 x 10^{-3} M Ce^{3+} extracted from 0.2 M HNO_3 into an organic phase containing 0.75 M HDBP and 0.25 M TBP in *n*-dodecane.

Each scan takes approximately 40 minutes to complete and the sample remains in the beam throughout the full sequence of scans. The data in Figure 19 indicates that the Ce that was originally extracted into the organic phase in the form of Ce^{3+} was oxidized to Ce^{4+} as evident by the formation of the double peak in the L_3-edge that became more pronounced as time in the beam increased. Reduction of Np and Ce has been previously observed in synchrotron beams but oxidation has not yet been seen.[75,76] Unfortunately, there was insufficient beam time to investigate the oxidation of Ce in the synchrotron beam further.

3.8 Fluorescence Study of the Complexes Formed

The immediate next step in this study is to complete the investigation into the hydration number of the metal complexes formed in the organic phases. Experimental determination of the hydration number of these complexes would further solidify the source of the oxygen atoms about the central metal ion and provide a more complete understanding of the complex environment observed when trivalent metal ions are extracted into a organic phase consisting of 1 M TBP, 1 M HDBP, or mixtures thereof. A useful tool that will allow us to achieve this goal is luminescence studies, specifically time-resolved laser induced fluorescence spectroscopy (TRLIFS). Initial luminescence studies were carried out on all trivalent lanthanides and the uranyl ion to determine the fluorescence spectra and to rule out those unsuitable for investigation. These studies have allowed us to narrow our current search to Dy^{3+} and Eu^{3+} alone since most other trivalent lanthanides do not provide a sufficient luminescent signal. Unfortunately, in this regard, it was discovered that La^{3+} and Lu^{3+} do not provide adequate fluorescent signals to allow luminescence studies to be conducted. Figure 20 shows the 2D spectra for Eu^{3+}. This data does show a change in peak morphology that is acid dependent, which Zhang et al. has previously attributed to a change in the coordination environment around the metal centers for this system.[77]Additionally, the intensity of the dominant peaks seems to be dependent on the water concentrations in the organic phases as the maximum intensity correlates with the maximum water uptake for the TBP:HDBP system.

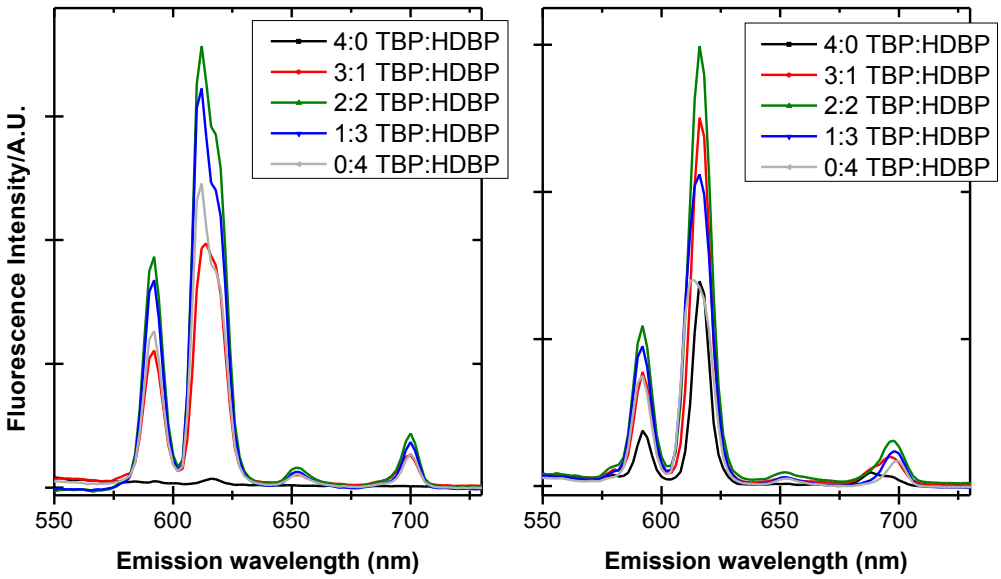

Figure 20: Fluorescence spectra for 10^{-3} M Eu^{3+} extracted from 0.2 M HNO_3 (left) or 2 M HNO_3 (left).

Time-resolved laser induced fluorescence spectroscopy (TRLIFS) has been used for the determination of the hydration number of complexes formed by the extraction of Eu^{3+} and can also be used for determination of hydration number in Dy^{3+} due to its powerful fluorescence after excitation with a 355 nm laser.[77,78] Preliminary studies with Eu^{3+} TRFS have been carried out at Lawrence Berkeley National Laboratory (LBNL) with a Xenon flash lamp and show hydration numbers to be less than 1 on average in accordance with the formula for hydration number for Eu^{3+} given by Zhang and Kimura,[77] shown in Eq. 3.6.

$$\mathbf{n_{H_2O} = 1.05 \times 10^{-3} k_{obs}(H_2O) - 0.44} \qquad 3.6$$

where k_{obs} (H_2O) is the decay constant determined experimentally from fitting the fluorescence signal decay with an exponential trend. Table 7 shows the calculated hydration numbers for the europium extractions. These hydration numbers are in line with complexes that are formed predominantly with monodeprotonated dimers of HDBP alone with the presence of some

complexes formed with TBP that would include some water in the inner coordination sphere. Unfortunately, although Dy^{3+} does exhibit similar fluorescence properties that can be linked to hydration number in much the same way as Eu^{3+}, it has not been studied in great detail in literature and only one instance of a relation between hydration number and luminescence decay constant could be found.[78]

Table 7: k_{obs} and hydration number for Dy^{3+} or Eu^{3+} from either 2 M HNO_3 or 0.2 M HNO_3. Errors associated with these calculations are ±0.5 n_{H2O}.

	Europium Extraction				Dysprosium Extraction			
	0.2 M HNO_3		2 M HNO_3		0.2 M HNO_3		2 M HNO_3	
Sample	$k_{obs}(s^{-1})$	n_{H2O}	$k_{obs}(s^{-1})$	n_{H2O}	$k_{obs}(ms^{-1})$	n_{H2O}	$k_{obs}(ms^{-1})$	n_{H2O}
4:0 TBP:HDBP			653.8	0.24			22.13	-0.27
3:1 TBP:HDBP	753.4	0.35	694.6	0.28	16.81	-0.39	23.61	-0.24
2:2 TBP:HDBP	754.8	0.35	823.4	0.42	24.72	-0.21	26.80	-0.17
1:3 TBP:HDBP	802.6	0.40	966.2	0.57	22.21	-0.27	25.18	-0.20
0:4 TBP:HDBP	884.2	0.48	1035.6	0.64	23.43	-0.24	26.71	-0.17

To investigate the hydration of Dy in organic phase further, we conducted two separate experiments; one that is identical to all other previously completed experiments and one involving deuterium oxide and DNO_3 instead of water and nitric acid. The use of deuterium oxide allows us to make comparisons between the decay lifetime of water and D_2O, owning to the fact that $k_{obs}\,(H_2O) \gg k_{obs}\,(D_2O)$ and $k_{obs}\,(D_2O)$ is almost a constant, and ligands are not as effective as H_2O in causing the de-excitation of the exited state. The empirical formula can then be determined as follows:

$$\mathbf{n_{H_2O} = 1.05\left(\frac{1}{\tau_{H_2O}} - \frac{1}{\tau_{D_2O}}\right)} \qquad 3.7$$

where τ_{H_2O} is the time constant for the fluorescence decay for a system containing water and τ_{D_2O} is the time constant for a system containing deuterium oxide.[79] Kimura et al. had previously determined a relation between hydration number and k_{obs} for Dy(III) complexation with aqueous complexants and determined that the hydration number can be calculated with Eq. 3.8.[78]

$$\mathbf{n_{H2O} = 0.024k_{obs}(Dy) - 1.3} \qquad 3.8$$

We developed a similar relation between hydration number and luminescence decay constant utilizing a similar method as Kimura. Figure 21 shows the experimental luminescence decay constants versus hydration number for complexes of Dy with ethylenediaminetetraacetic acid (EDTA), diethylenetriaminepetaacetic acid (DTPA), and nitrilotriacetic acid (NTA).

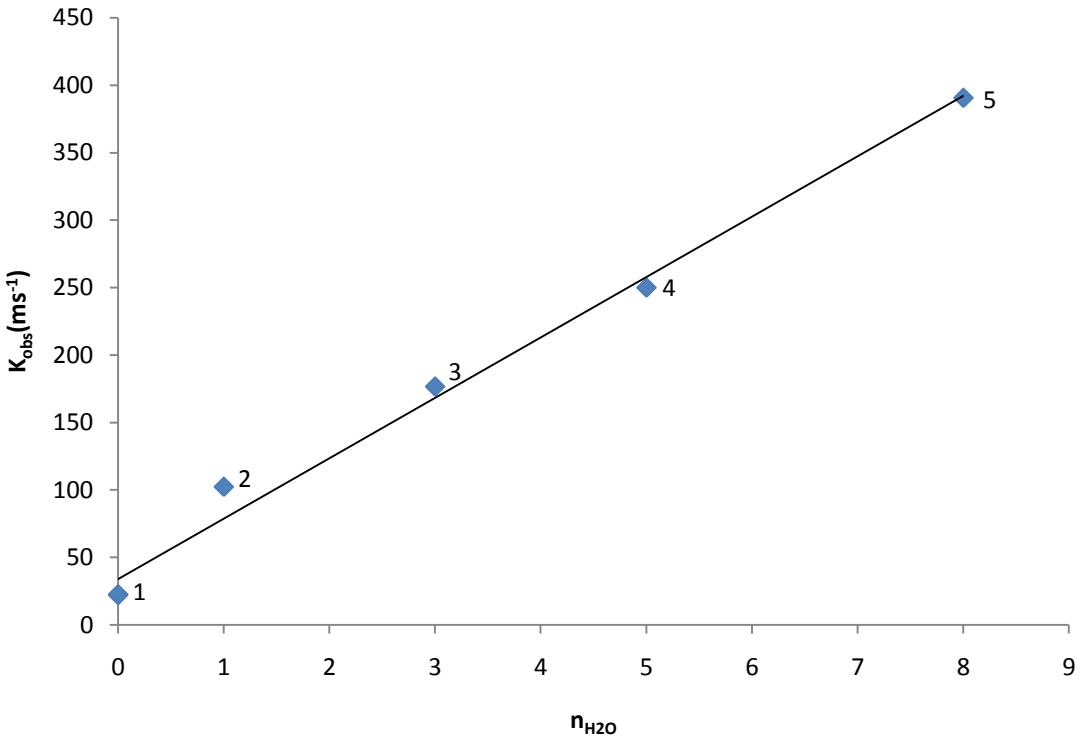

Figure 21: plot of $k_{obs}(ms^{-1})$ vs. n_{H2O} for Dy(III). The trend line shown is the relation shown in Eq. 3.9. The k_{obs} for Dy(III) in D_2O and H_2O as well as those for Dy(III)-polyaminopolycarboxylate complexes. They are numbered as 1) D_2O, 2) DTPA, 3) EDTA, 4) NTA, and 5) H_2O.

Utilizing the calibration curve from Figure 21, we were able to calculate a similar relation to Kimura, shown in Eq. 3.9.

$$\mathbf{n_{H2O} = 0.022k_{obs}(Dy) - 0.76} \quad 3.9$$

The results of the Dy hydration number calculations are shown in Table 7 and indicate a slightly different story to that of Eu(III), namely that there seems to be -1 to 0 water molecules bound to the metal centers of these complexes. It is also important to note that though the hydration numbers for Dy complexes are negative they do not lay below the experimental value for Dy-D_2O complexes which indicates the hydration number is highly likely to be very close to 0.

3.9 Conclusions

The EXAFS data presented in this chapter serves to indicate that there are 6 oxygen atoms about the central metal ion and between 3-5 phosphorus atoms in the second shell. Coupling this find with the hydration number calculations allows us to determine that the most probable source of the oxygen atoms is the extractants and not water or nitrate, though in the case of the 1 M TBP the source of the oxygen present is most likely bidentate bound nitrate ions. In view of the 4-6 phosphorus in the second coordination shell, it is quite possible that we are observing some sort of dinuclear species or complexes that may exist inside of some sort of macromolecular structure. To investigate these aggregation phenomena further, we must now turn to X-ray and neutron scattering techniques.

Chapter 4: Macromolecular Structures and Aggregate Formation

To investigate the macromolecular structures formed in the organic phase, small angle scattering techniques such as Small Angle X-ray Scattering (SAXS) and Small Angle Neutron Scattering (SANS) were utilized. These techniques allow us a different avenue to approach the extraction behavior of these organic extraction systems.

4.1 SAXS/SANS Theory and Data Analysis

Small angle scattering techniques are in essence a set of methods for studying structural features of a colloidal size. Colloidal dimensions may range between tens to several thousand angstroms and are large compared to the wavelength of the X-ray or neutron beam. The difference in wavelength and investigated particle size makes the angular range of observable scattering very small. These scattering processes are characterized by a reciprocity law which gives an inverse relationship between the particle size and scattering angle.[80] It is important to note that X-rays are primarily scattered by electrons while neutrons are scattered off of the atom nucleus which gives rise to a differing contrast between the two techniques and thus a different viewpoint to investigate these systems. Figure 22 shows two spherical particles of different size and their correspondingand simplified scattering behavior.

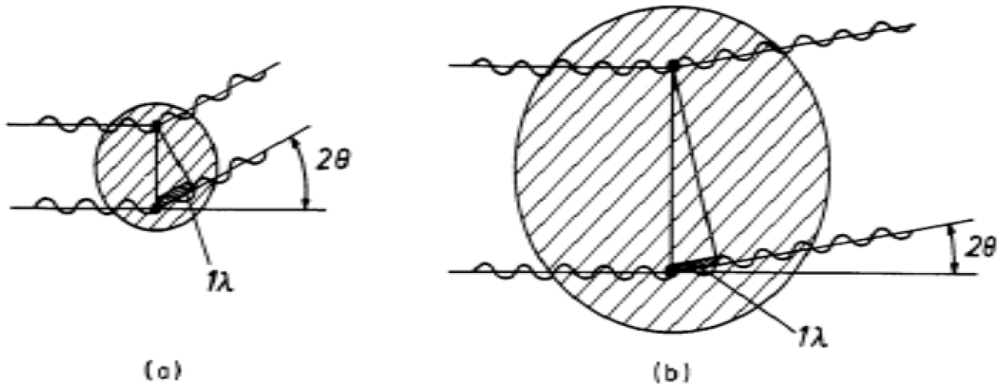

Figure 22: X-ray scattering of two spherical particles of different size. Figure reproduced from Small Angle X-ray Scattering.[80]

The following treatment of scattering data will be concerned with X-rays alone, though all analysis may be applied to neutron scattering as well with only slight modifications. To obtain meaningful information regarding the structures present in the organic phase, one first must average the intensities azimuthally in Q, where Q is the momentum transfer calculated by Eq. 4.1.

$$\mathbf{Q} = \frac{\mathbf{4\pi sin\theta}}{\boldsymbol{\lambda}} \tag{4.1}$$

Here, 2θ is the scattering angle and λ is the wavelength of the incident X-ray beam.

In systems where aggregation does not occur, the extractant monomers produce very weak scattering that is barely above the background. As reverse micelles form, each molecule participates in scattering by the square of the volume of the micelles so that the supramolecular structure dominates the SAXS data.[81] The radius of gyration, R_g(a shape-independent measure of particle size in terms of the root mean square of all the distances in the particle from its center of mass)[82] of the scattering particles and the scattering intensity at zero momentum transfer, I(0), can be determined through use of the Guinier Approximation (shown in Eq. 4.2) and the Unified fit method conducted with the Irena software package.[83]

$$\mathbf{Ln}\big(\mathbf{I(Q)}\big) = \mathbf{Ln}\big(\mathbf{I(0)}\big) - \frac{\mathbf{R_g^2 Q^2}}{\mathbf{3}} \tag{4.2}$$

The Guinier plots, log(I(Q)) vs Q^2, may show some indication of curvature which is typically indicative of structure factor interference. In this case the analysis of the low Q data with the

Guinier approximation alone is not always sufficient since it would yield an inaccurate R_g.[82] Further analysis can be made through use of a pair distance distribution function (PDDF).

For a dilute system, which is the simplest case, one can assume that all scatterers are uncorrelated, i.e. every particle of the system can be regarded as independent in respect of the translation and orientation and that there is no long range order or interparticle interactions.[84] This assumption leads to the formulation shown in Eq. 4.3

$$\mathbf{I(Q) = 4\pi \int_0^{\infty} p(r) \frac{\sin(Qr)}{Qr} dr} \qquad 4.3$$

where p(r) is the pair distance distribution function (PDDF) that yields information about particle shape. In principle, the PDDF can be calculated from I(Q) by an inverse Fourier transformation. In non-dilute systems, such as those found in solvent extraction systems like ours, we must take the interparticle interactions into consideration.

The GIFT method[85-87] can be used to obtain p(r) functions (structure information in real space) from scattering data in Q space from non-dilute systems. GIFT interprets the globular particle system, I(Q) = nP(Q)S(Q), where P(Q) is the average form factor corresponding to the shape and size of the scattering particles, S(Q) is the average structure factor from interparticle interactions, and n is the number of particles per unit volume. P(Q) is the Fourier transformation of its real space counterpart, p(r), according to Eq 4.4:

$$\mathbf{P(Q) = 4\pi \int_0^{\infty} p(r) \frac{sinQr}{Qr} dr} \qquad 4.4$$

Thus to determine p(r), the inverse Fourier transformation (IFT) of an experimental P(Q) must be calculated. In concentrated systems, such as those involved in solvent extraction, the structure factor, S(Q), must be modeled and subtracted from the scattering data, I(Q), to give P(Q). The selection of the appropriate structure factor model is paramount to the determination of correct p(r) functions from GIFT, and the model selected for the current study was the Percus-Yevick (PY) closure relation[88] that has been shown to closely approximate the interaction effects of micelles in SAXS studies from numerous extraction systems.[34,89-92]

The PY closure relation for hard spheres solves the Ornstein-Zernike equation on the principle that the hard sphere potential is zero if the particles do not overlap andis infinity if they do. The resulting structure factor depends on the radius and volume fraction of particles with a modification to include polydispersity with a distribution function. The PY closure relation structure factor is simple, relatively fast, and can be used for non-hard sphere interaction potentials,sincemany potentials behave similarly to effective hard spheres.[93] According to Glatter,[94] this structure factor model holds true for both deviations from hard spheres and from perfect spherical symmetry, allowing its use to evaluate scattering data of interacting elongated particles. Many recent publications have used this method to great effect on systems that contain interacting nonionic surfactant reverse micelles in nonpolar solvents.[95-99] These studies have shown growth of spherical particles into elongated rod-like aggregates. A detailed discussion of the PY closure relation model in the GIFT treatment of SAXS data is given in a recent review article by Fritz and Glatter.[94]

4.2 Experimental Procedures

SAXS Experimental Procedures

To conduct SAXS/SANS experiments on the TBP/HDBP system, again only the organic phases are necessary. Samples were created identically as those described in section 2.1 of this thesis though the metal ion concentration investigated was 10^{-3} M. SAXS data from the organic phases from the experiments with 2 M HNO_3,0.2 M HNO_3, and 0.2 M HNO_3 + 1.8 M NH_4NO_3 (with and without the metal ion present) were collected at beam line 12-ID-C at the Advanced Photon Source (APS) at Argonne National Lab.The incident photon energy was 28keV, providing good X-ray transmittance for all compositions of the solution systems. Two separate experimental setups were used for the collection of SAXS data, one using a single 2 mm diameter quartz capillary tube for containment of all solutions to facilitate meaningful comparisons of the SAXS intensities, I(Q), where Q is the scattering vector ($Å^{-1}$) according to Eq. 4.1 and a second set of experiments performed with a pendant drop system. A cartoon schematic of the difference between both methods is shown in Figure 23.

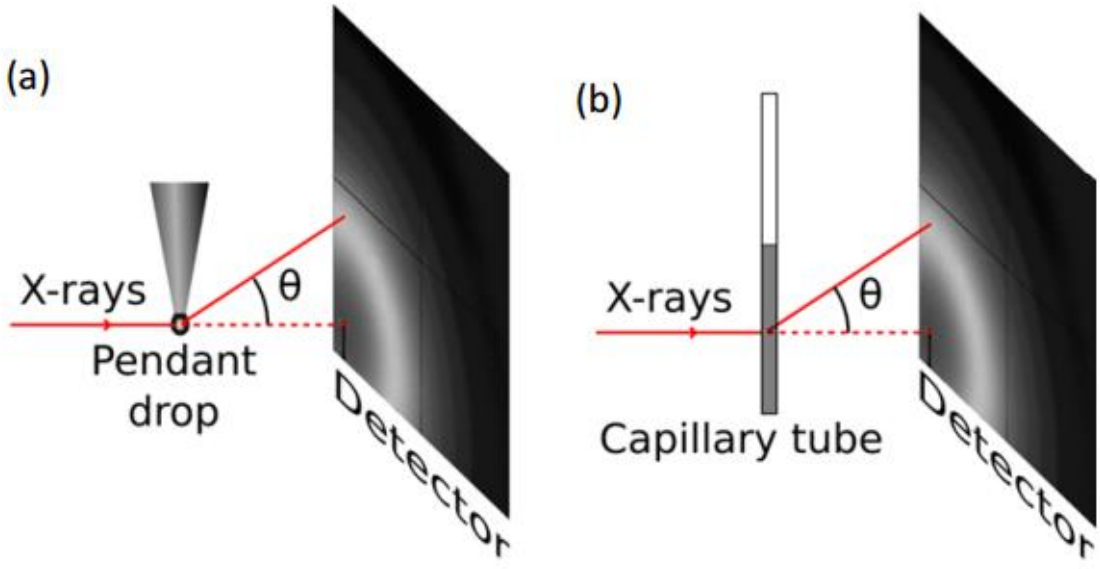

Figure 23: Schematics of (a) pendant drop and (b) capillary tube setup for small-angle X-ray scattering measurements.Figure courtesy of Dr. Mark Antonio.

Five 30 s exposures, obtained with a MAR CCD, for each sample (containing data with less than 1% shot-to-shot variation of all values of scattering vector, $0.03 Å^{-1} \leq Q \leq 0.86 Å^{-1}$) were averaged, and the background-subtracted data were analyzed following standard procedures.[89,100] The data for collected intensity versus Q were also analyzed with the Irena software package utilizing the unified fit method developed by Greg Beaucage.[83,101-103] All radius of gyration and I(0) data is given as the average of the values calculated from the Unified fit method and from the Moore Autocorrelation.[104]

SANS Experimental Procedures

SANS experiments were conducted at the High Flux Isotope Reactor (HFIR) at Oak Ridge National Lab on CG-2 GP-SANS. To conduct SANS experiments, the organic diluent must be deuterated along with the aqueous phase to ensure that the scattering observed is from the extractants and not from excess hydrogen in the system. N-dodecane-d26 was obtained from Sigma Aldrich to 98 atom % D. Deuterium oxide, D_2O, was obtained from Sigma Aldrich to 99.9 atom % D. DNO_3 was obtained from Sigma Aldrich as 65 weight % in D_2O with 99 atom % D. Solutions were prepared in an identical manner as described in section 2.1. Tb was chosen instead of La, Dy or Lu since the organic samples would be exposed to a neutron beam. Tb has a sufficiently low neutron absorption cross section which allows for minimal activity after extended exposure to the neutron beam. Additional experiments using deuterated TBP were also conducted to investigate the nature of the organic phase structures more closely and to investigate any potential shape and size changes in the organic phase microstructure. Samples were loaded into 1 mm path length Hellma “banjo” type quartz cells with a 20 mm diameter. The samples were loaded on a sample changer with capacity for up to 15 samples. All experiments were conducted with ambient temperature and pressure. The sample to detector distance was

chosen to be 0.25 m and 10 m to collect data over a Q range of 0.006 to 1 Å. The data collected at the two sample-to-detector distances were merged and corrected for absolute intensities. Samples were exposed to a neutron beam with a 4.75 Å wavelength until approximately 10 million counts were achieved (approximately 30 minutes to 2 hours depending on the scattering behavior of each sample).

4.3 SAXS Results and Discussion

To investigate aggregation phenomena in the organic phase as a function of TBP:HDBP, and how this affect the extraction of Ln^{3+} at low and high acid, SAXS measurements were performed on solutions with and without metal ion. The scattering intensities, I(Q) vs. Q, obtained from the SAXS experiments, varied with the molar ratios of the extractants as shown in Figure 24 for selected organic phases. The data selected for presentation are for the extraction of dysprosium from 0.2M HNO_3 and 2 M HNO_3. Dysprosium was chosen as a representative for all the lanthanides investigated since the trends are identical for each metal ion with respect to the aqueous acidity. The plots of the scattering intensities of La and Lu extraction into 2 and 0.2 M HNO_3 as well as the Dy scattering intensities for 2 M HNO_3 extraction can be found in appendix A5, A6, and A7. The most interesting aspect of this data is that the scattering contrast for the contacted organic solution using the mixture of TBP and HDBP is much higher than the arithmetic average for the contacted solutions of TBP and HDBP alone for $Q \leq 0.3$ $Å^{-1}$. Also, the SAXS data for systems with or without Dy^{3+} are essentially identical, showing that extraction of the metal ion, in this case, has very little impact on the macromolecular organic phase structure, as expected at these low metal loading conditions.This trend has been previously observed in this system.[99]The SAXS data further suggests that the mixture of TBP-HDBP solution has large assemblies of scatterers after contact and, in view of the water uptake into the organic phase

shown in Chapter 2 Figure8 is consistent with the formation of reverse micelles, such as, for example, when mixtures of HDHP (di-*n*-hexylphosphoric acid) and DMDOHEMA (dimethyl-dioctylhexylethoxymalonamide) are used for the extraction of trivalent lanthanide ions from nitric acid solutions.[89]

For globular systems, such as reverse micelles or microemulsions that are common in solvent extraction systems, the intensity at I(0) is dependent on the volume (V) of the core of the aggregates according to eq. 4.5:

$$\mathbf{I(0) = (\varphi V \Delta \rho)^2 P(0) S(0)} \qquad 4.5$$

Here, φ is the volume fraction of the scattering aggregates, $\Delta\boldsymbol{\rho}$ is the electron density contrast, and P(0) and S(0) are the form and structure factors of the aggregates, respectively. In a recent study by Dourdain et al.,[30] a predictable change in I(0) was observed between the pure end members, indicating no notable changes in aggregate state in the mixed HDEHP-TOPO system. A similar trend was observed in the dry HDBP-TBP mixtures of interest in this study, shown in Figure 25.Post contact with an aqueous phase, however, the trend in I(0) changes so that there are definitive peaks which indicates that the mixed systems form large micelles, with a different aggregated structure than the end members, or that the structure factor S(Q) has changed across the series.

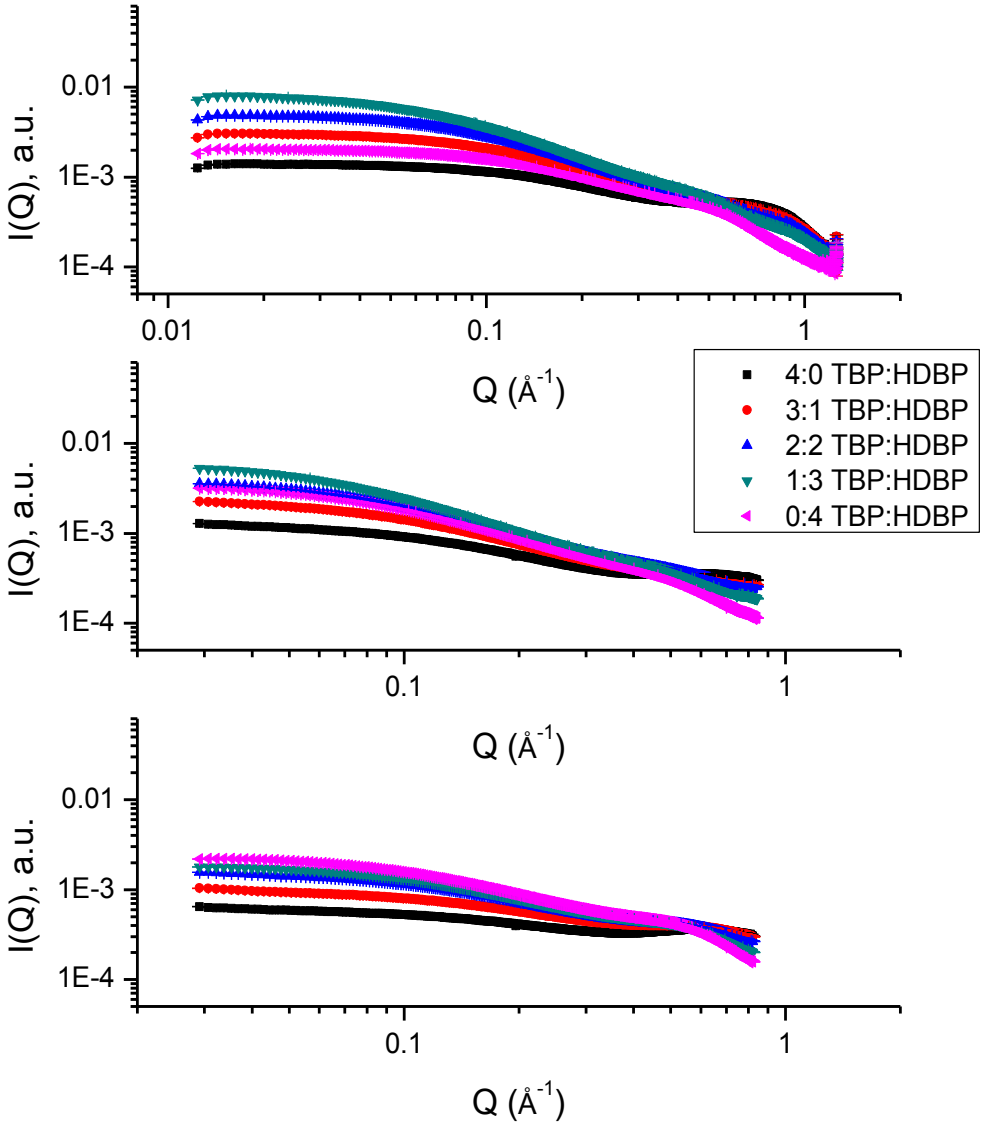

Figure 24: Log-log plot of the SAXS data for the three TBP:HDBP mixtures and the two individual extractant solutions after contact with 0.2 M HNO_3 aqueous phase (top) with Dy and (middle) without Dy. Dy concentration was 10^{-3} M. The responses for the pre-aqueous contact ("dry") organic solutions are shown bottom.

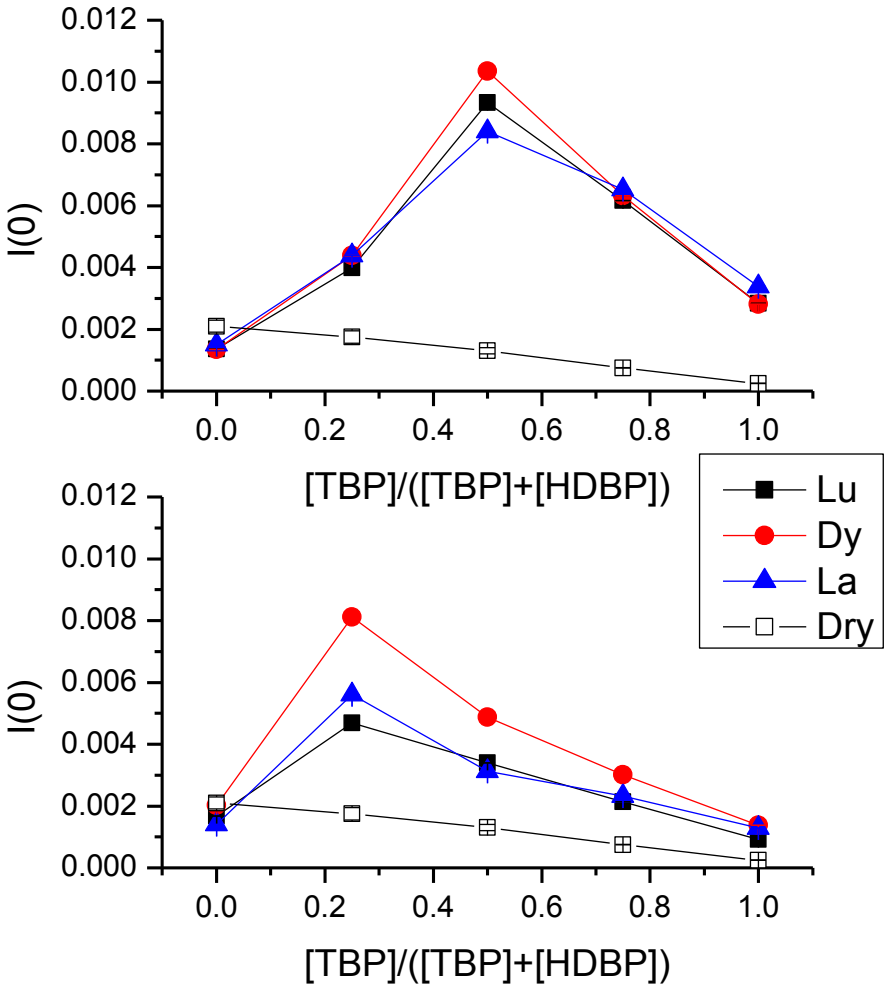

Figure 25: I(0) calculated from the entire scattering curves for the organic phases containing varying ratios of TBP and HDBP with constant extractant concentration after contact with aqueous phases containing 0.2 M HNO_3 (Top) and 2 M HNO_3 (bottom) and either La, Dy or Lu. Dry organic phase behavior is shown with open squares.

Information about the aggregates formed upon extraction of each metal ion is provided in terms of R_g values, which are plotted as a function of the mixing ratio of the extractants, as shown in Figure 26.

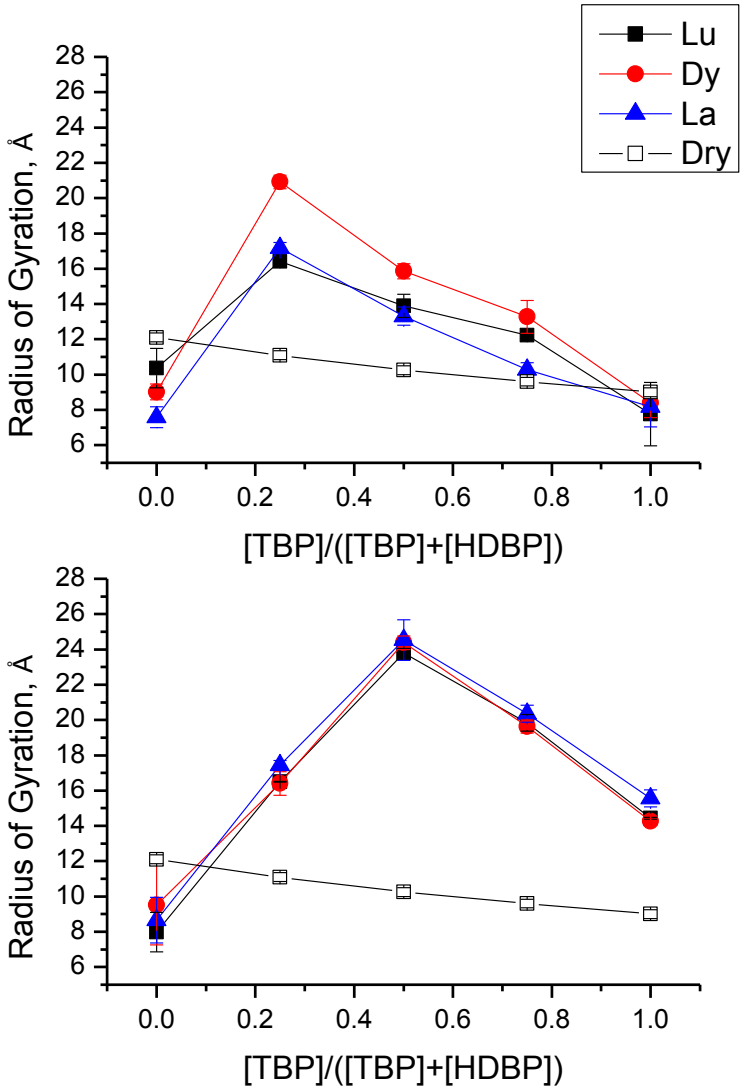

Figure 26: Radius of gyration (R_g, Å) calculated from the entire scattering curves for the organic phases containing varying ratios of TBP and HDBP with constant 1 M extractant concentrations after contact with 0.2 M HNO_3 (top) and 2 M HNO_3 (bottom) containing either La, Dy or Lu. The radius of gyration for the dry organic phase is shown with open squares.

The corresponding results for the precontacted, i.e. dry organic phases, show a predictable linear trend similar to that of the I(0) data.[99] However, after contact with a phase containing metal ions a distinct peak can be seen in the R_g that corresponds identically with the peak previously observed in the I(0) data. A similar peak in the R_g values for the TBP:HDBP system without the inclusion of metal ions was observed previously which indicates that the aggregates form with or without the metal ion present, as indicated by the I(Q) data and the water uptake into the organic

discussed in a previous chapter.[99]This variation in the experimentally determined R_g values clearly shows that, after contact with the aqueous phase, the particle scatterers assemble into larger entities in the mixed extractant phases than in either of the single component systems.

Additional information about particle morphology can be obtained from the p(r) functions, shown in Figure 27, obtained by the GIFT treatment of the SAXS data. For simplicity, only the p(r) functions for the extraction of Dy from 2 and 0.2 M HNO_3 and the dry organic phases will be shown in this text. The remaining p(r) functions for the extraction of La and Lu from 2 and 0.2 M HNO_3 solutions can be found in the appendix A8 and A9. The extended, tail like decay of the p(r) functions indicates elongated reverse micelles that are typically between globular/ellipsoidal in nature to cylindrical.[84,105] In the dry organic phases the intensity of the first peak decreases with increasing HDBP concentration, indicating a deviation from a globular system. Additionally, the formation of a second peak has been attributed to interactions between rod-shaped aggregates as a solution becomes more structure.[97,106] Analogous studies of nonionic surfactant micelles in aqueous and oil diluents observed similar secondary peaks in the GIFT-generated p(r) functions. After contact with an aqueous phase, the ordering across the series with the mixed system differs from the dry organic phases and indicates larger, more elongated structures than the end members when a mixture of TBP and HDBP exists. Additionally, the formation of a second peak is far more pronounced after contact with an aqueous solution than the corresponding dry organic phases, indicating a higher degree of order for the organic phases after contact with an aqueous phase.

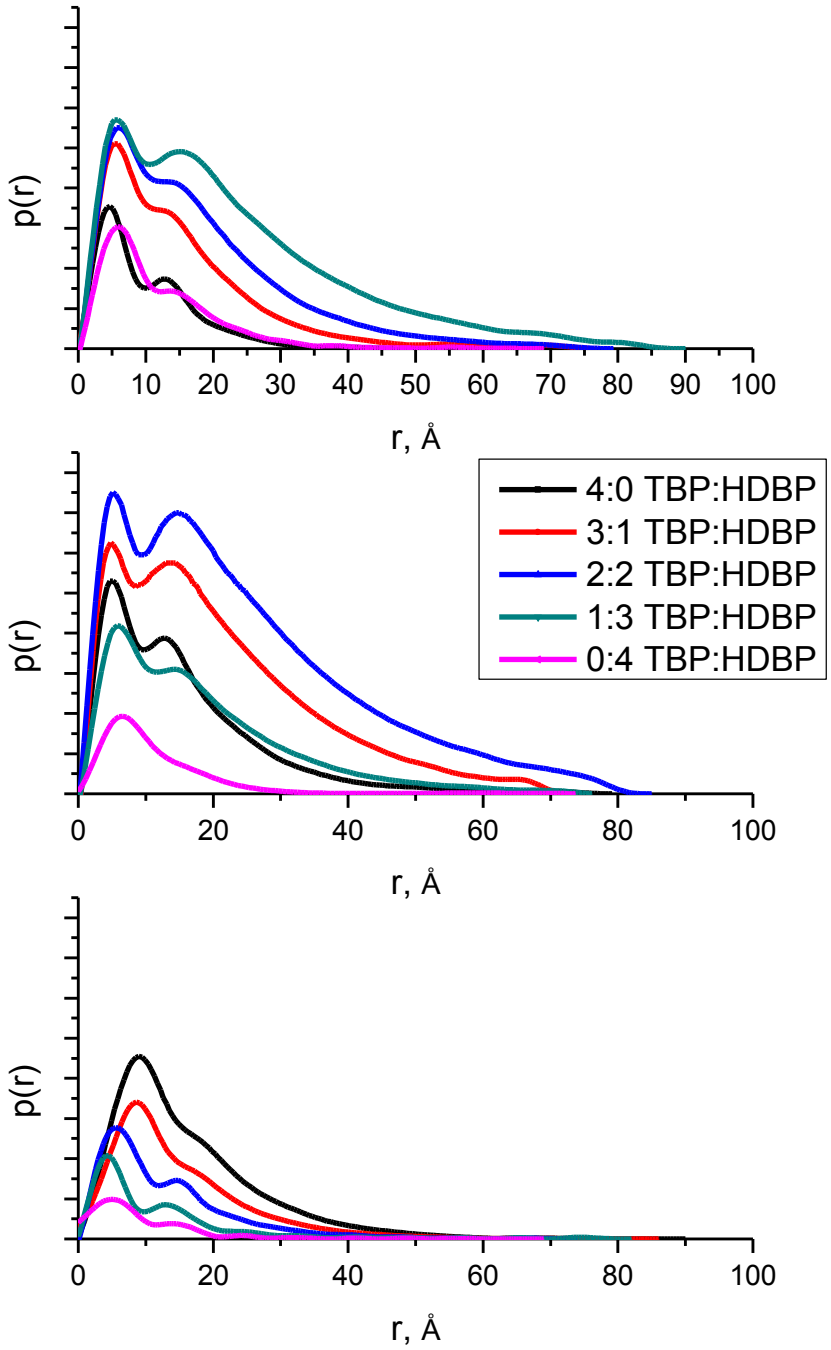

Figure 27: P(r) functions for the extraction of Dy from 0.2 M HNO_3 (Top), 2 M HNO_3 (middle) and the corresponding dry organic phases (bottom).

The point at which the p(r) functions decay to zero (r_{max}) corresponds to the maximum linear extent (MLE) of the aggregates or the length of the rod. The variation of the MLE values for

each of the five extractant ratios is shown in Figure 28. The largest MLE values (90 – 125 Å for 0.2 M HNO_3 extractions and 70 – 85 Å for 2 M HNO_3 extraction) are observed with mixtures of TBP and HDBP. The domed nature of the MLE with respect to the extractant ratio shows, once again, that the system behaviors with mixed TBP and HDBP extractants after aqueous contact are not simple arithmetic averages of the responses for the two end members.

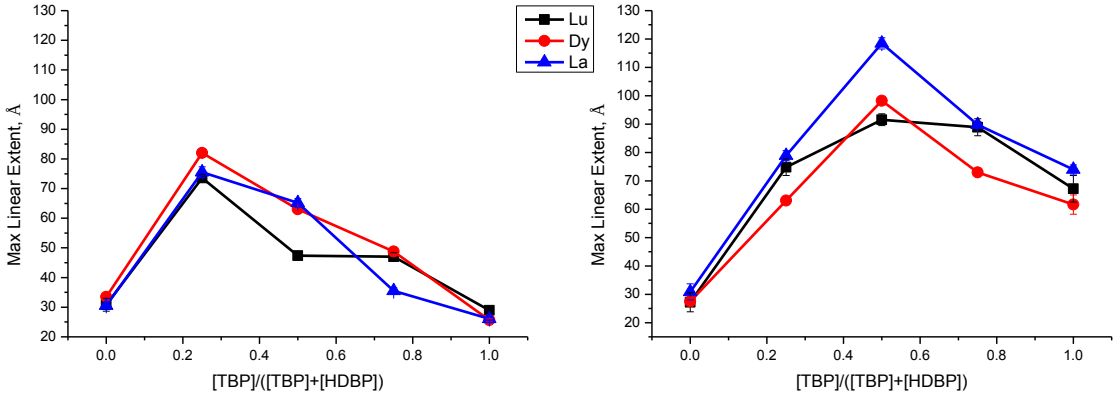

Figure 28: Miximum linear extent (MLE) for extraction of trivalent lanthanides from 2 M HNO_3(left) and 0.2 M HNO_3 (right).

Our SAXS results agree with the pioneering work by Osseo-Asare, who showed an enhanced extraction of metal ions using microemulsions,[28] and by the more recent work by Dourdain et al. that aggregation and synergy may be connected.[30] The SAXS results in the dryorganic phases show that mixing the two extractants does not result in any notable difference in aggregate structure than just a weighted-arithmetic sum of the components, as was observed by Dourdain.[30] However, after contact with the acidic aqueous phase, significant rearrangement of the organic phase structure occurs, with increased ordering and larger aggregates evident in the mixed systems relative to the end members, an effect that was not noted beforehand.[30] Of significant interest is the molar ratio of TBP and HDBP that yield the largest aggregates. In the 0.2 M HNO_3 extraction system, the largest aggregates are formed with 0.25 TBP mole fraction which seems to coincide with the apparent maximum in the extraction of metal ions, within errors, which

suggests there may be a correlation between aggregate size and synergy in these systems. It is important to note though that no such correlation can be observed in the 2 M HNO_3 extraction systems and the largest aggregates seem to only correlate with the maximum water uptake into the organic phase, which was found to be independent of metal ion.

4.4 SANS Results

Small angle neutron scattering, though a similar technique to small angle X-ray scattering, can be utilized to yield a different perspective of the aggregates formed in solvent extraction systems. X-rays scattering cross sections increase systematically in terms of Z^2 while neutron scattering cross sections show very little systemic variation with atomic number. Figure 29 below shows the scattering cross sections for x-rays and thermal neutrons for a few atoms.

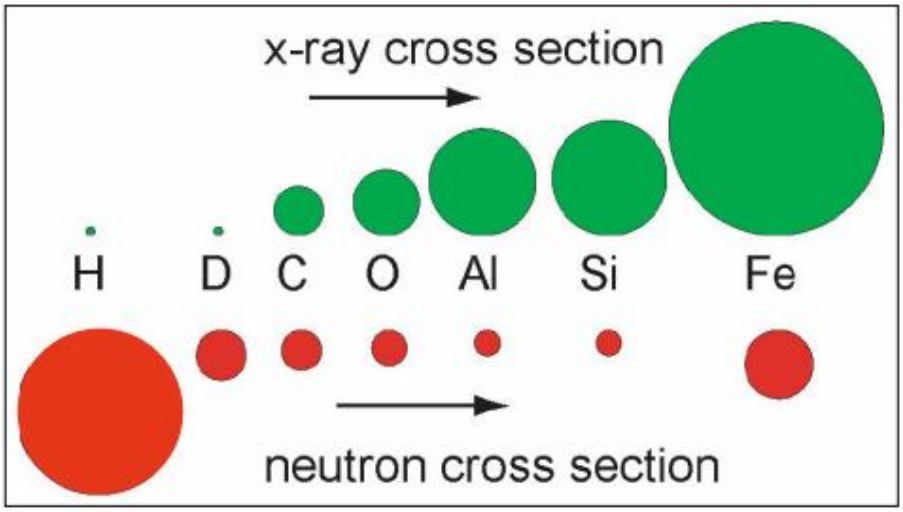

Figure 29: X-ray and neutron scattering cross section comparison. The X-ray scale has been reduced by a factor of 1.5 compared to the neutron scale. Figure reproduced from ncnr.nist.gov.

The difference in scattering cross section allows us to probe the polar core of the reverse micelles with SAXS measurements and the hydrocarbon corona with SANS. The I(Q) vs. Q data for the extraction of Tb^{3+} into organic phases containing TBP and HDBP at varying ratios and the respective dry organic phases are shown in Figure 30.

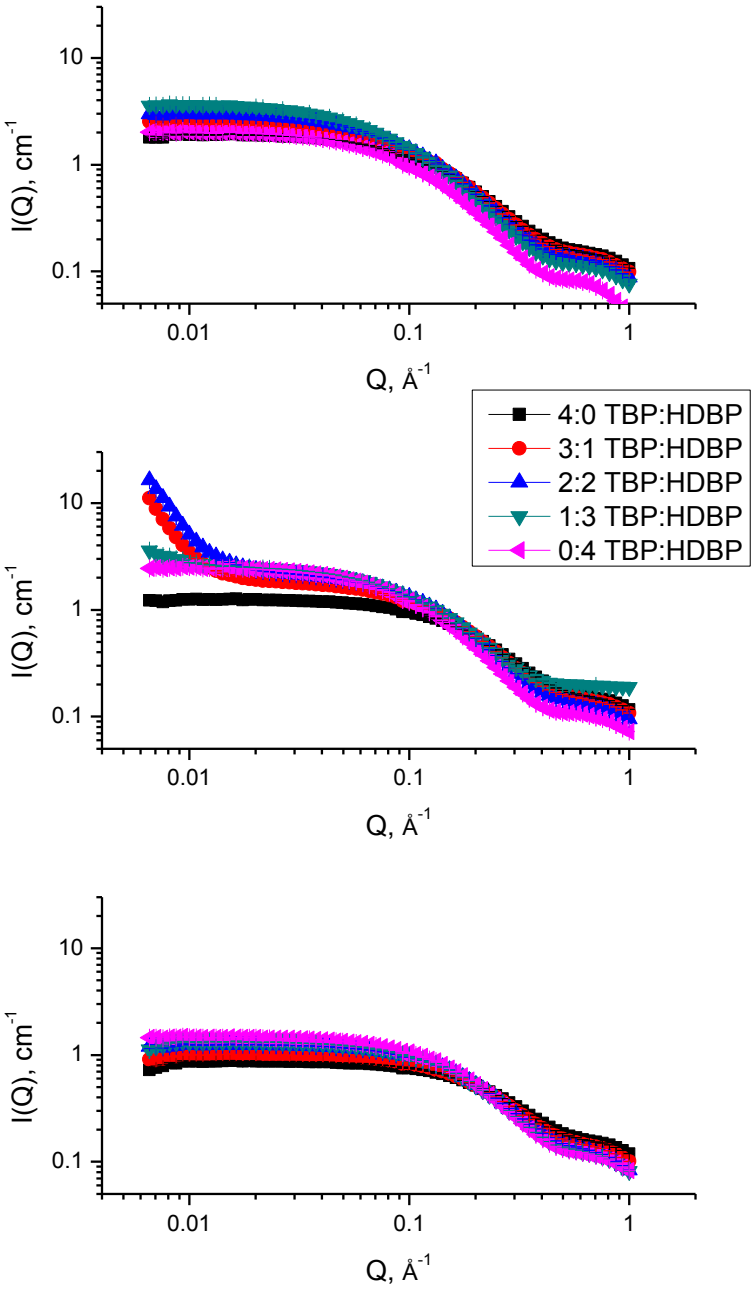

Figure 30: Log-log plot of the SANS data for the extraction of Tb into organic phases of varying TBP and HDBP ratio from 2 M DNO_3 (top) and 0.2 M DNO_3 (middle). The dry organic phase scattering behavior is shown bottom.

The SANS response for the dry organic phase yield identical results to that of the SAXS data, namely that the scattering increases with increasing HDBP concentration. After contact with an

aqueous phase, however, we observe a shift in the intensities and a reordering of the scattering curves with the 0.25 M TBP and 0.75 M HDBP organic phase yielding the highest scattering for both 2 M and 0.2 M DNO_3 extraction a Q of 0.025 and 0.1 Å. It is important to note though that this trend does not hold true outside of this range for either aqueous contact. For the 0.2 M DNO_3 contact, we see a ski slope type of response for the 3:1 and 2:2 TBP:HDBP organic phase concentrations which is indicative of the existence of larger structures present in the organic phase. Unfortunately, we were unable to probe sufficiently low Q with this particular SANS instrument to investigate these structures further.

In addition to the study with TBP and HDBP in *n*-dodecane-d26, we investigated how the organic phase structures change with respect to HDBP by utilizing deuterated TBP. The I(Q) vs. Q data for the extraction of Tb^{3+} into organic phases containing HDBP and deuterated TBP at varying ratios and the respective dry organic phases are shown in Figure 31. Once again, we observe that the scattering increases with increasing HDBP concentration uniformly in the dry organic phases. After contact with an aqueous phase, we again observe a ski slope type feature at low Q for the extraction of Tb from 0.2 M DNO_3 for the 3:1, 2:2, and now 1:3 TBP:HDBP concentrations indicating that there are larger assemblies present in the organic phase than we are able to probe with our current Q range. Additionally, we observe a similar ski slope feature at low Q in the 3:1 TBP:HDBP concentration during the extraction of Tb from 2 M DNO_3.

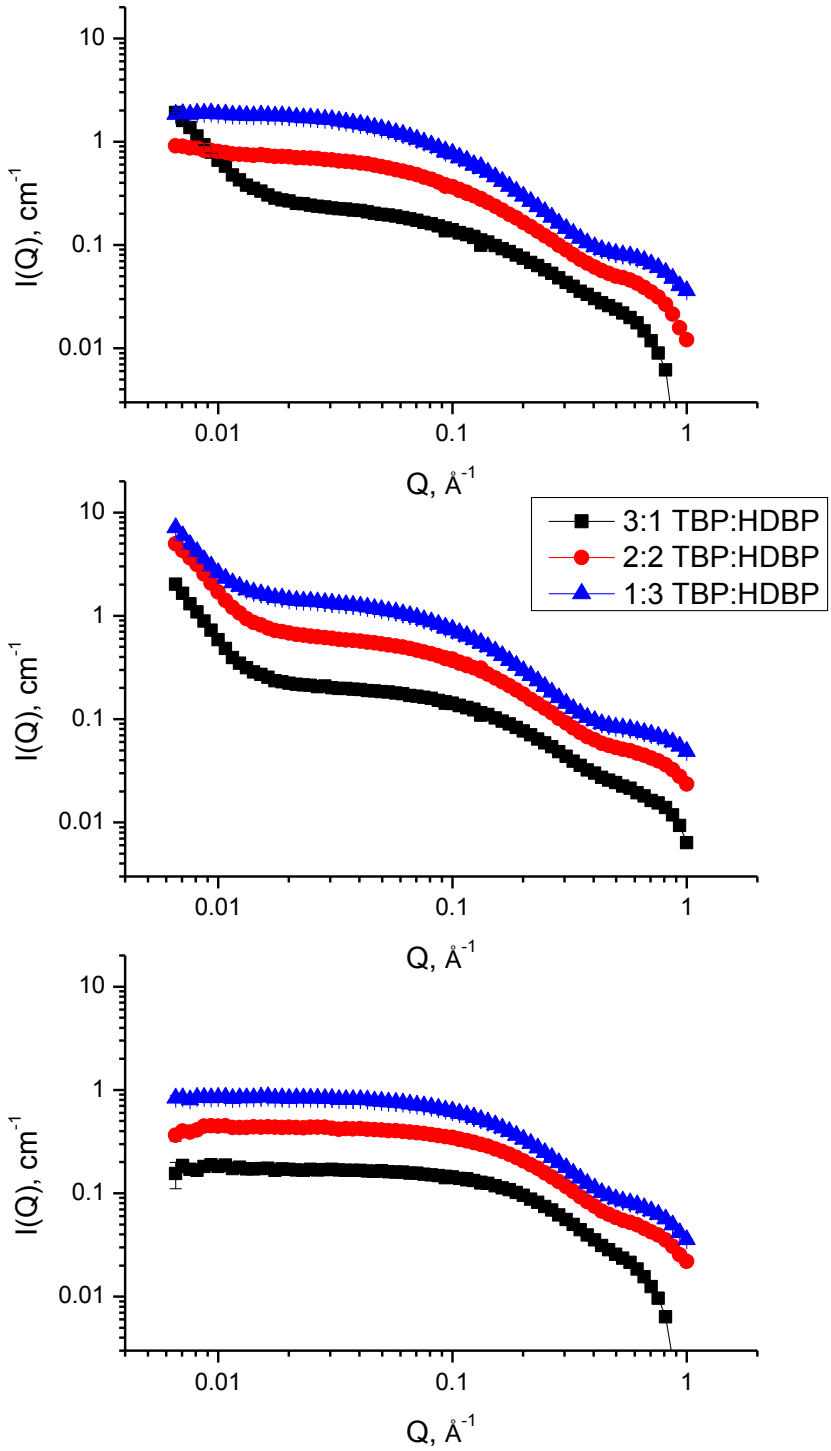

Figure 31: Log-log plot of the SANS data for the extraction of Tb into organic phases of varying HDBP and deuterated TBP ratio from 2 M DNO_3 (top) and 0.2 M DNO_3 (middle). The dry organic phase scattering behavior is shown bottom.

4.5 SANS Discussion

Information about the aggregates formed upon extraction of Tbcan be provided in terms of R_g and I(0) values, which are plotted as a function of the mixing ratio of the extractants, as shown in Figure 32.

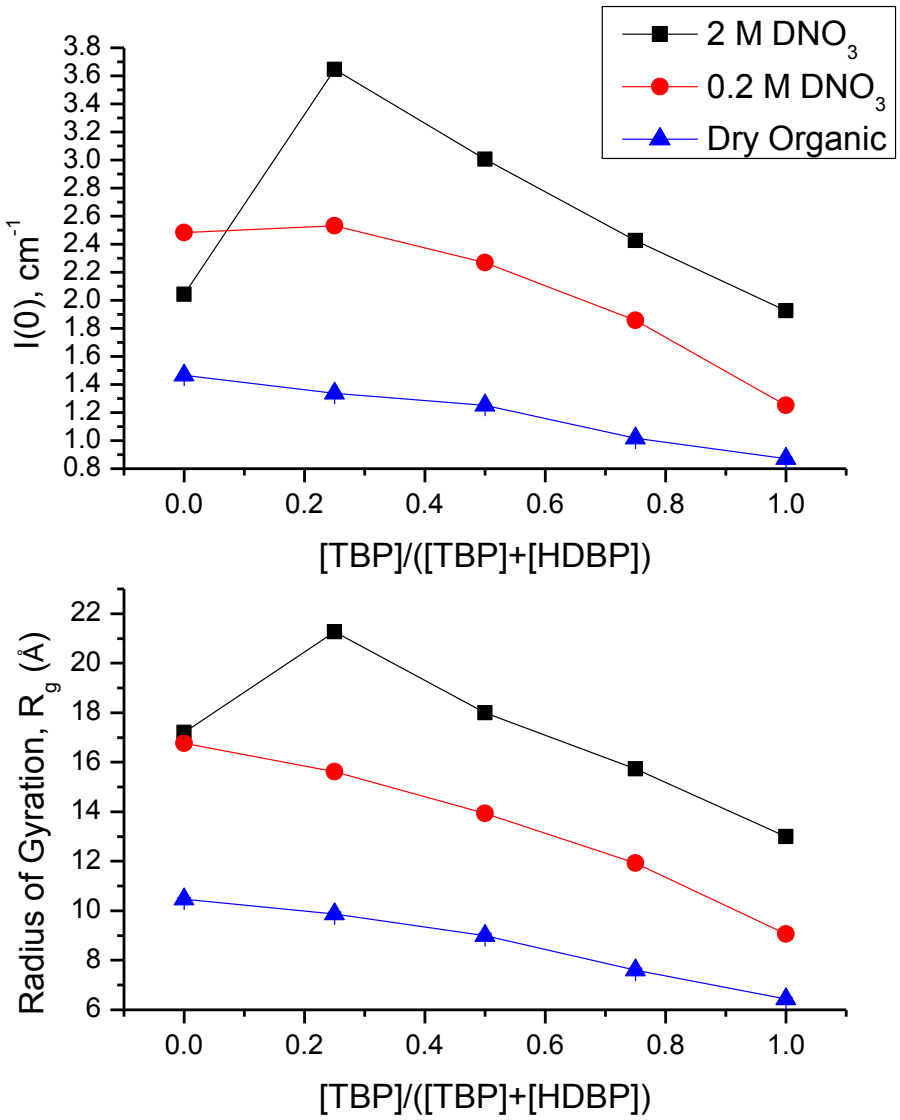

Figure 32: I(0) (top) and R_g (bottom) calculated from the entire scattering curves for the organic phases containing varying ratios of TBP and HDBP with constant 1 M extractant concentrations after contact with 0.2 M DNO_3 and 2 M DNO_3containing 10^{-3} M Tb. Dry organic phases are shown with blue triangles.

Similarly to the I(0) calculated from the SAXS data, the I(0) for the dry organic phases show a linear trend that increases with increasing HDBP concentration. Post contact with an aqueous

phase, however, the trend in I(0) changes so that there are definitive peaks after contract with 2 M DNO_3 which indicates that the mixed systems form large micelles, with a different aggregated structure than the end members, or that the structure factor S(Q) has changed across the series.

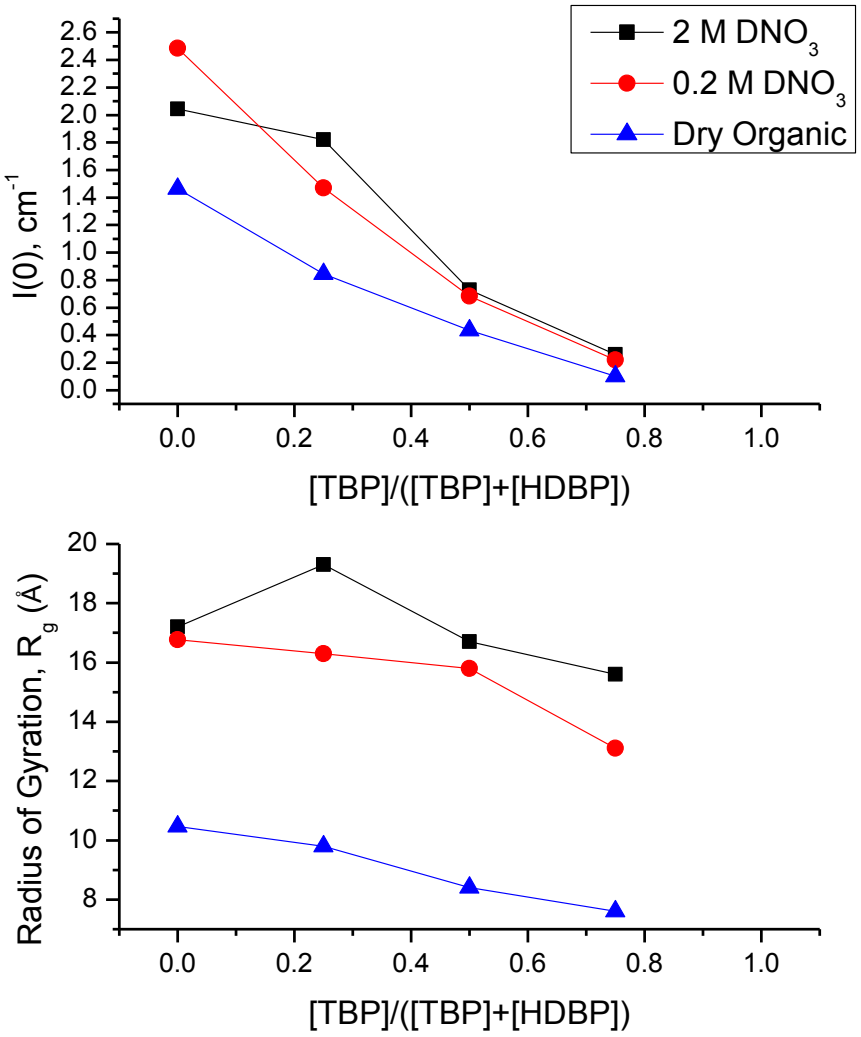

Figure 33: I(0) (top) and R_g (bottom) calculated from the entire scattering curves for the organic phases containing varying ratios of HDBP and deuterated TBP with constant 1 M extractant concentrations after contact with 0.2 M DNO_3 and 2 M DNO_3. Dry organic phases are shown with blue triangles.

It is important to note though that the organic phases contacted with 0.2 M DNO_3 do not show the same peak that the SAXS calculated I(0) values do and that the peak in the 2 M DNO_3 has shifted to a maximum at 0.25 M TBP rather than the 0.5 M TBP as seen with the SAXS

calculated values.This is most likely due to the differences in contrast mechanisms between neutrons and X-rays. Turning to the Radius of Gyration data, a similar trend to the I(0) data can be observed, namely that the dry organic phases show a linear increase with increasing HDBP concentration and a definitive peak present after contact with 2 M DNO_3.Looking now at the I(0) and R_g values obtained after deuterating one of the extractants, shown in Figure 33, we see a much more linear trend increasing with increasing HDBP concentration. Additionally, we observe slightly decreased values in R_g and I(0) indicating that the structures present in the organic phase include both TBP and HDBP in them which is expected in these binary extractant systems.

Additional structural information regarding the aggregates formed by extraction can be obtained from the p(r) functions. The p(r) functions obtained by using the ScÅtter software package developed at the SIBYLS beamline of the Advanced Light Source in Berkeley, CA are shown in Figure 34.[107]The extended, tail like decay of the p(r) functions observed previously with the GIFT treatment of the SAXS data are not observed with the ScÅtter treatment of the SANS data. This is mostly likely due to structure factor interference often present in concentrated solvent extraction systems. Additionally, the second peaks observed in the SAXS data does not appear in the p(r) functions calculated from the SANS data. The shape of the p(r) functions indicates a globular nature of the aggregates formed upon extraction, though without the proper subtraction of the structure factor the p(r) functions shown here may be inaccurate. It is also important to note that the data in Figure 34 is normalized to the same peak height.

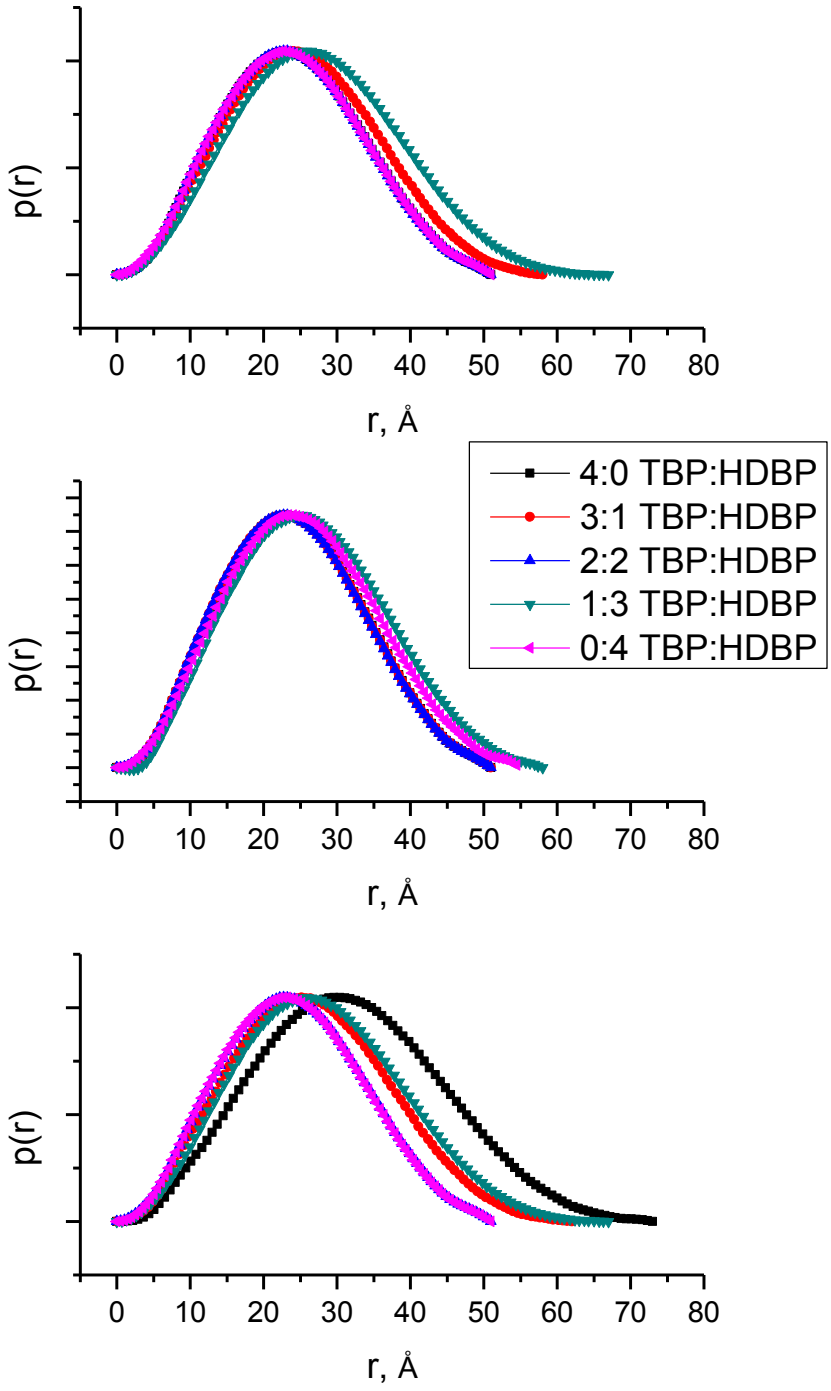

Figure 34: P(r) functions for the extraction of Tb from 2 M DNO_3 (top), 0.2 M DNO_3 (middle), and the corresponding dry organic phases (bottom).

4.6 Note on DLS

In an effort to probe larger aggregates structures, Dynamic light scattering (DLS) was investigated. Extraction experiments were carried out identically to the SAXS experiments and the organic phases were analyzed with a Malvern Zetasizer ZS Nano DLS for polydispersity and size distribution at 25° C and ambient pressures. The organic phases were loaded into quartz fluorescence cuvettes but it was noticed that a cloudy film coated the interior of the quartz as soon as the organic phase was added. The clouding observed on the walls of the cuvettes was most likely due to third phase formation and after sufficient time to allow for temperature equilibration the cloudiness dissipated in some samples and the samples could then be measured. Unfortunately, the samples where the cloudiness did not dissipate indicated too high a degree of polydispersity rendering the samples unfit for DLS measurements. Instead, use of an ultra small angle scattering method such as USAXS or USANS may yield information on larger aggregate structures in these solvent extraction systems.

4.7 Conclusions

The SAXS and SANS investigation of the TBP:HDBP extraction system sheds light on the shape and size of large macromolecular aggregates from two differing perspectives. The SAXS data indicates that there may be a link between the size of the reverse micelles and synergy for the 0.2 M HNO_3 extraction while for 2 M HNO_3 there does not seem to exist such a link and the size of the aggregates seems to only correlate with water content of the organic phases. The SANS data seems to indicate a more globular type system, as opposed to the elongated rod like aggregates shown with SAXS, though the current treatment of this data is not sufficient without the removal of the structure factor interference often present in such concentrated systems.

Chapter 5: Conclusions

Solvent extraction systems are highly complex and involve interactions on the atomic, molecular, and supramolecular scales that profoundly influence the delicate balance of energetic that underpin metal extraction. In term of the physicochemical properties on the TBP and HDBP extraction system, we observe a nonlinear trend in the extraction of trivalent lanthanides from 0.2 M HNO_3 solutions which indicates there may be some sort of interaction between the extractants and the existence of a slight synergistic extraction in this system. The extraction from 2 M HNO_3 however shows a much more linear trend that is typically expected in an extraction system where extractant interactions are not present. An interesting observation discovered during this work is that the distribution of metal ions into the organic phase does not seem to deviate with metal ion concentration which indicates that below the onset of third phase the extraction is independent of metal concentration. In view of the water uptake into the organic phase, a clear synergistic trend is observed with contacted with a 0.2 M HNO_3 phase while a more linear trend is observed when contacted with a 2 M HNO_3 aqueous phase. The stark contracts between the precontacted, i.e. dry, and postcontacted organic phases, however, suggests the presence of reverse micelles in the organic phase and coupled with the nonlinear trends observed in the extraction of trivalent lanthanides may indicate some correlation between the existence of micelles and synergic extraction.

In an effort to probe the potential link between reverse micelles and synergy, we turned to several techniques that would shed light on the complexes formed upon extraction. Extended X-ray absorption fine structure (EXAFS) was employed to determine the coordination environment around the metal ions and it was determined that there are 6 oxygen atoms about the central metal ion and between 4-6 phosphorus atoms in the second shell. Coupling this find with the

hydration numbers determined by Time Resolved Fluorescence allows us to determine that the most probable source of the oxygen atoms is the extractants and not the water or nitrate ions for all organic phases containing HDBP. The oxygen atoms for the complexes formed in the organic phases that contain 1 M TBP alone, however, are most likely due to the extractant molecules and the nitrate ions, either bound bidentate or monodentate. With the complexes formed in organic phase characterized, it may be quite possible that we are observing some sort of dinuclear species or complexes that may exist inside of some sort of macromolecular structure such as the reverse micelles present in this system.

To investigate the nature of the reverse micelles formed in the TBP:HDBP extraction system, we now turn to small angle X-ray and neutron scattering to determine the size and shape of the micelles formed. The SAXS data indicates that there may be a link between the size of the reverse micelles and synergy for the 0.2 M HNO_3 extraction while for 2 M HNO_3 there does not seem to exist such a link and the size of the aggregates formed seems to only correlate with the water uptake into the organic phase. The SANS data seems to indicate a more globular type of system of core-shell type geometry, as opposed to the elongated rod like aggregates shown with the SAXS investigation, though the current treatment of this data is not sufficient without the removal of the structure factor interference often present in such concentrated systems. It is also important to note that SANS and SAXS have differing contrast mechanisms, namely that for neutron scattering the contrast between the deuterated diluent and the extractant H atoms in the oleophilic corona of the reverse micelles is being probed, whereas for SAXS all of the contrast is from the phosphate head groups, acid, metal, and water in the hydrophilic core of the reverse micelles.

Chapter 6: Future Work

Though the TBP:HDBP binary extractant system has been probed extensively throughout the life of this study, there are several experiments and analysis techniques that can be conducted to yield additional information on the nature of this extraction system. The first and most pressing of which is conducting a model dependent analysis on the SANS data collected at Oak Ridge National Lab and the removal of structure factor interference from the p(r) calculations.The SANS data collected can be further analyzed with SASFit to conduct model dependent fits to determine core volume and radius as well as some other interesting parameters. To conduct the model dependent fit, SASFit will be used on all of the data collected at GP-SANS. Preliminary fits of the data indicate all the data can be fit adequately with a spherical core-shell type geometry. Additionally, the GIFT analysis that was conducted on the SAXS data may also be conducted on the SANS data to remove the structure factor from the calculation for the p(r) functions and will allow us to probe the shape and size of the reverse micelles in the organic phase without interparticle interferences. It would also be useful to conduct USANS (Ultra Small-Angle Neutron Scattering) experiments to obtain information regarding the structures formed at very low Q since the SANS data collected so far does indicate the presence of features in the I(Q) vs. Q data that continue into much lower Q that we were unable to probe with the GP-SANS instrumental capabilities.

As an additional investigative method of the TBP:HDBP extraction system, NMR could prove useful in investigating the aggregate structures and the presence of the metal ion within them. The use of advanced NMR techniques such as diffusion ordered NMR spectroscopy (DOSY) may allow us to utilize the difference in mobility and diffusion rate between different size molecules to study the aggregates more closely and overall how they form. Additionally, the

methods and procedures carried out in this thesis may be applied to other synergistic solvent extraction pairs to further elucidate the link between synergy and aggregate formation in other synergistic systems that also are shown to form reverse micellar structures.

References

1. Choppin, G. R.; Liljenzin, J. O.; Rydberg, J. *Radiochemistry and Nuclear Chemistry*; 3rd ed.; Butterworth-Heinemann, 2002.

2. *Nuclear Technology Review*, International Atomic Energy Agency, 2012.

3. *Blue Ribbon Commission on America's Nuclear Future*, 2012.

4. *Report of the American Nuclear Society President's special committee on used nuclear fuel management options*, American Nuclear Society, 2011.

5. Lanham, W. B.; Runion, T. C.; Oak Ridge National Laboratory: Oak Ridge, TN, 1949.

6. Herbst, R. S.; Baron, P.; Nilsson, M. In *Advanced Separation Techniques for Nuclear Fuel Reprocessing and Radioactive Waste Treatment*; Nash, K. L., Lumetta, G. J., Eds.; Woodhead Publishing: Philadelphia, PA, 2011, p 141-73.

7. *Spent Nuclear Fuel Management: Outreach Needed to Help Gain Public Acceptance for Federal Activities That Address Liability*, United States Government Accountability Office, 2014.

8. Blass, E. Solvent Extraction - A Historical Review, *Value Adding through Solvent Extraction***1996**, *1*, 3-10.

9. Grodowska, K.; Parczewski, A. Organic solvents in the pharmaceutical industry, *Acta Poloniae Pharmaceutica***2010**, *67*, 3-12.

10. Bernardis, F. L.; Grant, R. A.; Sherrington, D. C. A review of methods of separation of the platinum-group metals through their chloro-complexes, *Reactive and Functional Polymers***2005**, *65*, 205-17.

11. Tasker, P. A.; Plieger, P. G.; West, L. C. In *Comprehensive Coordination Chemistry II*; McCleverty, J. A., Meyer, T. J., Eds.; Elsevier Ltd.: Oxford, UK, 2004; Vol. 9, p 759-808.

12. Bautista, R. G. *Handbook on the Physics and Chemistry of Rare Earths*; North-Holland: Amsterdam, The Netherlands, 1995; Vol. 21.

13. Musikas, C.; Schulz, W. W.; Liljenzin, J. O. *Solvent Extraction Principles and Practice*; 2nd ed.; Mercel Dekker, Inc.: New York, 2004.

14. Warf, J. C. Extraction of Cerium(IV) Nitrate by Butyl Phosphate, *J. Am. Chem. Soc.***1949**, *71*, 3257-8.

15. Peppard, D. F.; Faris, J. P.; Gray, P. R.; Mason, G. W. Studies of the Solvent Extraction Behavior of the Transitions Elements. I. Order and Degree of Fractionation of the Trivalent Rare Earths, *J. Phys. Chem.***1953**, *57*, 294-301.

16. Peppard, D. F.; Gray, P. R.; Markus, M. M. The Actinide-Lanthanide Analogy as Exemplified by Solvent Extraction Behavior, *J. Am. Chem. Soc.***1953**, *75*, 6063-4.

17. Benedict, M.; Pigford, T. H.; Levi, H. W. In *Nuclear Chemical Engineering*; 2nd ed.; McGraw Hill: New York, 1981, p 457-564.

18. Marcus, Y.; Kertes, A. S. *Ion Exchange and Solvent Extraction of Metal Complexes*; Wiley-Interscience: London, UK, 1969.

19. Burger, L. L. The Neutral Organophosphorus Compounds as Extractants, *Nuclear Science and Engineering***1963**, *16*, 428-39.

20. Irving, H.; Edgington, D. N. Synergic effects in the solvent extraction of the actinides. I. Uranium(VI), *Journal of Inorganic Nuclear Chemistry***1960**, *15*, 158-70.

21. Mincher, B. J.; Modolo, G.; Mezyk, S. P. Review Article: The Effects of Radiation Chemistry on Solvent Extraction: 1. Conditions in Acidic Solution and a Review of TBP Radiolysis, *Solvent Extraction and Ion Exchange***2009**, *27*, 1-25.

22. Irving, H. M. N. H. In *Solvent Extraction Chemistry*; Dyrssen, D., Liljenzin, J.-O., Rydberg, J., Eds.; John Wiley & Sons, Inc.: New York, 1967, p 91-110.

23. Hardy, C. J. Alkylphosphoric Acids and Their Complexes with Metals, *Nuclear Science and Engineering***1963**, *16*, 401-4.

24. May, I.; Taylor, R. J.; Wallwork, A. L.; Hastings, J. J.; Fedorov, Y. S.; Zilberman, B. Y.; Mishin, E. N.; Arkhipov, S. A.; Blazheva, I. V.; Poverkova, L. Y.; Livens, F. R.; Charnock, J. M. The influence of HDBP on actinide extraction by 30% tributylphosphate, *Radiochemica Acta***2000**, *88*, 283-90.

25. Zangen, M. Some aspects of synergism in solvent extraction. II. Some di-, tri- and tetravalent metal ions, *Journal of Inorganic Nuclear Chemistry***1963**, *25*, 1051-63.

26. Hahn, H. T.; Vander Wall, E. M. Complex formation in the dilute uranyl nitrate-nitric acid-dibutyl phosphoric acid-tributyl phosphate-amsco system, *Journal of Inorganic Nuclear Chemistry***1964**, *26*, 191-202.

27. *Principles and Practices of Solvent Extraction*; Marcel Dekker, Inc.: New York, 1992.

28. Osseo-Asare, K. Enhanced Solvent Extraction with Water-in-Oil Microemulsions, *Sep. Sci. Technol.***1988**, *23*, 1269-84.

29. Osseo-Asare, K. Aggregation, reversed micelles and microemulsions in liquid liquid extraction: The tri-n-butyl phosphate-diluent-water-electrolyte system, *Adv. Colloid Interface Sci.***1991**, *37*, 123-73.

30. Dourdain, S.; Hofmeister, I.; Pecheur, O.; Dufreche, J. F.; Turgis, R.; Leydier, A.; Jestin, J.; Testard, F.; Pellet-Rostaing, S.; Zemb, T. Synergism by coassembly at the origin of ion selectivity in liquid-liquid extraction, *Langmuir : the ACS journal of surfaces and colloids***2012**, *28*, 11319-28.

31. Alcock, K.; Grimley, S. S.; Healy, T. V.; Kennedy, J.; McKay, H. A. C. The extraction of nitrates by tri-n-butyl phosphate (TBP). Part 1.?The system TBP + Diluent + H2O+HNO3, *Transactions of the Faraday Society***1956**, *52*, 39.

32. Antonio, M. R.; Chiarizia, R.; Jaffrennou, F. Third-Phase Formation in the Extraction of Phosphotungstic Acid by TBP inn-Octane, *Separation Science and Technology***2010**, *45*, 1689-98.

33. Chiarizia, R.; Briand, A. Third Phase Formation in the Extraction of Inorganic Acids by TBP inn-Octane, *Solvent Extraction and Ion Exchange***2007**, *25*, 351-71.

34. Chiarizia, R.; Jensen, M. P.; Borkowski, M.; Ferraro, J. R.; Thiyagarajan, P.; Littrell, K. C. Third phase formation revisited: The U(VI), HNO_3-TBP, *n*-dodecane system, *Solvent Extr. Ion Exch.***2003**, *21*, 1-27.

35. Nave, S.; Mandin, C.; Martinet, L.; Berthon, L.; Testard, F.; Madic, C.; Zemb, T. Supramolecular organisation of tri-n-butyl phosphate in organic diluent on approaching third phase transition, *Physical chemistry chemical physics : PCCP***2004**, *6*, 799-808.

36. Chiarizia, R.; Rickert, P. G.; Stepinski, D.; Thiyagarajan, P.; Littrell, K. C. SANS Study of Third Phase Formation in the HCl-TBP-n-Octane System, *Solvent Extraction and Ion Exchange***2006**, *24*, 125-48.

37. Chiarizia, R.; Stepinski, D.; Antonio, M. R. SANS Study of HCl Extraction by Selected Neutral Organophosphorus Compounds inn-Octane, *Separation Science and Technology***2010**, *45*, 1668-78.

38. Lumetta, G. J.; Gelis, A. V.; Vandegrift, G. F. Review: Solvent Systems Combining Neutral and Acidic Extractants for Separating Trivalent Lanthanides from the Transuranic Elements, *Solvent Extraction and Ion Exchange***2010**, *28*, 287-312.

39. Gannaz, B.; Chiarizia, R.; Antonio, M. R.; Hill, C.; Cote, G. Extraction of Lanthanides(III) and Am(III) by Mixtures of Malonamide and Dialkylphosphoric Acid, *Solvent Extraction and Ion Exchange***2007**, *25*, 313-37.

40. Dhami, P. S.; Chitnis, R. R.; Gopalakrishnan, V.; Wattal, P. K.; Ramanujam, A.; Bauri, A. K. Studies on the Partitioning of Actinides from High Level Waste Using a Mixture of Hdehp and Cmpo as Extractant, *Separation Science and Technology***2001**, *36*, 325-35.

41. Hagström, I.; Spjuth, L.; Enarsson, Å.; Liljenzin, J. O.; Skålberg, M.; Hudson, M. J.; Iveson, P. B.; Madic, C.; Cordier, P. Y.; Hill, C.; Francois, N. Synergistic Solvent Extraction of Trivalent Americium and Europium by 2-Bromodecanoic Acid and Neutral Nitrogen-Containing Reagents, *Solvent Extraction and Ion Exchange***1999**, *17*, 221-42.

42. Partridge, J. A.; Jensen, R. C. Purification of Di-(2-ethylhexyl)Phosphoric Acid by Precipitation of Copper(II) Di-(2-ethylhexyl)phosphate, *Journal of Inorganic Nuclear Chemistry***1969**, *32*, 2587-9.

43. Braatz, A. D.; Ellis, R. J.; Antonio, M. R.; Nilsson, M. In *Global 2013* Salt Lake City, Utah, 2013, p 1490-4.

44. Moeller, T. *The Chemistry of the Lanthanides*; Reinhold Publishing Corporation: New York, 1963.

45. Anderson, T. L.; Braatz, A.; Ellis, R. J.; Antonio, M. R.; Nilsson, M. Synergistic Extraction of Dysprosium and Aggregate Formation in Solvent Extraction Systems Combining TBP and HDBP, *Solvent Extraction and Ion Exchange***2013**, *31*, 617-33.

46. du Preez, J. G. H.; Sumter, N. M.; Viviers, C.; Rohwer, H. E.; van Brecht, B. J. A. M. Coordination Chemistry and the Developement of Metal Ion Specific Separating Agents, *Emerging Separation Technologies for Metals II, Proceedings of a Symposium, Kona, Hawaii, June 16-21, 1996***1996**, 265-78.

47. Svantesson, I.; Persson, G.; Hagström, I.; Liljenzin, J. O. Distribution Ratios and Empirical Equations for the Extraction of Elements in PUREX High Level Waste Solution - II: HDEHP, *J. Inorg. Nucl. Chem***1980**, *42*, 1037-43.

48. Trifonov, Y. I.; Tutov, A. G.; Legin, E. K.; Suglobov, D. N. Structure of Rare Earth Di-2-ethylhexyl phosphates, *Radiokhimiya***1991**, *33*, 63-9.

49. Trifonov, Y. I.; Legin, E. K.; Suglobov, D. N. Solvation and Phase Processes in Organic Solutions of Eu di-2-ethylhexylphosphate, *Radiokhimiya***1991**, *33*, 70-7.

50. Suglobov, D. N.; Trifonov, Y. I.; Legin, E. K.; Tutov, A. G. DEHP complexes of lanthanides(III) and actinides(III), *Journal of Alloys and Compounds***1994**, *213/214*, 523-7.

51. Tomita, A.; Kanki, T.; Asano, T.; Sano, N. Formation of crystal film at interface in processes of extraction of rare earth metals by D2EHPA, *Journal of Chemical Engineering of Japan***2000**, *33*, 661-4.

52. Naganawa, H.; Tachimori, S. Complex Formation between Tributyl Phosphate and Nitric Acid and the Hydration of the Complexes in Dodecane, *Chem. Soc. Jpn.***1997**, *70*, 809-19.

53. In *Science and Technology of Tributyl Phosphate*; Schulz, W. W., Navratil, J. D., Kertes, A. S., Eds.; CRC Press: Boston; Vol. IV, p 71-205.

54. Chaiko, D. J.; Vandegrift, G. F. A Thermodynamic model of nitric acid extraction by tri-n-butylphosphate, *Nucl. Technol.***1988**, *82*, 52-9.

55. Beno, M. A.; Engbretson, M.; Jennings, G.; Knapp, G. S.; Linton, J.; Kurtz, C.; Rutt, U.; Montano, P. A. BESSRC-CAT Bending Magnet Beamline at the Advanced Photon Source, *Nuclear Instruments & Methods in Physics Research, Section A***2001**, *467-468*, 699-702.

56. George, G. N., EXAFSPAK, **2001**

57. Ravel, B.; Newville, M. ATHENA, ARTEMIS, HEPHAESTUS: data analysis for X-ray absorption spectroscopy using IFEFFIT, *Journal of Synchrotron Radiation***2005**, *12*, 537.41.

58. Rehr, J. J.; Albers, R. C. Theoretical approaches to x-ray absorption fine structure, *Reviews of Modern Physics***2000**, *72*, 621-54.

59. Stern, E. A. Number of relevant independent points in x-ray-absorption fine-structure spectra, *Physical Review B***1993**, *48*, 9825-7.

60. Lukens, W. W.; Bucher, J. J.; Shuh, D. K.; Edelstein, N. M. Evolution of Technetium Speciation in Reducing Grout, *Environ. Sci. Technol.***2005**, *39*, 8064-70.

61. Ressler, T., WinXAS, **2013**

62. Rohler, J. In *Handbook on the Physics and Chemistry of Rare Earths*; Gschneidner, K. A., Eyring, L., Hufner, S., Eds.; Elsevier Science Publishers B.V.: Amsterdam, 1987; Vol. 10, p 453-545.

63. Healy, T. V.; McKay, H. A. C. The extraction of nitrates by tri-n-butyl phosphate (TBP). Part 2.?The nature of the TBP phase, *Transactions of the Faraday Society***1956**, *52*, 633.

64. Hesford, E.; McKay, H. A. C. The Extraction of Nitrates by Tri-n-Butyl Phosphate (TBP) Part 3. Extraction at Trace Concentrations, *Transactions of the Faraday Society***1958**, *54*, 573-86.

65. Gannaz, B.; Antonio, M. R.; Chiarizia, R.; Hill, C.; Cote, G. Structural study of trivalent lanthanide and actinide complexes formed upon solvent extraction, *Dalton transactions***2006**, 4553-62.

66. Antico, E.; Masana, A.; Hidalgo, M.; Salvado, V.; Iglesias, M.; Valiente, M. Solvent extraction of yttrium from chloride media by di(2-ethylhexyl)phosphoric acid in kerosene. Speciation studies and gel formation, *Analytica Chemica Acta***1996**, *327*, 267-76.

67. Shannon, R. D. Revised effective ionic radii and systematic studies of interatomic distances in Halides and Chalcogenides, *Acta Crystallography***1976**, *32*, 751-67.

68. Jensen, M. P.; Bond, H. Influence of aggregation on the extraction of trivalent lanthanide and actinide cations by purified Cyanex 272, Cyanex 301, and Cyanex 302, *Radiochimica Acta***2002**, *90*, 205-9.

69. Cocalia, V. A.; Jensen, M. P.; Holbrey, J. D.; Spear, S. K.; Stepinski, D. C.; Rogers, R. D. Identical extraction behavior and coordination of trivalent or hexavalent f-element cations using ionic liquid and molecular solvents, *Dalton transactions***2005**, 1966-71.

70. Antonio, M. R.; Soderholm, L. In *The Chemistry of the Actinide and Transactinide Elements*; 4 ed.; Morss, L. R., Edelstein, N. M., Fuger, J., Eds.; Springer: 2010, p 3086-198.

71. Jensen, M. P.; Chiarizia, R.; Urban, V. Investigation of the Aggregation of the Neodymium Complexes of Dialkylphosphoric, -oxothiophosphinic, and -dithiophosphinic acids in tluene, *Solvent Extr. Ion Exch.***2001**, *19*, 865-84.

72. Roehler, J. In *Handbook on the Physics and Chemistry of Rare Earths*; Gschneidner, K. A., Eyring, L., Huefner, S., Eds.; North-Holland: Amsterdam, 1987; Vol. 10, p 453-545.

73. Krause, M. O.; Oliver, J. H. Natural Widths of Atomic K and L Levels, K_{alpha} X-Ray Lines and Several KLL Auger Lines, *J. Phys. Chem. Ref. Data***1979**, *8*, 329-38.

74. Antonio, M. R.; Soderholm, L.; Ellison, A. J. G. Local environments of erbium and lutetium in sodium silicate glasses, *Journal of Alloys and Compounds***1997**, *250*, 536-40.

75. Skanthakumar, S.; Gorman-Lewis, D.; Locock, A.; Chiang, M.-H.; Jensen, M. P.; Burns, P. C.; Fein, J.; Jonah, C. D.; Attenkofer, K.; Soderholm, L. In *Materials Reserach Society Symposium Proceedings* Boston, Massachusetts, 2003; Vol. 802.

76. Miyake, C.; Ichinose, N.; Sakamoto, J. In *The Third International Conference on Nuclear Fuel Reprocessing and Waste Management* Sendai, Japan, 1991; Vol. II.

77. Zhang, P.; Kimura, T. Complexation of Eu(III) with Dibutyl Phosphate and Tributyl Phosphate, *Solvent Extraction and Ion Exchange***2006**, *24*, 149-63.

78. Kimura, T.; Kato, Y. Luminescence study on determination of the hydration number of Sm(III) and Dy(III), *Journal of Alloys and Compounds***1995**, *225*, 284-7.

79. Horrocks, W. D.; Sudnick, D. R. Lanthanide Ion Probes of Structure in Biology. Laser-Induced Luminescence Decay Constants Provide a Direct Measure of the Number of Metal-Coordinated Water Molecules, *J. Am. Chem. Soc.***1979**, *101*, 334-40.

80. *Small Angle X-ray Scattering*; Academic Press: New York, 1982.

81. Guinier, A.; Fournet, G. *Small-Angle Scattering of X-rays*; Wiley: New York, 1955.

82. Putnam, C. D.; Hammel, M.; Hura, G. L.; Tainer, J. A. X-ray solution scattering (SAXS) combined with crystallography and computation: defining accurate macromolecular structures, conformations and assemblies in solution, *Quarterly reviews of biophysics***2007**, *40*, 191-285.

83. Ilavsky, J.; Jemian, P. R. Irena: tool suite for modeling and analysis of small-angle scattering, *J. Appl. Cryst.***2009**, *42*, 347-53.

84. *Neutrons, X-rays and Light: Acattering Methods Applied to Soft Condensed Matter*; Elsevier, 2002.

85. Brunner-Popela, J.; Mittelbach, R.; Strey, R.; Schubert, K. V.; Kaler, E. W.; Glatter, O. Small-angle scattering of interacting particles. III. D[sub 2]O-C[sub 12]E[sub 5] mixtures and microemulsions with n-octane, *The Journal of Chemical Physics***1999**, *110*, 10623.

86. Fritz, G.; Bergmann, A.; Glatter, O. Evaluation of small-angle scattering data of charged particles using the generalized indirect Fourier transformation technique, *The Journal of Chemical Physics***2000**, *113*, 9733.

87. Glatter, O.; Fritz, G.; Linder, H.; Brunner-Popela, J.; Mittelbach, R.; Strey, R.; Egelhaaf, S. U. Nonionic Micelles near the Critical Point: Micellar Growth and Attractive Interaction, *Langmuir : the ACS journal of surfaces and colloids***2000**, *16*, 8692-701.

88. Percus, J.; Yevick, G. Analysis of Classical Statistical Mechanics by Means of Collective Coordinates, *Physical Review***1958**, *110*, 1-13.

89. Antonio, M. R.; Chiarizia, R.; Gannaz, B.; Berthon, L.; Zorz, N.; Hill, C.; Cote, G. Aggregation in Solvent Extraction Systems Containing a Malonamide, a Dialkylphosphoric Acid and their Mixtures, *Separation Science and Technology***2008**, *43*, 2572-605.

90. Chiarizia, R.; Jensen, M. P.; Borkowski, M.; Ferraro, J. R.; Thiyagarajan, P.; Littrell, K. C. Sans Study Of Third Phase Formation In The U(vi)-hno3/tbp-n-dodecane System, *Separation Science and Technology***2003**, *38*, 3313-31.

91. Chiarizia, R.; Jensen, M. P.; Rickert, P. G.; Kolarik, Z.; Borkowski, M.; Thiyagarajan, P. Extraction of Zirconium Nitrate by TBP in n-Octane: Influence of Cation Type on Third

Phase Formation According to the "Sticky Spheres" Model, *Langmuir : the ACS journal of surfaces and colloids***2004**, *20*, 10798-808.

92. Chiarizia, R.; Briand, A.; Jensen, M. P.; Thiyagarajan, P. Sans Study of Reverse Micelles Formed upon the Extraction of Inorganic Acids by TBP inn-Octane, *Solvent Extraction and Ion Exchange***2008**, *26*, 333-59.

93. Barker, J. A. Perturbation Theory and Equation of State for Fluids. II. A Successful Theory of Liquids, *The Journal of Chemical Physics***1967**, *47*, 4714.

94. Fritz, G.; Glatter, O. Structure and interaction in dense colloidal systems: evaluation of scattering data by the generalized indirect Fourier transformation method, *Journal of Physics: Condensed Matter***2006**, *18*, S2403-S19.

95. Sharma, S. C.; Shrestha, R. G.; Shrestha, L. K.; Aramaki, K. Viscoelastic Wormlike Micelles in Mixed Nonionic Fluorocarbon Surfactants and Structural Transition Induced by Oils, *J. Phys. Chem. B***2009**, *113*, 1615-22.

96. Shrestha, L. K.; Shrestha, R. G.; Aramaki, K. Intrinsic parameters for the structure control of nonionic reverse micelles in styrene: SAXS and rheometry studies, *Langmuir : the ACS journal of surfaces and colloids***2011**, *27*, 5862-73.

97. Shrestha, L. K.; Yamamoto, M.; Arima, S.; Aramaki, K. Charge-free reverse wormlike micelles in nonaqueous media, *Langmuir : the ACS journal of surfaces and colloids***2011**, *27*, 2340-8.

98. Shrestha, L. K.; Sato, T.; Dulle, M.; Glatter, O.; Aramaki, K. Effect of Lipophilic Tail Architecture and Solvent Engineering on the Structure of Trehalose-Based Nonionic Surfactant Reverse Micelles, *J. Phys. Chem. B.***2010**, *114*, 12008-17.

99. Ellis, R. J.; Anderson, T. L.; Antonio, M. R.; Braatz, A.; Nilsson, M. A SAXS study of aggregation in the synergistic TBP-HDBP solvent extraction system, *The journal of physical chemistry. B***2013**, *117*, 5916-24.

100. Meridiano, Y.; Berthon, L.; Crozes, X.; Sorel, C.; Dannus, P.; Antonio, M. R.; Chiarizia, R.; Zemb, T. Aggregation in Organic Solutions of Malonamides: Consequences for Water Extraction, *Solvent Extraction and Ion Exchange***2009**, *27*, 607-37.

101. Beaucage, G. Small-Angle Scattering from Polymeric Mass Fractals of Arbitrary Mass-Fractal Dimension, *J. Appl. Cryst.***1996**, *29*, 134-46.

102. Beaucage, G.; Rane, S.; Sukumaran, S.; Satkowski, M. M.; Schechtman, L. A.; Doi, Y. Presistence Length of Isotactic Poly(hydroxy butyrate), *Macromolecules***1997**, *30*, 4158-62.

103. Beaucage, G. Approximations Leading to a Unified Exponential/Power-law Approach to Small-Angle Scattering, *J. Appl. Cryst.***1995**, *28*, 717-28.

104. Moore, P. B. Small-Angle Scattering. Information Content and Error Analysis, *J. Appl. Cryst.***1980**, *13*, 168-75.

105. Glatter, O. The Interpretation of Real-Space Information from Small-Angle Scattering Experiments, *J. Appl. Cryst.***1979**, *12*, 166-75.

106. Glatter, O.; Fritz, G.; Lindner, H.; Brunner-Popela, J.; Mittelbach, R.; Strey, R.; Egelhaaf, S. U. Nonionic Micelles near the Critical Point: Micellar Growth and Attractive Interaction†, *Langmuir : the ACS journal of surfaces and colloids***2000**, *16*, 8692-701.

107. Rambo, R., SCATTER, **2015**

Appendix

A1.

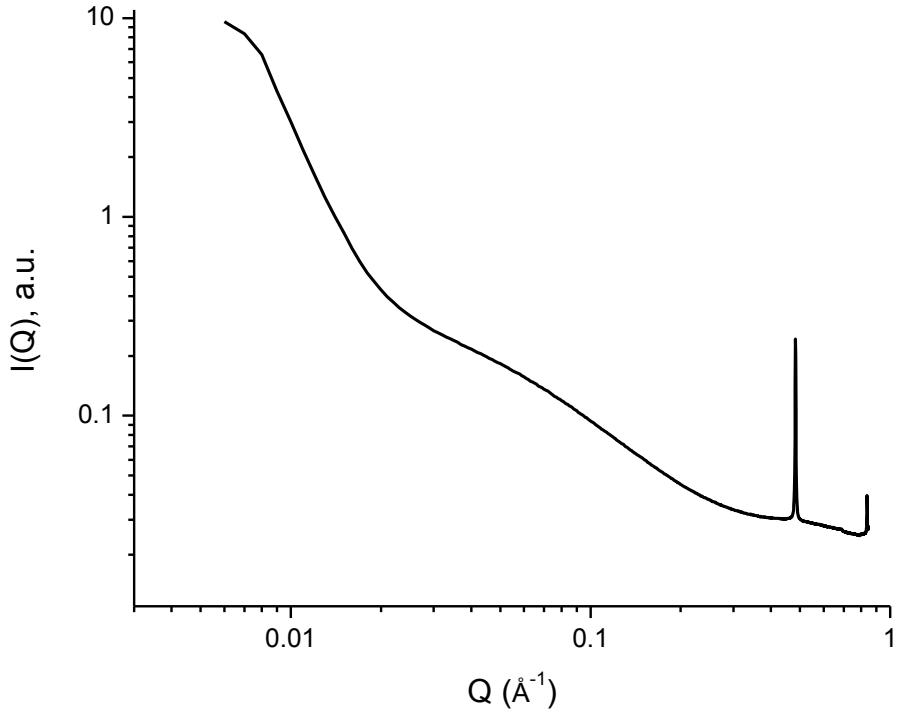

Appendix 1: I(Q) vs. Q data for 1.25 x 10^{-3} M Lu extractions into an organic phase that contains 0.5 M TBP and 0.5 M HDBP in *n*-dodecane. The distinctive peak in the graph is evidence of highly ordered and crystalline structures present in the organic phase. A photograph taken of the sample with an optical microscope showed the existence of small needle like crystals present in some of the organic phases contacted with Lu containing aqueous phases. All subsequent data for the extraction of Lu into organic phase is taken at 0.001 M concentration instead of 0.00125 M Lu.

A2.

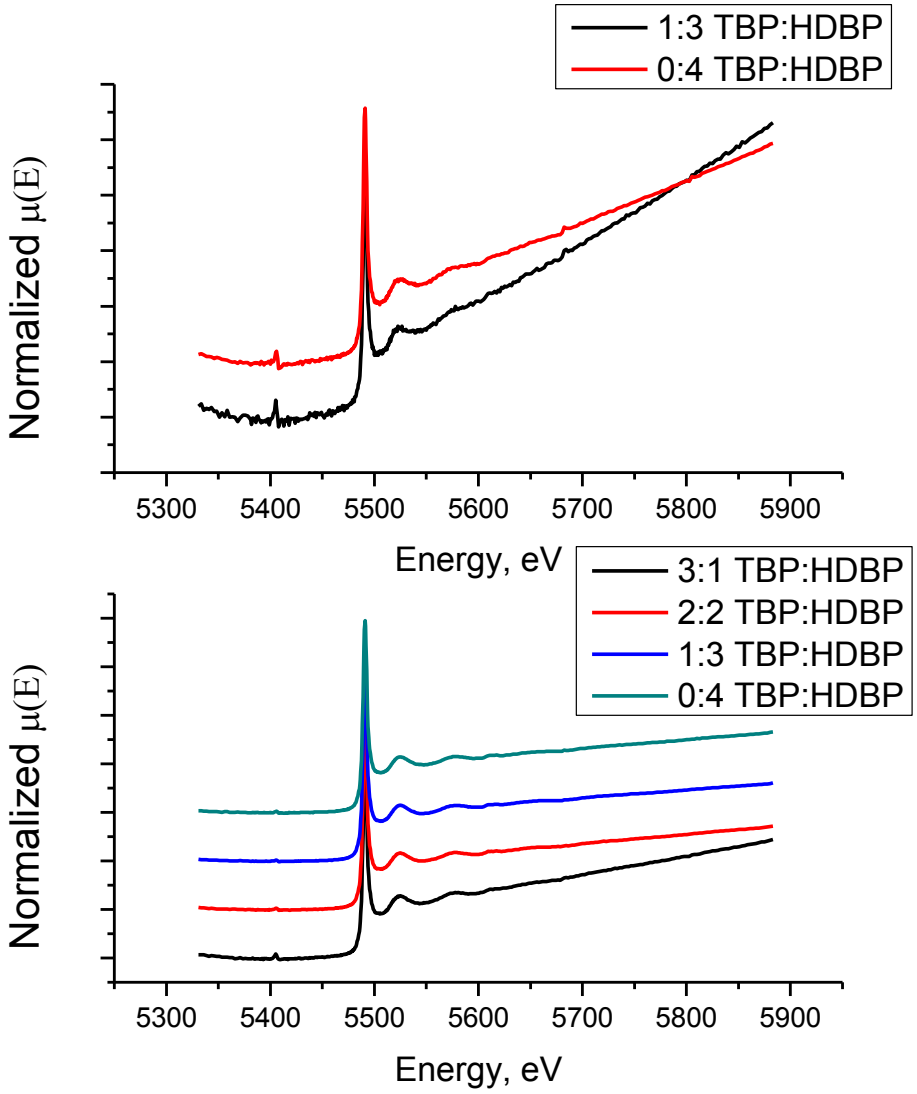

Appendix 2: Normalized μ(E) vs. E data for La(III) extraction into organic phases consisting of TBP and HDBP in varying ratios. Data for 2 M HNO_3 extraction is shown top and 0.2 M HNO_3 extraction is shown bottom.

A3.

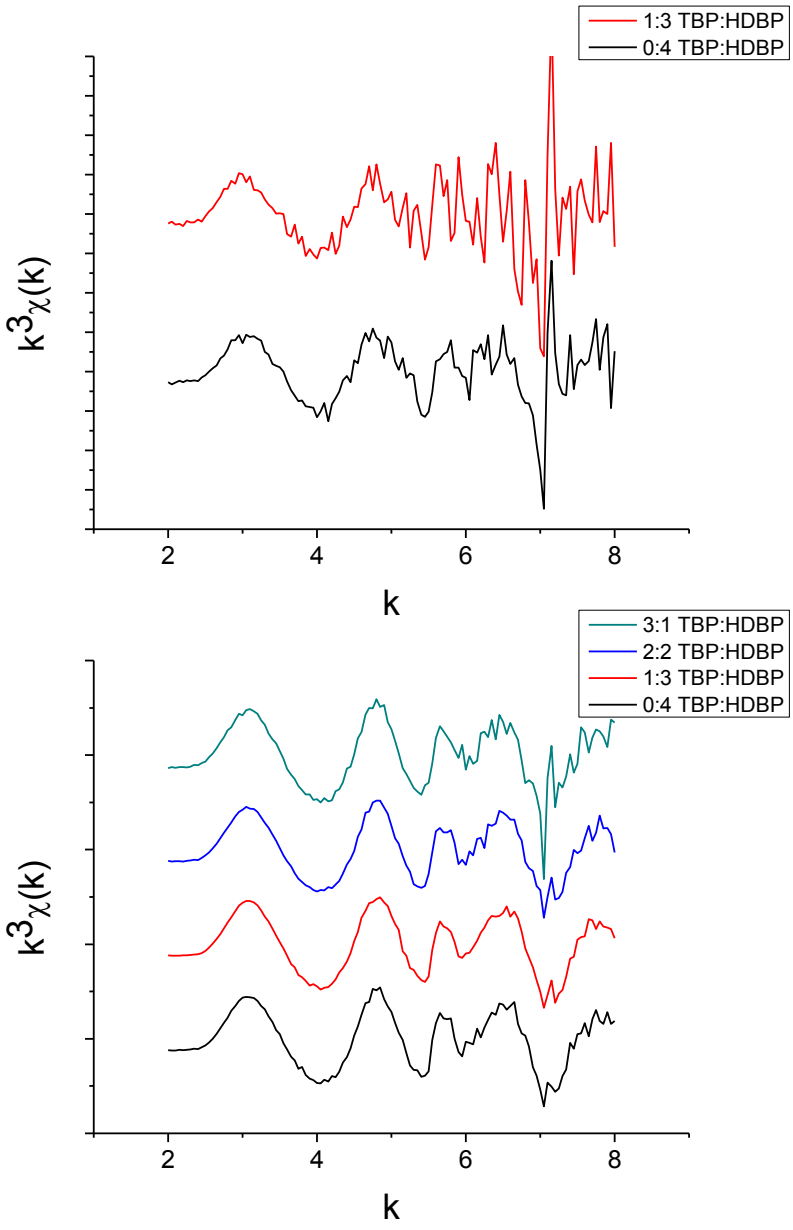

Appendix 3: $k^3\chi(k)$ data for La(III) extraction into organic phases consisting of TBP and HDBP in varying ratios. Data for 2 M HNO_3 extraction is shown top and 0.2 M HNO_3 extraction is shown bottom.

A4.

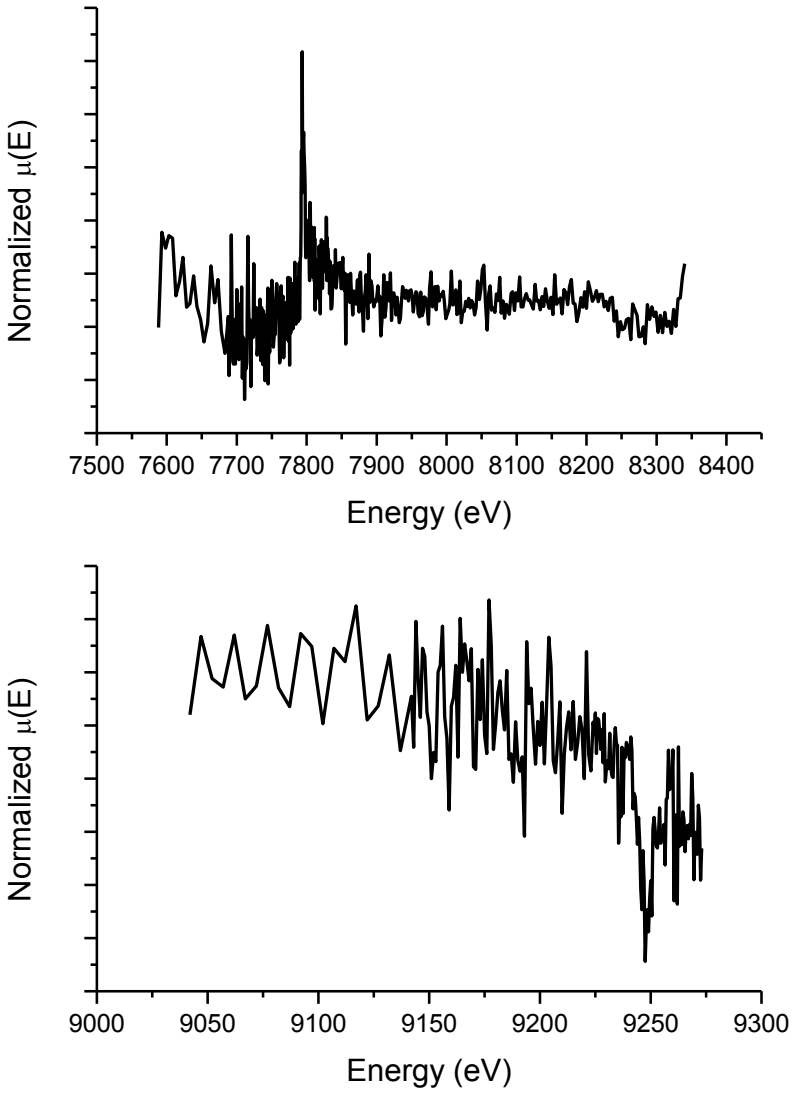

Appendix 4: Normalized μ(E) data for Dy (top) and Lu (bottom) extraction into organic phases contained 1 M TBP in *n*-dodecane. The data for Lu was cut off just after the L_3-edge should have appeared to save beamtime for additional samples.

A5.

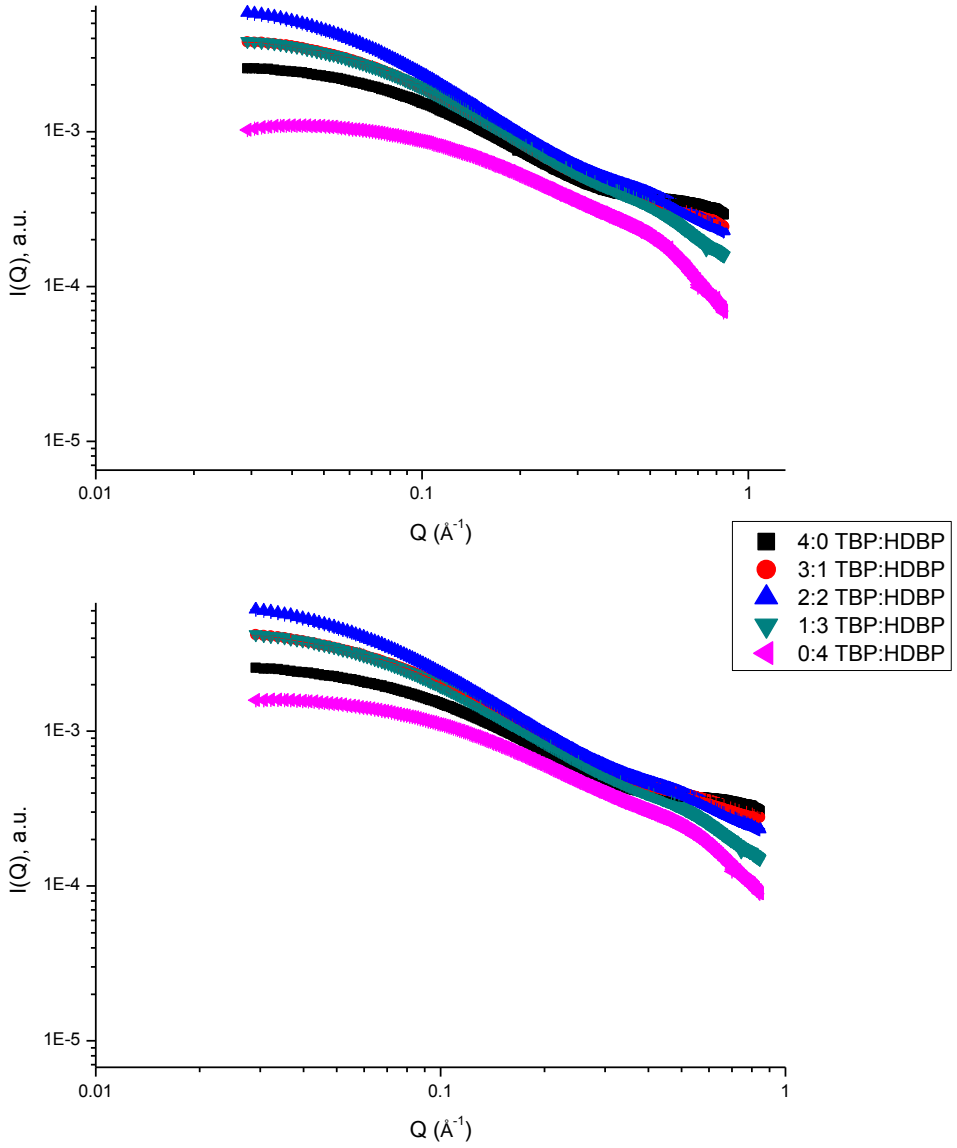

Appendix 5: I(Q) vs. Q data for extraction of Dy from 2 M HNO_3 (top) and the organic phases contacted with 2 M HNO_3 without a metal ion (bottom).

A6.

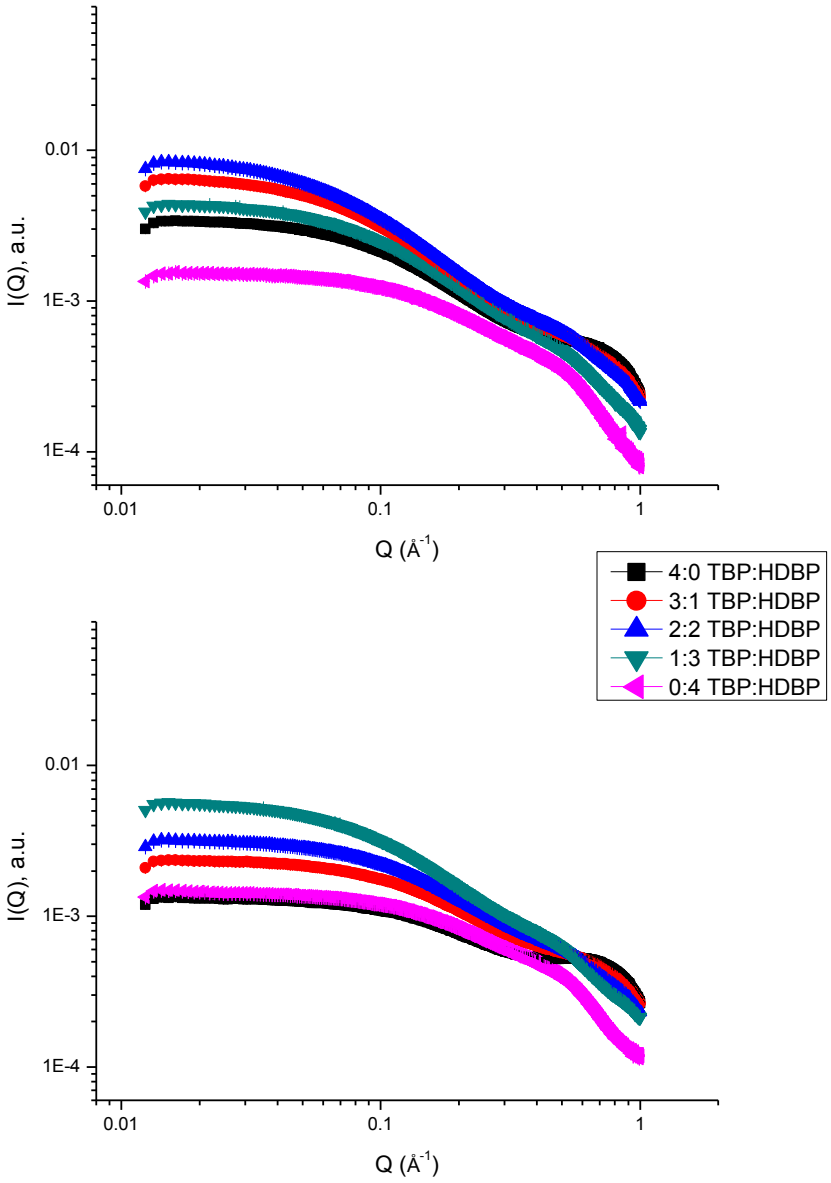

Appendix 6: I(Q) vs. Q data for extraction of La from 2 M HNO_3 (top) and from0.2 M HNO_3 (bottom).

A7.

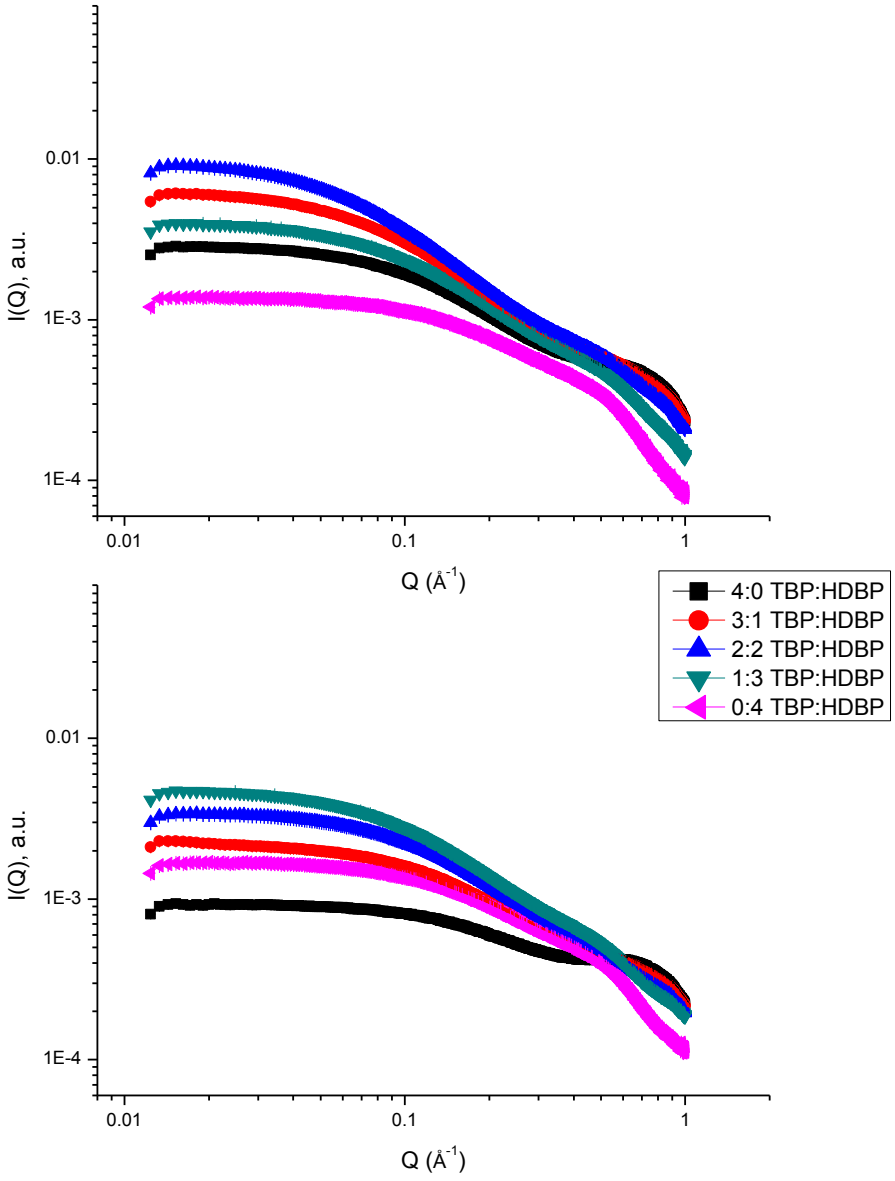

Appendix 7: I(Q) vs. Q data for extraction of Lu from 2 M HNO_3 (top) and from 0.2 M HNO_3 (bottom).

A8.

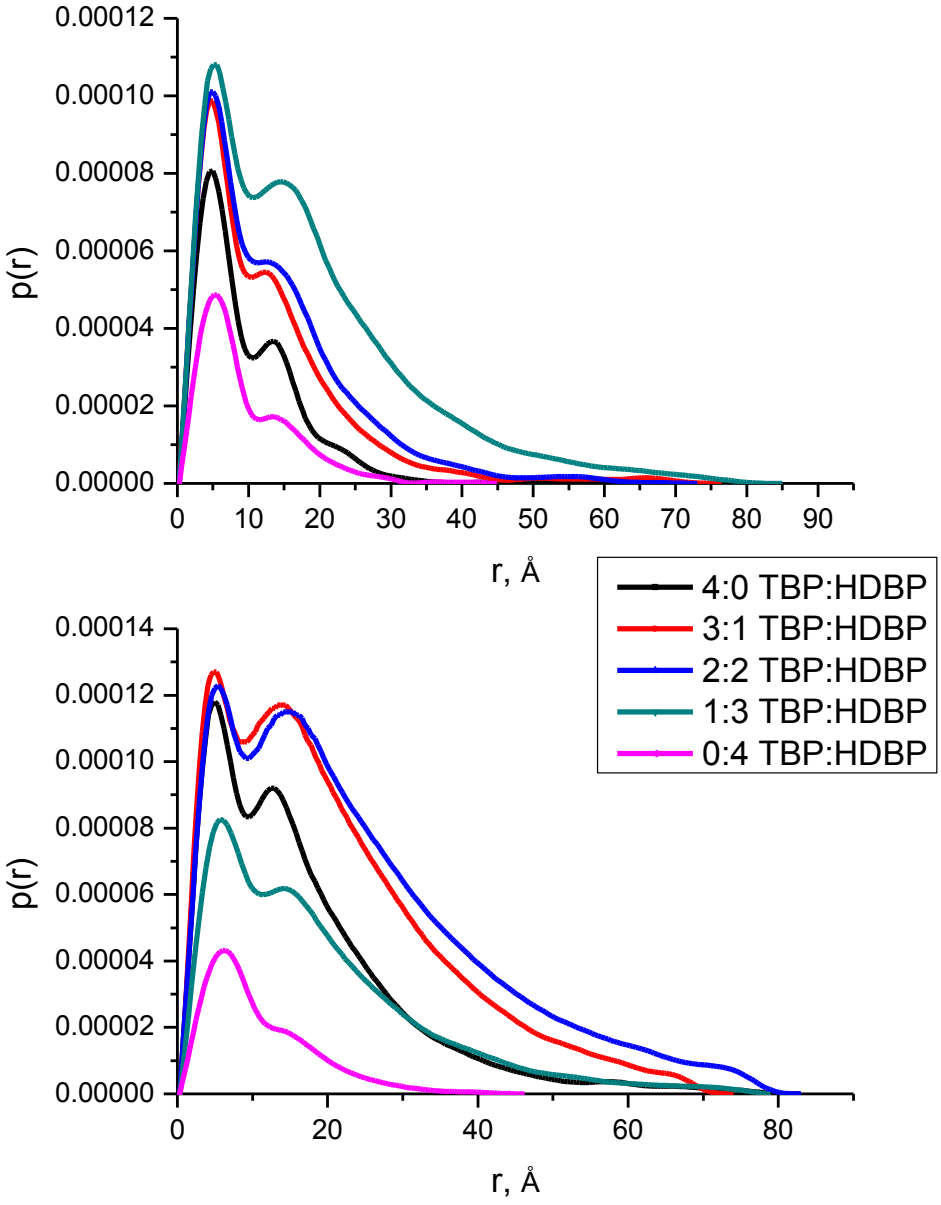

Appendix 8: P(r) functions for the extraction of La from 0.2 M HNO_3 (top) and 2 M HNO_3 (bottom).

A9.

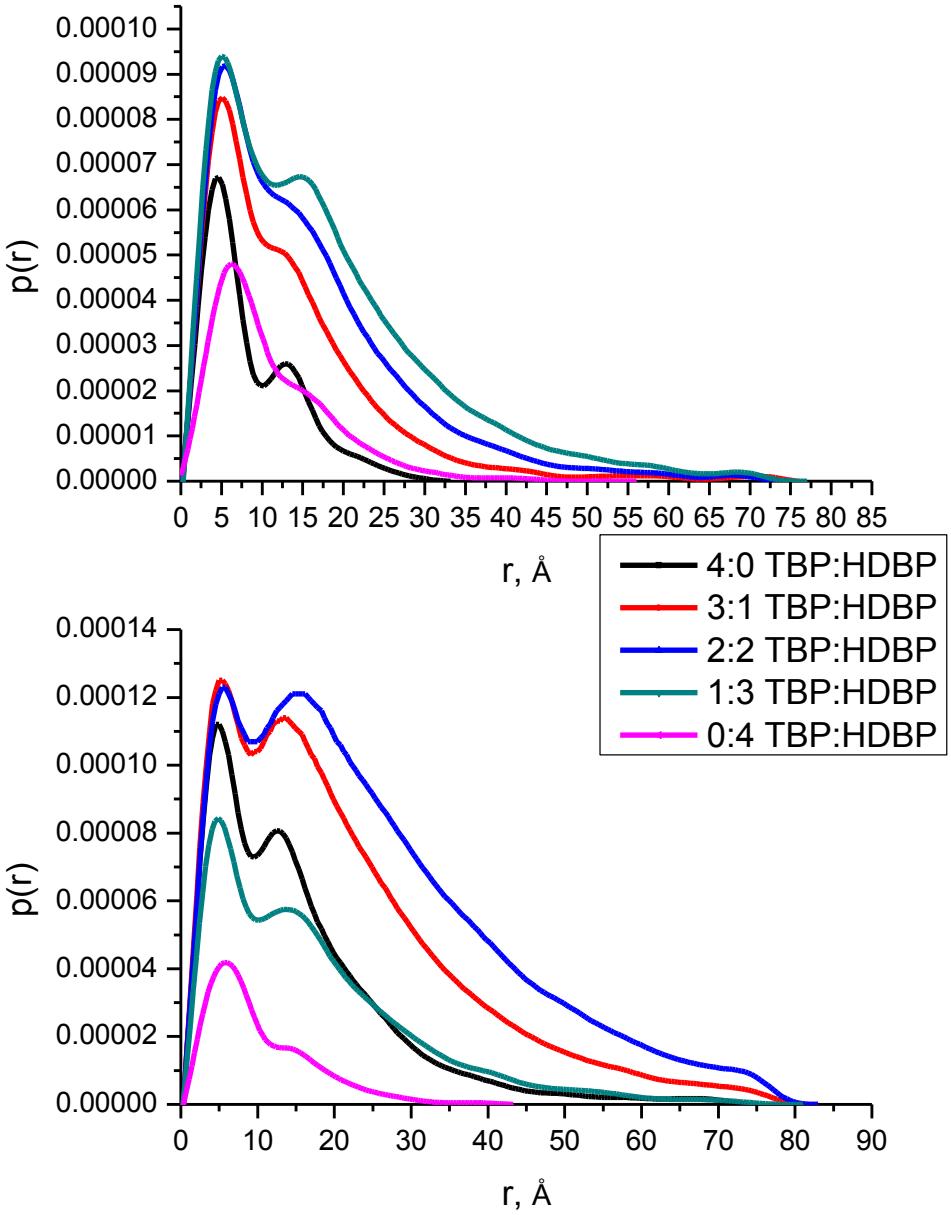

Appendix 9: P(r) functions for the extraction of Lu from 0.2 M HNO_3 (top) and 2 M HNO_3 (bottom).